Encoding of Odour Blends in the Moth Antennal Lobe

Thesis submitted for the degree of

Doctor of Philosophy

at the University of Leicester

by

Kwok Ying Chong

Department of Engineering

University of Leicester

March 2007

Abstract

Encoding of Odour Blends in the Moth Antennal Lobe,
Kwok Ying Chong

Olfaction is a vital sense that informs moths of their environment, and as such moths are adept at chemical sensing. Natural odours are often complex mixtures of different compounds. These mixtures can be perceived to have qualities that are different from their components, sometimes making components difficult to distinguish within a blend. Thus, odour components can interact along the olfactory pathway in a nonlinear fashion such that the mixture is not perceived simply as the sum of its components. Here an investigation is made into possible nonlinear interactions in the olfactory system of moths at two stages along the olfactory pathway. These are the input to and the output from the antennal lobe, the region of the insect brain responsible for the first neural processing of odour information.

The input to the antennal lobes is the neural representation of odours carried by the receptor neurons. By use of a calcium sensitive dye, this activity was observed optically as odour-evoked changes in Ca^{2+} concentration in the moth *Spodoptera littoralis*. This reveals the input pattern to functionally distinct neuropil in the antennal lobes, the so-called glomeruli. Such a calcium imaging analysis requires the identification of the glomeruli, and a novel method was developed to facilitate the automatic identification of olfactory glomeruli. By applying unsupervised clustering analysis to sets of calcium images, glomeruli were functionally identified. Binary odour blend responses were then analysed for nonlinear interactions, but no strong interactions were found.

The output from the antennal lobe, the projection neuron responses, was assessed by computational models. It was demonstrated in pheromone processing models that a spatiotemporal odour code is better able to encode for blend ratios than a spatial code. And it was shown that a spatiotemporal general odour model produces nonlinear component interactions, despite the data-motivated input having none.

For my wife. I met you because I started this, but I finished it because of you. Now, you are my life.

Contents

List of Figures

Acknowledgements

Firstly, great thanks go to Tim Pearce as my supervisor, for his constant flow of ideas and optimism. And not least for his inspiring chats.

Secondly, thanks go to Mikael Carlsson for doing most of the experiments and for our invaluable discussions, which have influenced this work beyond where he has been credited.

Huge thanks go to my parents, Brenda and William, for absolutely everything! It is difficult to overstate how much I owe to them. Your continued support made my whole life possible, and you're still boosting me through life now.

Thanks also go to my wife's parents, Sue and Anthony, for their unwavering encouragement and enthusiasm.

I am grateful to all my friends, especially those with whom I shared many interesting lunches. You picked me up in the bad times, and shared with me the good times. Thank you for keeping me sane. Well, almost.

Most of all, special thanks go to my wife, Hannah. Without your unfaltering care and support throughout and endless love I would never have got this far.

Publications

Peer reviewed articles:

Chong, K.Y., Carlsson, M.A., Hansson, B.S. and Pearce, T.C. (2007). Automatic Identification of Functionally Equivalent Olfactory Glomeruli across Individuals. The 3rd International IEEE EMBS Conference on Neural Engineering, *manuscript accepted.*

Carlsson M.A.*, Chong, K.Y.*, Daniels W., Hansson, B.S. and Pearce, T.C. (2007) Component information is preserved in glomerular responses to binary odour mixtures in the moth *Spodoptera littoralis*. Chemical Senses, *manuscript accepted.*

* Joint first authorship

Book chapter:

Pearce T.C., Chong K.Y., Verschure P.F.M., Bermudez I Badia S., Carlsson M.A., Eric Chanie and Bill S. Hansson (2004). Chemotactic Search in Complex Environments: From Insects to Real-World Applications. In J.W. Gardner & J. Yinon (Eds.), *Electronic Noses & Sensors for the Detection of Explosives* (pp 181–208), Kluwer.

Poster presentation:

Chong, K.Y., Carlsson, M.A., Hansson, B.S. and Pearce, T.C. (2004) Encoding Linearity of Binary Odour Blends in the Antennal Lobe of *Spodoptera littoralis*. 7th International Congress of Neuroethology, Nyborg, Denmark.

Chapter 1

Introduction

Insects, in particular moths, are adept at chemical sensing. This can be seen from behavioural studies regarding the complex responses of insects to olfactory stimuli (Quero, Fadamiro, & Baker, 2001; Kerguelen & Carde, 1997; Baker & Haynes, 1996; Kuenen & Carde, 1994; Harris & Foster, 1991; Hartlieb & Anderson, 1999; Laing, 1989). Insects are able to use olfaction to locate food and host plants, and can even be trained to locate particular scents (Kerguelen & Carde, 1997). In species of moths that use pheromones for sexual communication, males are able to detect and distinguish minute amounts of female pheromones from a background of other chemicals. Calling females release pheromones, becoming a point source of a pheromone plume. Males are able to locate females of their own species by identifying the correct pheromone plume, and altering their flight behaviour accordingly to perform chemotaxis. Males switch behaviour between so called 'casting' and 'surging' depending on the presence, quality, and time dynamics of pheromone plume (Hartlieb & Anderson, 1999).

In short, olfaction is a vital sense that informs insects of their environment. Insects must be able to extract and process relevant chemical information about its environment (Pearce *et al.*, 2004). Chemical information

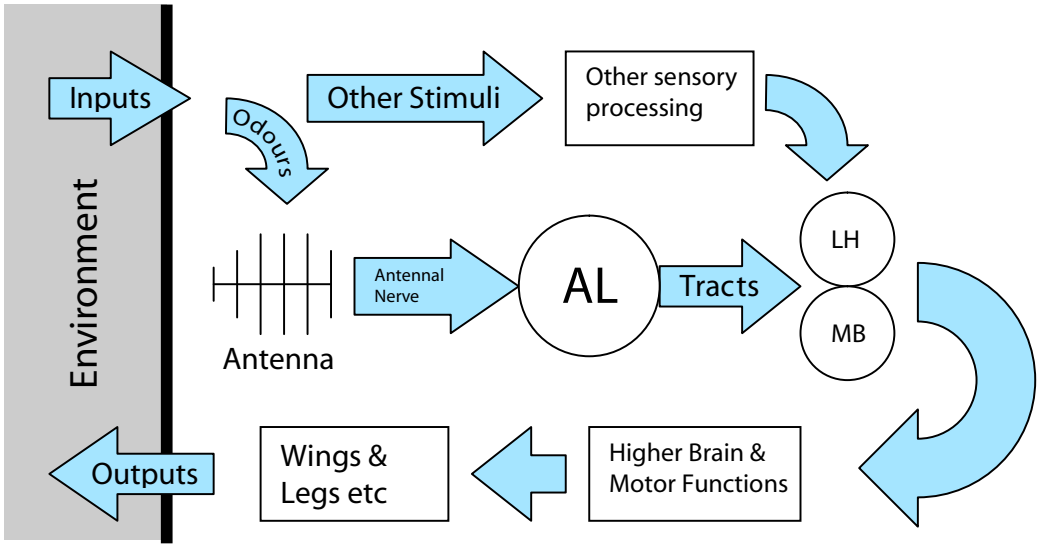

Figure 1.1: Overall system context of the antennal lobe. AL is the antennal lobe, MB the mushroom bodies and, LH the lateral horn. This schematic shows the role of the AL in relation to the animal and its environment. The AL is a vital stage in the olfactory pathway.

is first captured by the olfactory receptor neurons (ORNs) at the antennae. On each antenna, these ORNs send axons down to an antennal lobe (AL), where their dendrites arborise into dense neuropil, called glomeruli, and form synapses onto interneurons. The role of the AL is to aggregate and encode this olfactory information, preserving the aspects that are relevant, and encapsulating this for higher brain processes and motor functions. The relevant coding parameters include odour identity, quality, concentration, component ratios and temporal aspects. The AL must be able to encode some or all of these parameters using a spatiotemporal output, which is then passed onto the lateral horn (LH) and mushroom body calyces (MB) for sensory integration and memory. As such, the AL is a crucial part of the olfactory system of insects, and indeed plays a vital role in insect behaviour (Figure 1.1).

The insect must interact with its environment to achieve its goals, be that locating a mate or food or other activities. Critically, its environment determines its behaviour, but its behaviour is also designed to change its environment to maximise its ability to attain its goals (Vickers, Christensen, Baker, & Hildebrand, 2001). Therefore, what is relevant to the animal behaviourally determines its biological setup. For instance, the odour stimuli in which moths are primarily interested are odour plumes with fast temporal features and complex blends. This has implications for the form and function of the AL and its inputs. It has been suggested that there are ORNs that respond only to the changes in odour concentration because this flux may provide information of odour plumes (Todd & Baker, 1999; K. E. Kaissling, 1998). Another example is that of the pheromone detection subsystem of the AL called the macroglomerular complex (MGC). Pheromones are a very precise, species-specific blend of pheromone components, and this has consequences for the workings of the MGC, which cause the MGC and the general odour system to have significant differences.

Odours in the natural environment for moths are usually found as mixtures. General odours, or more relevantly host-plant odours, are usually composed of many chemical compounds in a range of ratios. Yet most studies so far have investigated single component odours. Much of what is known regarding the neural representation of odour blends is derived from how blends are perceived compared to the blend components. Psychophysical and behavioural studies in invertebrates (Chandra & Smith, 1998; Hosler & Smith, 2000) and vertebrates (Wiltrout, Dogra, & Linster, 2003; Laing & Livermore, 1992; Laing, Panhuber, & Slotnick, 1989) show that blends are sometimes

perceived elementally where the blend is perceptually the combination of the components, and sometimes perceived configurally where the blend is perceptually novel and distinct from its components. An elemental perception would imply a coding scheme that does not change the neural representation of components within a blend. In this case, component information can easily be extracted from the blend. A configural perception would imply the opposite, with component representations interacting non-trivially and generating a blend representation from which component information cannot easily be extracted. It has been suggested that such configural coding can be a result of nonlinear interactions in the neural representations such as synergy and suppression (Duchamp-Viret, Duchamp, & Chaput, 2003), where synergy is an increased neural response from odour component interactions and suppression is a lessened response due to interactions.

This thesis investigates the encoding of odour blends in the antennal lobe. This is done through analysis of data from antennal lobes and also through computer modelling of networks of neurons that approximate the interneurons and their interconnections found in the antennal lobe. Chapters 2 and 3 deal with optical imaging of the antennal lobes. This imaging was achieved by bathing the antennal lobe in a calcium sensitive dye, which mainly reports the cumulative presynaptic activity of the receptor neurons innervating each glomerulus. As such, it reflects the input to the glomeruli. Chapter 2 develops a new technique for automatically identifying glomeruli just from the pattern of these calcium signals. This new technique is then used in Chapter 3, which searches for sources of configural processing, in the form of synergistic and suppressive nonlinearities in the olfactory code as it enters the glomeruli.

In Chapters 4 and 5, models of the MGC and general AL were created and studied. Modelling allows the assessment of the connectivity of the interneurons, to see how different connection schemes will affect the odour code. Chapter 4 compares and contrasts two inhibition schemes and their respective responses to binary blend ratios. One model generates a predominantly spatial code and the other a spatiotemporal code, and they are analysed for their ability to encode blend ratios. In Chapter 5, a general odour model is built and realistic odour input to the glomeruli is created that is motivated by the data from Chapter 3. This general odour model is an extension of the spatiotemporal MGC model. The odours are then presented as blends, and an assessment is made as to whether this spatiotemporal blend code generates any nonlinear interactions that might be a source of configural coding.

The remainder of this introduction provides some background information with a brief review of existing knowledge of insect antennal lobes, and a review of previous antennal lobe modelling efforts.

1.1 Biological Constraints

1.1.1 Morphology

Sensilla

The moth has two antennae, but each antenna (and its associated brain functions) can be regarded as a separate olfactory organ and the two systems only combine at the highest level of brain processes. The ORNs are located in sensilla. The number of ORNs in each sensillum depends on the type of sensillum. A sensillum is too small a complex to merit the status of organ, but shows a highly stereotyped organisation (Keil, 1999). Sensilla are evenly

dispersed all over the antenna. In the males of the moth *Manduca sexta*, there are around 3×10^5 ORNs on each antenna (Anton & Homberg, 1999). The axons of the ORNs are sent into the antennal nerve and down to the AL.

Glomeruli

In the AL, the ORNs innervate the glomeruli – spheroids of tightly packed dendritic and axonal branches. These first-order synaptic neuropil are where ORNs, PNs and LNs interconnect. *M. sexta* males have around 66 glomeruli, 360 LNs and 900 PNs (Anton & Homberg, 1999).

There are many different receptor types, since the ORNs are tuned to respond to a variety of chemicals. Functionally characterised ORNs have been found to project in a chemotypic manner (Carlsson, Galizia, & Hansson, 2002; Hansson, Almaas, & Anton, 1995; Hansson, Ljungberg, Hallberg, & Lofstedt, 1992). In *Drosophila melanogastor*, the number of receptor gene types equals the number of glomeruli (Carlsson *et al.*, 2002; Vosshall, 2001). Thus, it is thought that, although different ORN types are intermingled on the antennae, ORNs of the same type send axons to the same glomerulus. Thus each glomerulus is a site of convergence for ORNs of the same type. Synapses in the AL are almost entirely restricted to the glomeruli. ORNs synapse directly to both LNs and PNs, and are largely excitatory. The most common is dyadic synapsing where one presynaptic bouton contacts two post synaptic elements (Anton & Homberg, 1999; Homberg, Christensen, & Hildebrand, 1989).

In moths there is sexual dimorphism of the AL (Anton & Homberg, 1999; Christensen, Mustaparta, & Hildebrand, 1989; King, Christensen, & Hildebrand, 2000). Males have large glomeruli at the top of the AL called the

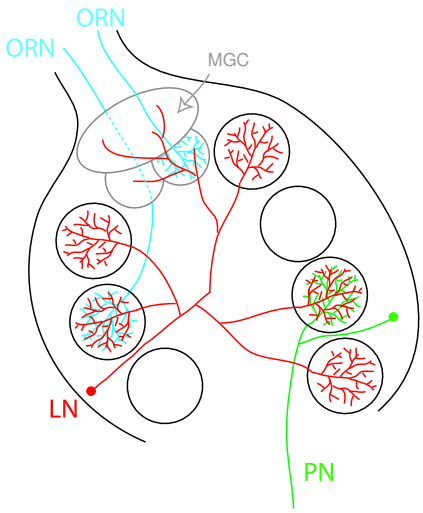

Figure 1.2: Ramifications in the glomeruli. ORNs (blue) and PNs (green) typically innervate single glomeruli, whereas LNs (red) tend to innervate many glomeruli.

macroglomerular complex (MGC) which are responsive to sex-pheromones (actually, males and females have the same glomeruli, but males have become morphologically different (Rospars & Hildebrand, 2000)). The pheromone sensitive ORNs will branch mainly to the MGC. In the moth *Spodoptera littoralis*, the MGC is composed of three glomeruli. The largest glomerulus is the Cumulus, which sits atop two smaller ones. The MGC is the pheromone processing subsystem and is largely separate to the rest of the olfactory system. There is some, but very little interaction between the MGC and the rest of the glomeruli. Even the LNs and PNs within the MGC are sexually dimorphic (Homberg *et al.*, 1989; Homberg, Montague, & Hildebrand, 1988). The rest of the AL is composed of general olfactory glomeruli.

LNs and PNs

LNs are amacrine interneurons with processes restricted to the AL, while PNs are output interneurons with axonal processes to other brain regions as well

as dendritic processes within the AL. Each glomerulus receives arborisations from around 13 or 14 PNs. Using high powered light microscopy as well as electron microscopy on ultrathin slices of glomeruli, Distler and colleagues directly studied the synapses in these glomeruli. The different neurons were stained and labelled, and it was found that ORNs form synapses directly onto LNs and PNs (Distler & Boeckh, 1996), LNs form GABA-ergic synapses onto PNs and also back onto ORNs (Distler & Boeckh, 1997a, 1997b), and PNs can synapse back onto LNs (Distler, Gruber, & Boeckh, 1998). Although these observations were made of the AL in the American cockroach, *Periplaneta americana*, these studies illustrate some of the possible interconnections between neuron classes in insect AL. In the moth *M. sexta*, indirect evidence of the synaptic connectivity, that is implied by the neural activation patterns (Christensen, Waldrop, Harrow, & Hildebrand, 1993), shows that ORNs give monosynaptic excitatory input to both the LNs and PNs. The LNs can have inhibitory synapses onto PNs and LNs in its own glomerulus and, importantly, inhibitory synapses onto PNs and LNs in other glomeruli. Since the majority of PNs are uniglomerular or innervate just a few glomeruli, LNs are the main mechanism for inter-glomerular interaction. PNs receive excitation from ORNs, but they are influenced greatly by the inhibition from LNs.

Figure 1.2 shows the spread of the influence of LNs. While ORNs are always uniglomerular and about half of PNs are uniglomerular, LNs are usually multiglomerular. Morphologically, there are two types of LN: symmetric and asymmetric. Symmetric LNs have arborisations throughout the AL glomeruli. They are so called because each major neurite innervates in approximately the same number of glomeruli. However, some symmetric LNs

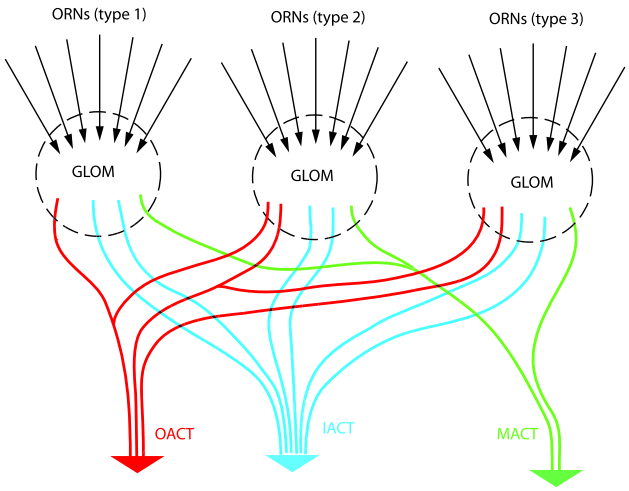

Figure 1.3: Neural pathways. ORNs of the same type converge on their respective glomeruli. Here they synapse onto LNs and PNs. Most PNs are organised so that their axons exit the AL through one of three main tracts. These are shown in the diagram as the colour coded tracts. There are PN axons from each glomerulus that run through the IACT (blue), PN axons from each glomerulus that run through the OACT, and the same for the MACT (green).

innervate more globally, and some are more specific to certain glomeruli. An asymmetric LN may also have arborisations throughout, but is very densely arborised in one glomerulus, and very sparse in others. Another type of asymmetric LN has localised fields of arborisations (just two or three fields) (Anton & Homberg, 1999; Hartlieb, Anton, & Hansson, 1997; Anton & Hansson, 1995).

Antenno-Cerebral Tracts

The encoded olfactory information feeds out of the AL into the mushroom bodies (MB) and the lateral horn (LH) via five antenno-cerebral tracts. These are the inner antenno-cerebral tract (IACT), outer (OACT), middle (MACT), dorso-median (DMACT) and dorsal (DACT) antenno-cerebral

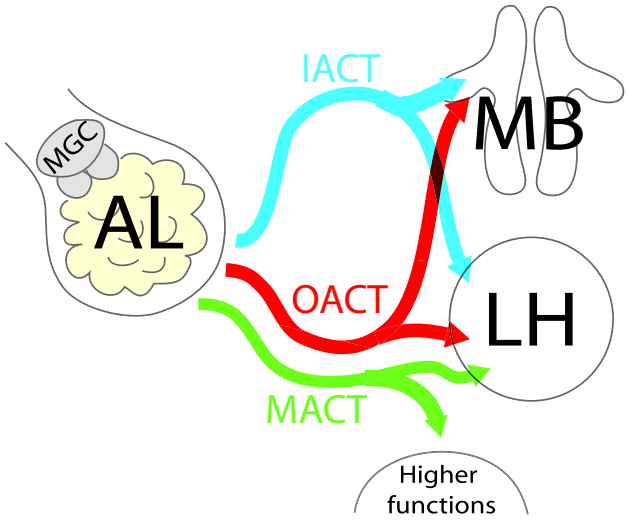

Figure 1.4: Three main antenno-cerebral tracts. These tracts are composed of the axons of the PNs. The IACT and the OACT visit the LH and the MB calyces in a different order. This gives insight into the function of the PNs. MACT PNs do not innervate the MB at all, only the LH, before going to higher brain and motor regions.

tracts (Anton & Homberg, 1999). In *M. sexta*, the IACT has 360 PNs with an additional 40 from the MGC in males; the OACT has 340; the MACT 120; DACT 30; and DMACT 10 (Homberg *et al.*, 1989) (see Table 1.1). So, of these tracts, the three main pathways are the IACT, OACT and MACT. Each PN within the AL sends its axon down one of the tracts, and then sends ramifications into the calyces of the MB, the LH and other higher brain regions. The MB is thought to deal with memory and learning functions (Homberg *et al.*, 1989, 1988). The LH is where the senses are integrated along with past experiences, and possibly where decisions are made.

1.1.2 Function and Physiology

ORN Selectivity and Sensitivity

ORNs respond most intensely and with the lowest thresholds to specific kinds of molecules. The molecule or type of molecule which elicits a response with the lowest threshold is said to be the one to which the ORN is tuned. Tunings may be optimised for molecular shapes, lengths, electron distribution, location of double bonds, and other aspects. However, this tuning does not mean that they only respond to those molecules. For the general odour system ORNs respond to many chemical compounds with varying levels of response, and this defines their receptive field. The ORNs have overlapping receptive fields, so a molecule would elicit responses from many ORN types, and it is the pattern of response that allows the AL to identify the molecule (Todd & Baker, 1999).

ORNs are also sensitive to concentrations of the odour stimulus, in both an absolute and a relative sense. They are able to detect changes in concentration strengths, even of blends. So when the concentration of a particular odour blend changes, the relative ratios of firing of the different ORNs will remain consistent and will accurately report that blend ratio to the brain (Todd & Baker, 1999).

It has been suggested that in fact ORNs are flux detectors rather than concentration detectors, and this is certainly true of ORNs in moths tuned for pheromone components (K. E. Kaissling, 1998). By flux I mean a change of concentration.

LN Types and Functions

There are (at least) three postsynaptic response types of LN: i) short latency excitatory response that represents a monosynaptic input from ORNs, ii) delayed excitatory response, and iii) delayed inhibitory response (Christensen *et al.*, 1993). This does not mean that there are three classes of LN, but three ways each LN could respond to ORN input.

Monosynaptic, short latency excitatory responses are by far the most common. This begins with membrane depolarisation and a brief period of firing (approximately matching duration of stimulus), followed immediately by a moderate period of hyperpolarisation during which firing is abruptly suppressed (up to 2 seconds) (Christensen *et al.*, 1993). Delayed excitatory responses display depolarisation at 200–300 ms after odour stimulus and are followed by little or no hyperpolarisation. Delayed inhibitory responses are hyperpolarisations during which firing is completely suppressed at 200–250 ms. The latency to the hyperpolarisation is greater than 5 ms, indicating that the input from antennal-nerve afferents is probably polysynaptic (Christensen *et al.*, 1993).

LNs can clearly be seen to shape PN responses. The inhibitory effect of LNs can be used in different ways. The obvious one is to reverse an excitatory input from ORNs into an inhibitory one. This allows enhancement of the output of one glomerulus while reducing the output of other glomeruli, thus enhancing the contrast between activity in the glomeruli. Another role is the indirect excitation of PNs through a disinhibition mechanism, when a LN is itself inhibited and releases PNs from inhibition and thus allowing PNs to spike. Yet another role is to sharpen the temporal response of PNs. Without

inhibition, PNs would take a long time to return to a normal firing rate after excitation, and any fast temporal characteristics of the stimulus would be lost.

PN Types and Functions

PNs are the output neurons of the AL. They usually have excitatory output, but can also be inhibitory such as some PNs in the MACT and DACT. The antenno-cerebral tracts outlined above are an important indicator of functional subgroups of PNs. If all the PNs were functionally the same, then a single tract would suffice and the animal would likely not have expended resources in this fashion. Table 1.1 summarises the PN types as described by Homberg *et al.* (1988).

The most common PN types in the honeybee are m-act and l-act PNs. m-act PNs are equivalent to IACT PNs in the moth, and l-act PNs are equivalent to OACT PNs although they are multiglomerular in the moth and uniglomerular in the honeybee. It is argued that these PN types are quite different with different roles to play (Muller, Abel, Brandt, Zockler, & Menzel, 2002). IACT PNs innervate the MB calyces and the LH in reverse order to OACT PNs as described above. The significance of this is that the signals from the IACT and OACT arrive at the MB and the LH with different timings. But more than this, IACT PNs and OACT PNs are physiologically different neurons. IACT PNs have a higher background activity level and respond in an odour specific manner, while OACT PNs have lower background activity and are generalists, responding to many different odours (Muller *et al.*, 2002). This indicates that the spatial code encapsulates odour identity and may be conveyed by the IACT PNs. OACT PNs may instead convey

Cell type	Cells per AL	Arborisation type	Arborisations outside AL	Possible neurotransmitter
PIa(MGC)	35-40	u	MB Calyces, LH	-
PIb(MGC)	(male only)	u	MB Calyces, LH	-
PIa(G)	360	u	MB Calyces, LH	-
PIb		-	Superior Protocerebrum	-
PIc		m	MB Calyces, LH	-
POa	340	m, u	LH	-
POb		m	LH	ACh, peptides
POc		m	MB Calyces, LH	-
POd		m, u	Inferior protocerebrum	-
PM	120	m, u	LH, inferior protocerebrum	GABA
PD	30	m	LH	GABA, peptides
PDM	10	u	MB Calyces, LH	peptides

Table 1.1: Details of PN types. These details are of *M. sexta* taken from Homberg *et al.* (1989). PI refers to PNs that go through the IACT, of which there are 3 types – a, b, c. The types have different properties such as arborisation pattern and axon destination. The IACT also contains PN axons from the MGC. These PNs are not present in females. PO refers to PNs that go through the OACT; PM those that go through the MACT; PD through the DACT; and PDM through the DMACT. The number cells are the totals for each tract. m means multiglomerular and u uniglomerular. The dash indicates where no data was available

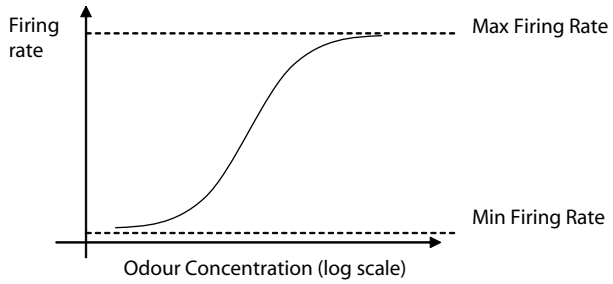

Figure 1.5: Sigmoid shaped response curve. PN responses have a sigmoidal shape as odour concentrations increase on a logarithmic scale (Carlsson & Hansson, 2003). There is a minimum firing rate for which the cell does not fall below, and a maximum firing rate that the cell cannot exceed. This means that there is a lower threshold of odour concentration at which the cell will start to respond, and an upper threshold above which the cell cannot distinguish between concentration levels. Between these, the cell has an approximately linear response to the log of the concentration.

other information about odour stimuli, perhaps about concentration or time dynamics of odour plumes. It is also apparent that IACT PNs and OACT PNs have different connections with LNs. IACT PNs show multi-phasic patterns that indicate strong inhibitory influence, whereas the OACT PNs show low latency response onsets with a gradual decay in activity showing little influence from inhibition (Muller *et al.*, 2002).

Like the ORNs, the PNs have specific sensitivity tunings. It is likely that the PNs have sigmoid shaped response curves to odour concentration as in Figure 1.5. Each PN is only sensitive to concentration change across the range where that PN response has the largest slope. Therefore, in order to cover all possible relevant odour concentrations, there must be many PNs that are sensitive to many different concentration ranges. Hence, it is the resulting population code that encodes for concentration.

Neuroactive Substances

There is a large variety of neurotransmitters and neuromodulators present in the AL, and not all are yet known. The main neuromediators are acetylcholine (ACh) and γ-amino-butyric acid (GABA). ACh is the principal neurotransmitter of ORNs and predominantly elicits an excitatory response in LNs and PNs (Homberg & Muller, 1999). GABA appears to be the principal neurotransmitter of LNs (Homberg & Muller, 1999; Christensen, Waldrop, & Hildebrand, 1998). It is unclear what neurotransmitters are used by PNs. However, GABA is also used by many PNs in the MACT and the DACT. This indicates that these PNs are perhaps inhibitory (Hoskins, Homberg, Kingan, Christensen, & Hildebrand, 1986).

LNs use a high number of other neuroactive substances, most probably only as cotransmitters with GABA (Homberg & Muller, 1999). There is apparently a high degree of heterogeneity in the LNs with respect to cotransmitters of GABA. Biogenic amines (serotonin, dopamine) can be used by feedback centrifugal neurons to modulate the activity of the glomeruli. These centrifugal neurons have axons that descend into the AL from higher brain regions.

1.2 Antennal Lobe Modelling Review

1.2.1 Level of Modelling Detail

Full Spiking Dynamics

Modelling of invertebrate olfactory neural systems comes in many flavours. From large networks of firing-rate or phase description oscillating neurons

which are analytically tractable (Ermentrout, Flores, & Gelperin, 1998; Ermentrout, Wang, Flores, & Gelperin, 2001), to small networks of highly detailed and biologically realistic olfactory interneurons (Av-Ron, 1994; Av-Ron & Rospars, 1995; Av-Ron & Vibert, 1996). High detail models that are built from ion currents upwards are usually adapted from Hodgkin-Huxley equations for a spiking neuron (Wilson, 1999a). Sodium and potassium are modelled and action potentials are generated from this single-compartment neuron model when a particular level of input current creates a limit cycle in the system. Communication between cells are mediated by these action potentials. Slow calcium currents can be added to create neurons with further features, such as bursting activity (Av-Ron, 1994; Av-Ron & Rospars, 1995; Av-Ron & Vibert, 1996) and adaptation (Bazhenov, Stopfer, Rabinovich, Huerta, *et al.*, 2001; Bazhenov, Stopfer, Rabinovich, Abarbanel, *et al.*, 2001). Studies by Av-Ron *et al.* (1994, 1995, 1996) show that the firing patterns that are observed in biological studies of antennal lobes can be reproduced by connecting four or fewer of these neurons together.

Spiking neurons can also be modelled by FitzHugh-Nagumo equations (Wilson, 1999c). This has been used in antennal lobe modelling by Rabinovich *et al.* (2001). These equations are not based on biophysical variables like ion channels, but instead have an abstract recovery-variable which creates a limit cycle that forms the action potentials. The advantage of FitzHugh-Nagumo equations is that they are computationally less expensive, yet are able to emulate the dynamics of the membrane potential of neurons including action potential generation. Rabinovich *et al.* (2001) use FitzHugh-Nagumo neurons to demonstrate that the Winnerless Competition theory they develop applies to biologically realistic spiking neurons.

Integrate and Fire

The next level of abstraction avoids biophysical descriptions of action potentials and involves only the membrane potential. Information is still mediated by spikes, with presynaptic spikes influencing the membrane potential depending on whether they are excitatory or inhibitory. Neurons will simply release a 'spike' whenever the membrane potential reaches a threshold. When a spike is released, the membrane potential is reset to a resting level, and the integration process starts again. The membrane potential is modelled as a first order linear equation, and as such, the influence of presynaptic spikes decays exponentially with time. Thus, many presynaptic spikes are needed in a short space of time to reach threshold level and evoke a spike. Variability can be incorporated into integrate-and-fire neurons either by a probabilistically fluctuating threshold (Linster, Masson, Kerszberg, Personnaz, & Dreyfus, 1992), or by relating the membrane potential to a probability which determined if the neuron will fire at any point in time (Linster, Masson, Kerszberg, Personnaz, & Dreyfus, 1993; Masson & Linster, 1995; Linster & Dreyfus, 1996; Linster & Masson, 1996; Linster & Cleland, 2004; Linster, Sachse, & Galizia, 2005).

Firing-rate

Simplifying the model allows mathematical analysis of high level properties of the system. An example is the mathematical proof of the existence of limit cycles in Winnerless Competition (WLC) inhibitory networks (Afraimovich, Rabinovich, & Varona, 2004). With mutually inhibitory networks, the case with symmetric connection strengths is the well known Winner-Takes-All

(WTA) network. WLC networks are mutually inhibitory networks with asymmetric connections. The asymmetry unbalances any neurons dominating activity, and thus the activity state of the system spontaneously changes. These switches of state generate a sequence of neuronal firing. Here, the firing-rates of neurons are modelled with equations based on Lotka-Volterra (predator-prey) equations (Afraimovich *et al.*, 2004). The proof guarantees the existence of such a sequence under certain circumstances, since it will be an attractive limit cycle. WLC is applied to model the antennal lobe and are found to resemble the neural response patterns in the antennal lobe when asymmetric mutual inhibition connects neurons with FitzHugh-Nagumo spiking dynamics (Rabinovich *et al.*, 2000, 2001). Different odours elicit different sequences of neural activity patterns, and in this way, a spatiotemporal code is generated for the odours.

A limiting factor that has caused a trade-off between high neuronal detail and network size in models is mathematical and computational complexity. With the ever increasing processing power available, this limit is being raised continually for simulations (Bazhenov, Stopfer, Rabinovich, Huerta, *et al.*, 2001; Bazhenov, Stopfer, Rabinovich, Abarbanel, *et al.*, 2001). However, for models that pursue an analytical understanding of aspects of olfactory encoding, it will always be necessary to make simplifications.

1.2.2 Spatial Aspects

Network Morphology and Connectivity

Generally in the antennal lobe, the exact connectivity between the neurons is not known. However, there are some general principles across species: afferent input from the antennae come from olfactory receptor neurons that send

axons down to the antennal lobe, forming synapses with antennal lobe interneurons and providing excitation directly; antennal lobe interneurons are divided into two broad classes, namely local interneurons and projection neurons; local interneurons are amacrine cells that form GABA-ergic synapses onto other interneurons; projection neurons form excitatory synapses onto other interneurons within the antennal lobe, but also have axonal processes to higher brain regions and are thus the output neurons of the antennal lobe.

There are different abbreviations used by researchers of different genera. Thus to prevent confusion, the following abbreviations, taken from *Lepidoptera* literature, will be used to refer to all species: antennal lobe, AL; olfactory receptor neuron, ORN; local interneuron, LN; projection neuron, PN. ORNs are divided into subpopulations, with each subpopulation expressing a different receptor type. On the antennae, these populations are thought to be inter-mingled and distributed evenly. However, ORNs of a subpopulation expressing the same receptor type will send axons that converge to a specific, spatially localised neuropil in the antennal lobe (Couto, Alenius, & Dickson, 2005; Fishilevich & Vosshall, 2005). Such neuropil of convergence are called glomeruli. It is within these glomeruli that ORNs, LNs and PNs form densely interwoven processes upon which synapses can form between neurons.

In the moth systems, there exist in males of the species a specialised subsystem called the macroglomerular complex (MGC) which is dedicated to the detection of pheromones. Since it is almost entirely functionally separate from the rest of the antennal lobe, and since it has a much simplified task of detecting only one specific pheromone blend, the MGC provides a starting point from which to investigate the antennal lobe.

Recreating Spiking Patterns

High-detailed models of neurons can be created by using Hodgkin-Huxley equations. The inclusion to the model of a calcium current and a calcium-dependent potassium current extends the spiking dynamics of a standard Hodgkin-Huxley neuron with bursting behaviour, exhibiting excitability and oscillatory behaviour (Av-Ron, 1994). The exact parameters for these bursting neurons can be modified to create different response behaviours, in particular firing patterns that are observed in moth MGC physiology. These patterns include bursting that is time-locked to the stimulus or spike bursts that last for the same duration as the stimulus.

Furthermore, these neurons can be connected into very small networks of 4 or fewer neurons that can produce biologically realistic response patterns. Different configurations of these neurons in simple networks can produce neurons that are responsive to the presence of different pheromone components during stimulation (Av-Ron & Rospars, 1995; Av-Ron & Vibert, 1996). As has been observed in biological recordings from the moth *M. sexta*, which uses two major sex pheromone components, there are neurons that are excited by: either of the two major pheromone components; excited by one and inhibited by the other; or excited only by the blend of both components (Christensen, Mustaparta, & Hildebrand, 1989).

A mechanism that is explored is that of disinhibition. This is an excitatory mechanism that is transmitted through inhibitory neurons which are connected in series. In a disinhibitory chain (ORN $\rightarrow$ LN $\rightarrow$ LN $\rightarrow$ PN), a PN is inhibited by a LN so that the PN has a low firing-rate when the system is at rest. During stimulation, that LN is itself inhibited by another

LN, and the PN is released from inhibition resulting in a bursting response of postinhibitory rebound. Av-Ron and Rospars (1995) show that by arranging neurons in a disinhibitory chain, the model can exhibit PN output that resembles intra-cellular recordings from actual PNs. Applying this disinhibition mechanism in network models inspired by moth MGC, temporal patterns of PN responses were mimicked, allowing some PNs in the model to follow pulsed stimuli (Av-Ron & Vibert, 1996). This work demonstrated that the theoretical disinhibition pathway could realistically be involved in antennal lobe processing. However, this disinhibition pathway remains as only a theoretical possibility, and has not been shown empirically.

Connectivity

Antennal lobe modelling studies by Linster *et al.* have concentrated on reproducing biologically realistic distributions of interneuron response patterns (Linster & Dreyfus, 1996; Linster *et al.*, 1992, 1993, 2005; Linster & Smith, 1997). Generally in these studies, the interneuron response patterns are categorised into one of three: pure inhibitory, pure excitatory, and mixed. These models were based upon the model described in Linster *et al.* (1992). It was demonstrated that as connectivity is increased, interneurons that exhibit mixed responses increase in number until all interneurons show mixed responses, while pure excitatory or pure inhibitory response interneurons decrease. This was derived analytically by considering the distributions of excitatory and inhibitory presynaptic interneurons, and the subsequent effect on the input to post-synaptic interneurons that receive this further downstream. As such, the response of an interneuron was defined by the synaptic input it received. The analytical results were also confirmed experimentally by

simulations with integrate-and-fire neurons. This model was useful in giving a very general result since it avoided any biological detail such as differentiation between antennal lobe interneurons, and any morphological details of glomerular structures and the consequences for interneuron connections. Neural networks were created for simulations with random all-to-all connections, and receptor neurons synapsing onto any antennal lobe interneuron. Thus by increasing the probability of synapses forming between neurons, the connectivity in the network was increased.

Subsequent MGC studies by Linster addressed more biological details from moth and cockroach physiological data, with distinction between PNs and LNs (Linster & Dreyfus, 1996; Linster *et al.*, 1993) and separate receptor types (Linster & Dreyfus, 1996). These two papers investigate the effect of stimulating the models with blend ratios of two odour components. However, the only assessment of these models was, as before, the distribution of response patterns, although there is some discussion of the existence of neurons that are "selective" to one odour component and neurons that are "non-selective". There is even an example of a neuron that is most responsive to the 1:1 blend, giving less response to either component presented singly at the same concentration.

Associative Learning

Now we move from MGC subsystem for pheromone detection to the general odour detection of the non-pheromone glomeruli of the antennal lobe. In behavioural psychophysics: 'overshadowing' is when an animal is taught to associate an unconditioned stimulus (US, in this case sucrose) to an odour mixture, and yet the animal associates the US with one odour component

more strongly than with the other; 'blocking' is when an animal is pre-trained to associate an US with one odour component (for instance, odorant A), then trained to associate the US with an odour mixture containing that component (odorants A + B), and the animal fails to associate the US with the other component of the odour mixture (odorant B).

In the honeybee antennal lobe, a neuron named VUMmx1 has been found that responds to the US sucrose. Importantly, it has been found to innervate several regions of the brain including the glomeruli of the antennal lobes, and so potentially can influence the odour code or be influenced by odours. This neuron is integral to associative pairing of sucrose US to odours (Linster & Smith, 1997; Menzel, 1993; Hammer & Menzel, 1995). Furthermore, the behavioural effects can be reproduced by VUMmx1 activation instead of an US. Once an animal is taught to associate an odour with the sucrose, this VUMmx1 neuron also responds to the presence of that odour in the absence of the US (Hammer, 1993).

Modelling efforts have shown that the overshadowing and blocking behaviours could be explained by how the odour is represented in the antennal lobe, and how this may interact with associative learning through a plasticity mechanism (Linster & Smith, 1997) following Hebbian rules (Dayan & Abbott, 2001). By incorporating this VUMmx1 neuron (shortened to VUM) to mediate information of the sucrose US into the antennal lobe glomeruli, Linster and Smith (1997) have built a model that develops a hypothesis about the connections of the VUM neuron in order for overshadowing and blocking effects to occur.

In this multiglomerular model, there were LNs receiving excitation from receptors of a single glomerulus, lateral inhibition between LNs of neighbouring glomeruli, and PNs activated by disinhibition. Crucially, the VUM neuron has Hebbian modulated synaptic connections to antennal lobe interneurons as the mechanism by which an animal can associate an odour with a sucrose US.

Overshadowing can be simulated in the model when the PN-to-VUM synaptic connections were allowed to change; and when the VUM-to-LN synaptic connections were also plastic, the model was also able to demonstrate the 'blocking' effect (Linster & Smith, 1997). This was because the additional VUM-to-LN variable synapses allowed the VUM neuron to modulate and alter PN activity. This allowed the VUM neuron to influence the representation of odour mixtures after pre-training with a single odour component, such that the spatial PN representation of the odour mixture was closer to that of the pre-trained component. Linster *et al.* (1997) argue that intrinsic connections of the AL model are not altered, thus preserving its ability to encode a wide range of odours. This modulatory VUM neuron clearly has a profound effect on the PN representation of odours. It illustrates a mechanism by which modulatory LNs (with similar connectivity to the VUM neuron modelled) may be able to affect the PN spatial code.

Functionally Organised Inhibition

Modelling efforts have also given insights into the organisation and function of the inhibitory output of LNs. Lateral inhibition is a commonly used mechanism to achieve contrast enhancement. In olfaction, this helps to generate an odour code in which similar odours are easier to differentiate (Linster &

Cleland, 2004). Thus, odours with overlapping receptor representation does not imply odours with overlapping output neuron representation. However, this will give rise to non-trivial odorant interactions in the glomeruli and odour mixtures may gain a representation that is unique and entirely distinct from its components. Since the odour code for the components and the blend diverge at this stage of processing, this has implications for the perception of odour mixtures. Indeed this helps to explain the contradiction between configural (mixtures perceived as novel qualities) and elemental (sum of components) perception that have both been observed (Linster & Cleland, 2004).

Contrast enhancement in olfaction also hints at the likely organisation of the inhibitory connections between neurons. It tells us that inhibition should be strongest between glomeruli that have highly correlated activity, since it is between similar and overlapping responses that we need to contrast. In a model of general odour detection inspired by the honeybee (Linster & Smith, 1997), multiple glomeruli are incorporated into the model with asymmetric LNs that favour a particular glomerulus, in which it innervates more densely than in other glomeruli (so called Hetero-LNs (Fonta, Sun, & Masson, 1993)). It was assumed that Hetero-LNs receive receptor input only from its favoured glomerulus, and that it provides inhibition to interneurons in other glomeruli. Optical imaging data was used to ascertain both average receptor input and PN output for glomeruli in honeybee antennal lobe. It was shown that a model with 'functionally' organised inhibition gave the closest simulated output to the biological data (Linster *et al.*, 2005). In this functionally organised model, inhibition between two glomeruli

was weighted depending on the similarity of the receptor tunings for those two glomeruli (strong inhibition for high similarity). This outperformed a 'stochastic' model with randomly distributed inhibitory connections, and a 'morphological' model with morphologically distributed inhibitory connections (with strongest inhibition for morphologically neighbouring glomeruli). This demonstrates that LNs do not just play a modulatory role, in which case a 'stochastic' model would suffice, but LNs play an active role, not just shaping PN activity but determining PN activity.

1.2.3 Temporal Aspects

Transient Activity

The antennal lobe of insects is now thought to utilise time as well as space as an encoding dimension (Laurent *et al.*, 2001). Delivery of information is not constrained to the identity of activated neurons, but is also carried by the timing of neuron activation, giving a so-called spatiotemporal or identity-temporal code. What these temporal aspects entail remain as yet undefined. However modelling efforts have provided some insights into how time may be incorporated into an olfactory code.

There have been modelling attempts to investigate temporal coding in insect antennal lobe motivated by cockroach and honeybee data (Getz & Lutz, 1999) and locust data (Bazhenov, Stopfer, Rabinovich, Huerta, *et al.*, 2001; Bazhenov, Stopfer, Rabinovich, Abarbanel, *et al.*, 2001). Getz and Lutz (1999) created a neural network with excitatory receptor cells, inhibitory local interneurons, and projection neurons excited through disinhibition. In addition, there was also feedback excitation from the PNs to LNs. The

performance of the network was measured by how well the network can discriminate different odours compared to the consistency of the code for the same odour. A genetic algorithm was then used to optimise the parameters of the network (such as the synaptic weights and delays) to improve its performance. Unsurprisingly, the network was able to perform very well after 5000 generations. This approach studied the workings of antennal lobe simply as a 'black box' with a known input and known output. The network demonstrated use of a temporal PN code, with odour discrimination in some cases only possible when taking into account the transient PN activity. Thus, the odour code was shown to be improved when the progression and sequence of activation was considered before the steady state attractor of the system (if it existed) was reached.

Winnerless Competition

Taking the coding by temporally patterned activity further, WLC provides some theoretic framework for competitive neural networks that can create attractive limit cycles rather than stationary points. The well known Winner-Takes-All competitive network utilises all-to-all connections between mutually inhibitory neurons. When the strength of these inhibitory connections is strong, this creates a multi-stable dynamical system. This means that activation of any one neuron will inhibit all other neurons, and thus there is competition between all the neurons to become the active dominant neuron. In this strict case, there is always only one dominant neuron, which remains dominant until the input to the network pushes the system to another neuron (Afraimovich *et al.*, 2004). In contrast, WLC networks encorporate asymmetrical inhibitory connections which ensure that neurons can

only dominate activity transiently, since the asymmetries allow other neurons to activate and shift the centre of activity. This is because, instead of multi-stable attractors, the system generates unstable saddle-points that are attractive from certain directions but unstable in other directions. To illustrate, take a simple three-neuron network where each neuron receives inhibition from one neuron and inhibits the other, creating a cyclical chain of inhibitory connections. When this system receives excitatory input from upstream neurons, activity switches in turn between each of the three neurons in the network.

It has been proved that, given a network of three or more neurons, with each neuron forming inhibitory connections with all neurons but one, and for each pair of neurons at least one will inhibit the other (hence creating the asymmetry in connectivity), then there will always be a limit cycle in the region around the union of heteroclinic contours connecting the saddle points (Afraimovich *et al.*, 2004). Each saddle point is the activation of a single neuron, and the heteroclinic contour leads to the activation of the one neuron that is not inhibited. Although the proof requires some very strong conditions to guarantee the existence of the limit cycle, WLC networks can still produce switching dynamics under less stringent conditions (Rabinovich *et al.*, 2001, 2000). When simulations were performed using FitzHugh-Nagumo spiking neurons, the spatiotemporal pattern generated by a WLC network was similar to that seen of PN output in the antennal lobe. Furthermore, the spatiotemporal patterns in the WLC models were specific to the afferent input, just as PN spatiotemporal patterns were odour specific (Rabinovich *et al.*, 2001, 2000).

An advantage of an odour code that converts an entirely spatial code from the receptor neurons into a spatiotemporal code is that the theoretical information capacity of the code is much increased with this temporal enhancement. The network is now not limited by the number of available steady state attractors it can support, but can now encode with trajectories of activation. By considering all possible sequences from a network with N neurons, Rabinovich *et al.* (2001) have shwon that the capacity C is bounded,

$$\left(1 - \frac{1}{e(N-2)!}\right) < \frac{C}{e(N-1)!} < \frac{N}{3}\left(1 - \frac{1}{e(N-2)!}\right).$$

In reality, however, it is unlikely that the antennal lobe could utilise all possible sequences. The mutual information measure between the input and the output of the simulated antennal lobe reaches maximum only after three activity switches after stimulus onset (Rabinovich *et al.*, 2001, 2000).

WLC networks provides some underlying general theory as to how a temporal component may be added to the odour code. Only general assumptions are made about cell physiology, and the temporal features arise purely from the network connectivity and not from intrinsic qualities on the neurons. The spatiotemporal code created is of a sequence of spatial PN activation patterns. The instantaneous spatial patterns can be thought of as letters that are used in sequence to create words. However, this is not the only way to utilise time as an extra coding dimension.

Spike Timing against Local Field Potential

Bazhenov *et al.* (2001) generated a temporal code of a different kind, generating synchronous behaviour in the PNs and, subsequently, oscillations in

the activity of the whole population of PNs. These oscillations were primarily caused by self-inhibition of LNs when the system is driven by receptor cell input. The effects of fast and slow inhibition on the timing of PN spikes relative to the phase of each oscillatory cycle were investigated (Bazhenov, Stopfer, Rabinovich, Huerta, *et al.*, 2001). Furthermore, slower dynamics were also investigated, involving the timing of PN spikes in terms of the oscillatory cycle in which such spikes occured (Bazhenov, Stopfer, Rabinovich, Abarbanel, *et al.*, 2001). However, neither oscillatory population behaviour nor odour dependent synchrony has been observed in moth antennal lobe (Christensen, Pawlowski, Lei, & Hildebrand, 2000). Furthermore, locust antennal lobe physiology is very different from that of moths, with non-spiking LNs, and many more glomeruli that are smaller and not paired with particular receptor types. The AL of locust are organised more homogeneously, with less spatial structure, and it is likely that the locust utilises a temporal code, indeed a coding strategy, that is very different from that of moths.

Chapter 2

Optical Imaging and Processing Techniques

2.1 Introduction

Odours are encoded in the olfactory pathway through distributed patterns of activity across a population of broadly-tuned olfactory receptor neurons (ORNs). These ORN responses at the periphery are reliably reported at the point of first synaptic contact, inside glomeruli (Galizia, Nagler, Holldobler, & Menzel, 1998), where the outer layer of each glomerulus is dominated by axonal processes from ORNs (Homberg *et al.*, 1989). Thus, each glomerulus provides a convenient site of integration to study the olfactory code, which taken together reflects the ORN population input underlying the combinatorial coding of simple and complex odours (Malnic, Hirono, Sato, & Buck, 1999). Calcium imaging of subsets of glomeruli is currently the most common approach to assessing this neural code, by providing an indirect measure of neuronal activity at the periphery (Galizia, Sachse, Rappert, & Menel, 1999; Galizia, Sachse, & Mustaparta, 2000; Galizia & Menzel, 2000, 2001; Carlsson *et al.*, 2002; Carlsson & Hansson, 2003).

Assessing the olfactory code through calcium imaging of glomeruli requires that these can be reliably identified from the resultant images. Glomerular structures are typically identified by visual inspection, usually requiring morphological stainings or an anatomical atlas. For instance, in invertebrates olfactory glomeruli are typically identified morphologically through post-experimental staining of the glomerular membranes to ascertain their boundaries (Galizia *et al.*, 1999; Sachse, Rappert, & Galizia, 1999; Wang, Wong, Flores, Vosshall, & Axel, 2003). Such morphological stainings are often difficult or impossible to attain and may cause glomeruli to swell and distort, which in addition to animal-to-animal variation means that glomeruli can be difficult to identify across individuals. These disparities often make alignment and identification of glomerular responses in any general sense a challenge for the experimenter. Carlsson *et al.* (2002) avoid the need for morphological stainings by identifying glomeruli by localising regions of high response over many trials. It was then shown that these centres of high activity correspond to individual glomeruli (Carlsson & Hansson, 2003). However, all these techniques require the judgement of the experimenter as well as complex experimental procedures.

In this chapter, I develop a novel technique that identifies glomeruli using only their physiological response characteristics. Also, an investigation was made as to whether this method can be extended to automatically registrate across individual animals those glomeruli that are functionally equivalent. Where this was successful, the consistency of the position of glomeruli between individual animals was assessed. By comparing the positions of functionally equivalent glomeruli after applying linear transformations to correct for perspective, it was possible to study glomerular positioning between animals without need of morphological staining or an anatomical atlas.

2.2 Experimental Procedures and Data Processing

2.2.1 Animals and Staining

A detailed description of the preparation of the animals and the experimental setup can be found elsewhere (Carlsson *et al.*, 2002; Carlsson & Hansson, 2003), but the following gives a brief summary of the experimental procedures. Experiments were performed on 1–5 days post emergence male moths. The head capsules were cut open between the compound eyes, and extraneous material removed to expose the antennal lobes (ALs). A calcium-sensitive dye (CaGR-2-AM, Molecular Probes, Eugene, OR) was applied to the uncovered brain, bathing the whole brain. The dye was dissolved in 20% Pluronic F-127 in DMSO (Molecular Probes, Eugene, OR) and diluted in moth saline (Christensen & Hildebrand, 1987) to a final concentration of $\sim$30 μM. After incubation (approximately $\sim$60 minutes in 10–12°C) and rinsing in moth saline, recordings were done in vivo.

A TILL Photonics air-cooled imaging system (Germany) with a 12 bit slow-scan CCD camera was used. Filter settings were dichroic: 500 nm; emission LP 515 nm and the preparation was excited at 475 nm. Sequences of 40 frames and a sampling rate of 4 Hz (200 ms exposure time) were recorded through an upright microscope (Olympus) with a 20× (NA 0.50; Olympus) water immersion objective. On-chip binning (2×2) was performed, which resulted in a pixel size corresponding to $\sim$1×1 μm.

The flower odours, linalool and geraniol were prepared separately in solution by dissolving and diluting pure odorants in paraffin oil. For each odorant, solutions of different concentration, 1 μg μl^{-1}, 2 μg μl^{-1} and 3 μg μl^{-1}

were created. Binary mixtures were then created by separately placing 10 μl of a linalool solution and 10 μl of a geraniol solution onto a piece of filter paper, which was then placed into a Pasteur pipette. Single component stimuli (or blanks) were created by using pure paraffin oil instead of one (or two) of the solutions. The blank (control) stimulus was created using only paraffin oil. In total, 16 different stimuli were used: 2 pure odours at 3 different concentrations each; 9 binary blends, each component being one of three concentration levels, and the blank. The stimuli were shuffled and presented in a randomised order to prevent systematic bias in the results.

A continuous carrier air stream ($30\,\mathrm{ml\,s^{-1}}$) ventilated the antenna. A further $5\,\mathrm{ml\,s^{-1}}$ of air was continually injected into this stream via an empty pipette, and during stimulation this was switched to the odour laden pipette, thus introducing the stimulus. A view of the antennal lobes was recorded by a CCD camera (TILL Photonics GmbH, Germany) as a series of 40 frames at 4 frames per second. Stimuli were presented at 3 seconds from the start of each recording (frame 12) and lasted for 1 second (ending at frame 16).

Dissection of the animals and working of the experimental apparatus was performed by a collaborator on this work, Mikael A. Carlsson (Swedish University of Agricultural Sciences). Creating the odour blend stimuli and operating recording equipment was done jointly by Carlsson and the author. All processing and analysis of these data is the work of the author.

2.2.2 Correction for Movement Artefacts

Movements by the animal during and between trials caused the positioning of the antennal lobe to shift in the camera view. These shifts were small during

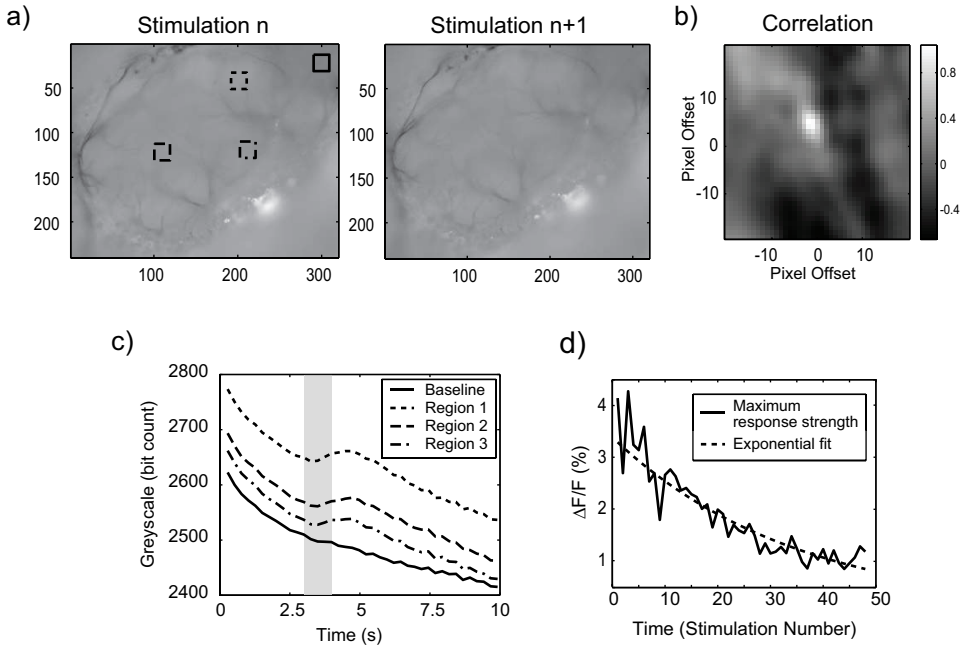

Figure 2.1: Adjustments to the data. (a) and (b): Correcting for movements of the moth using correlation. The two panels show images of the antennal lobe for two consecutive stimulations. The left image was displaced, and for each displacement, the correlation coefficient between the images was calculated. This correlation is summarised in (b). The peak is at pixel offset (-1,5), indicating that the image has shifted by this vector. (c): Correcting for the bleaching effect. The grey shading indicates the presentation of the stimulus, while the solid, dotted, dashed and dash-dotted lines show the time-courses of different regions of the antennal lobe as indicated in the left panel of (a). The solid-lined square is located in the macroglomerular complex, which is sensitive only to pheromones and not the odours used here. Thus, this region, or a region depicting the antennal nerve, can be used to obtain a baseline with which to negate the bleaching effect. (d) Normalising for the weakening of the animal. The solid line shows the maximum response magnitudes, and the dotted line is a least-squares exponential fit.

a single trial, but would accumulate over multiple trials, and so needed to be corrected for between trials. To determine these shifts, a correlation method was used. For two consecutive trials, the first frame from each trial was correlated with each other after displacing one of these frames by some pixel offset and calculating the average correlation over all corresponding pixels pairs in the images. This was repeated for a range of offsets, and the displacement resulting in the highest correlation was taken to be the movement vector between the two trials (Figure 2.1a and b). This vector allows any shifts in the camera view to be corrected.

2.2.3 Correction for Dye Bleaching

The magnitude of the dye's fluorescence decayed with time irrespective of the level of free calcium ions. Thus, the fluorescence of the dye, F, comprises the response to free Ca^{2+} sitting atop a much larger overall bleaching decay (Figure 2.1c). To correct for this, a bleaching baseline, a function of time $F_b(t)$, was taken from a non-responding region of the antennal lobe. The macroglomerular complex (MGC) is a sexually dimorphic part of the AL found in males that is dedicated to pheromone encoding, and so does not respond to general odours. Since linalool and geraniol are not pheromone components, this region was used to generate the baseline function (solid trace in Figure 2.1c). For *S. littoralis*, the MGC is close to the entrance of the antennal nerve in the AL, and the baseline was taken to be the spatial mean of the fluorescence of a 20×20 pixel square in this region. The bleach corrected response, $r(t_i)$, was taken to be the relative change in fluorescence $\frac{\Delta F(t_i)}{F_b(t_i)}$ where $\Delta F(t_i) = F(t_i) - F_b(t_i)$ for each time step t_i at each frame $i = 1, \ldots, 40$.

2.2.4 Correction for Reduction in Response Magnitude

In addition to the bleaching effect of the dye, as more odours were presented to the animals the animals would weaken, leading to decay in response magnitude. This caused a strong time dependence of the magnitude of the responses (Figure 2.1d) that added extra variability in the data. The stimuli were presented in a random order and this weakening was not found to be stimulus dependent but systematic in nature. We found that this weakening over stimulations could adequately be fitted (in a least-squares sense) by an exponential decay of the form $ae^{-n/\lambda}$, where the amplitude a and the decay constant λ are free parameters, and n is the chronological index of the stimulation. This artefact was then normalised from the data series by dividing the magnitude of each response by this exponential fit, evaluated at n, which also has the effect of adjusting to 1 the mean of maximum response magnitudes over all trials. This made the responses comparable across different animals.

2.2.5 Time Integration

After correction of pixel time series, the data were time-integrated between stimulus onset at 3 seconds and the end of recording at 10 seconds, giving $R = \int_3^{10} r(t)dt$. In practice, since we have discrete time steps, this gives $R = \sum_{i=12}^{40} r(t_i)\delta t$ where $\delta t = 0.25$ s. Integrating the responses over time in this way provides a more robust estimate of activity at each point in space, since the integration averages out uncorrelated noise generated by the camera. To further combat the camera noise, the responses were also spatially

averaged. For each pixel, the response was taken to be the mean response of the surrounding 5×5 pixel region. To average out noise, the region size should be as large as possible, yet the region should be as small as possible to ensure the spatial features are not lost. Given that the glomeruli are around 50 pixels across, the region size is a good compromise.

The results of these operations for three different animals are shown in Figure 2.2. We can clearly identify the responding glomeruli – there are two glomeruli that respond to both linalool and geraniol, and one that responds only to linalool. All three respond to the blend. This shows the spatial aspect of the coding, but to quantify the magnitude of these responses, the individual glomeruli need to be registrated across individuals so that their responses may be pooled. In Figure 2.2, Animal B appears to have activity that is distributed across the antennal lobe, and is not as well confined to glomeruli as for Animals A and C. This is because Animal B gave weak responses (compared to the other animals) and subsequently required more amplification during normalisation, which also amplified the background activity and noise in the image.

2.3 Identification of Glomeruli

2.3.1 Correlated Activity within each Glomerulus

Glomeruli are known to be convergent sites for olfactory receptor neurons expressing the same type of receptor (Couto *et al.*, 2005; Fishilevich & Vosshall, 2005; Gao, Yuan, & Chess, 2000; Vosshall, Wong, & Axel, 2000). Since the activity we observe is dominated by presynaptic activity of these receptor neurons, each glomerulus can be considered as a single functional unit. This

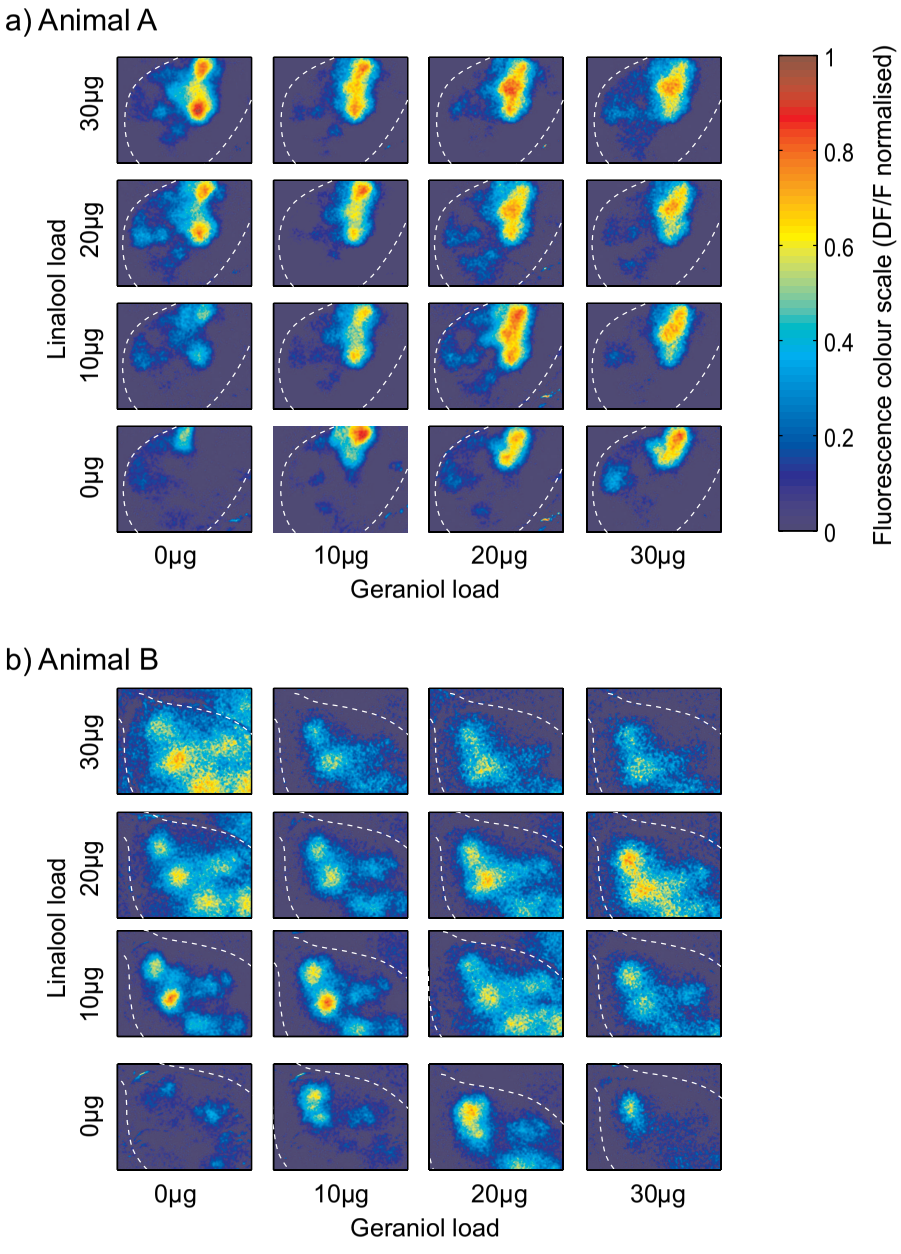
a) Animal A
30µg
20µg
10µg
0µg
Linalool load
0µg
10µg
20µg
30µg
Geraniol load
1
0.8
0.6
0.4
0.2
0
Fluorescence colour scale (DF/F normalised)
b) Animal B
30µg
20µg
10µg
0µg
Linalool load
0µg
10µg
20µg
30µg
Geraniol load

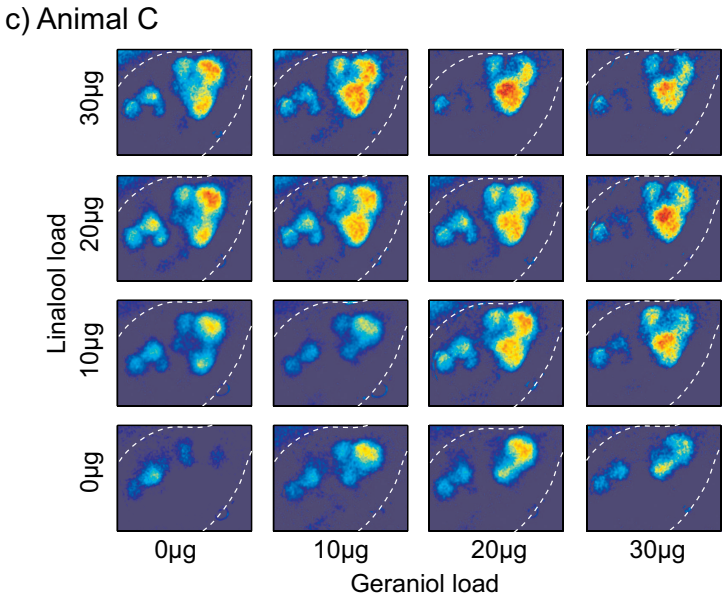

Figure 2.2: Blend responses. The responses to the blends organised into matrices according to the stimuli. The same colour scale is used for all three animals' responses. These responses have been normalised (as described in Figure 2.1) and time integrated. They are organised so that the columns indicate the geraniol loading while the rows indicate the linalool load. The dotted white lines show estimated boundaries of the AL. There are many glomeruli that seem to be activated to a low level, but in an unreliable manner. Responses in Animal B were weak when the odours were presented, and so these responses needed greater normalisation. Thus, background noise has been further amplified, resulting in seemingly more distributed activity foci than in the other animals.

is verified in Figure 2.3 in the case of Animal A. First, the positions of glomeruli of Animal A were estimated from the time-integrated responses (Figure 2.2) by visual inspection (Figure 2.3a). Regions of high activity (more than 50%) were identified as glomeruli as described by Carlsson *et al.* (2002). Then, a line of 30 sampling squares was defined that intersected three of these glomeruli. For each of these squares, $x = 1, \ldots, 30$, we can define a response profile vector, $\vec{P_x} = (R_x(S_1) \cdots R_x(S_k) \cdots R_x(S_{16}))$, where the scalar $R_x(S_k)$ is the response for square x to stimulus k. The order of stimuli in the vector is unimportant as long as it is preserved across pixel regions. These response profile vectors were then mutually correlated (Figure 2.3b), and the result shows that sampling squares within the same glomerulus are highly correlated, while those in different glomeruli are not, since a glomerulus acts as a single functional unit. This leads to the stepped appearance observed in Figure 2.3b, and from this we can estimate where the line of sampling squares crosses glomerular boundaries. Estimating the glomerular boundary in this way gives results that concur with the method described by Carlsson *et al.* (2002).

Thus, response profiles contain enough information to allow discrimination between glomeruli, and we exploit this idea of correlated response profiles to locate glomeruli. Firstly, we define a response space as follows. To each pixel, denoted by the location (i, j) of that pixel, we assign the response profile vector $\vec{P_{ij}}$, where $R_{ij}(S_k)$ is now the mean response of the 5×5 pixel region around pixel (i, j) to the stimulus $k = 1, \ldots, 16$. Hereafter, this will be called the pixel response. Pixels that have correlated response profiles are located in neighbouring regions of this response space. Thus, since a glomerulus is

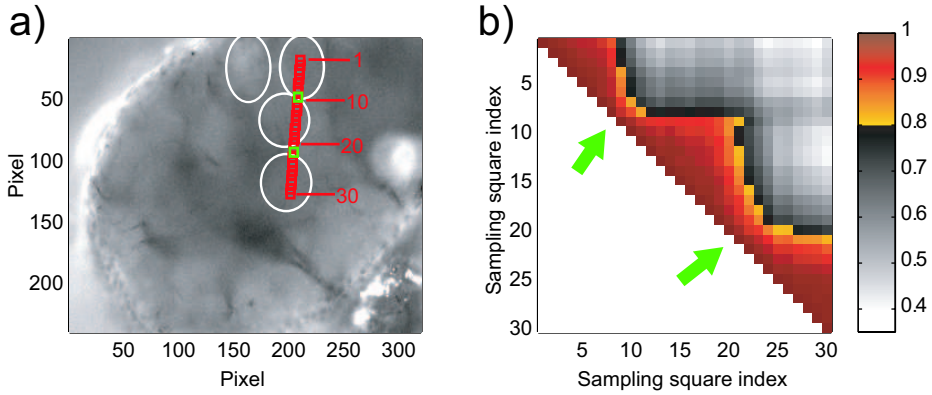

Figure 2.3: Correlation of the activity patterns across the stimulus set within and between glomeruli. (a) Definition of sampling squares that are shifted gradually from square 1 to square 30, as labelled. The white circles are estimated locations of glomeruli, identified using a visual inspection technique described by Carlsson *et al.* (2002). Green squares indicate a correlation-based identification of glomerular transition. The glomeruli boundaries identified by these two methods match well. (b) Mutual correlation of response profiles. For each sampling square, a response profile (see text) was derived, and these response patterns were correlated. The numbers on the x- and y-axes correspond to the numbers of the sampling squares in panel (a). The correlation matrix has a stepped appearance. The regions indicated by the green arrows are where neighbouring sample squares do not correlate well, indicating the boundary between glomeruli.

a single functional unit, so pixels from the same glomerulus can be expected to cluster together. Moreover, pixels from different glomeruli, which respond differently to this stimulus set, will have differing pixel responses and so will be separated in response space. Thus, the glomeruli will form distinct clusters.

2.3.2 Cluster Analysis

Cluster analysis was applied to these pixel responses in order to identify functionally equivalent pixel regions. Ward's method (Ward, 1963) was used for calculating the separation between clusters in response space (Rencher, 2002a). This approach is akin to that of analysis of variance. Firstly, for a given cluster G of pixel responses, the centroid was defined as $\vec{\bar{G}} = \frac{1}{N_G}\sum_{\vec{P_{ij}}\in G}\vec{P_{ij}}$, where N_G is the number of points in G. The sum of squares of the deviation from the centroid was defined to be $\sigma^2(G) = \sum_{\vec{P_{ij}}\in G}\left|\vec{P_{ij}} - \vec{\bar{G}}\right|^2$. The distance D_W between two clusters, G and H, is calculated as the increase in the sum of squares if these two clusters were combined into one cluster: $D_W(G,H) = \sigma^2(G\cup H) - [\sigma^2(G) + \sigma^2(H)]$. The algorithm is started with all the pixel responses as separate clusters, with the clusters containing just one point each. At each iterative step, the Ward linkage method combines those two clusters into a single cluster that causes the smallest increase in the sum of squares of deviations. The iterations stop when a predetermined number of clusters has been reached.

For agglomerative clustering methods, the number of clusters must first be specified *a priori*. This number has been obtained iteratively, to minimise the number of clusters, yet still portray the main features. However, this results in many clusters unrelated to glomeruli due to a slight general increase

in activity of the whole antennal lobe, or glomeruli that are activated, but only faintly above the background level and not in a reliable manner (Figure 2.4b). Salient glomeruli, which have strong responses, therefore, can be distinguished from this background simply by applying a threshold of 50% of maximum response magnitude (Figure 2.4a and c). This 50% threshold has been used in previous studies to distinguish glomeruli from background activity (Carlsson *et al.*, 2002). The resulting glomeruli have reduced resolution because the pixels were binned into 5×5 squares and averaged in these bins to reduce the total number of points to process during cluster analysis.

Figure 2.4a illustrates how each pixel is mapped to its pixel response in the response space. For Animal A, the pixel location depicted by the red dots in the time-integrated responses is mapped to the pixel response in the response space, according to its response across the 16 different stimuli. Green pixels and blue pixels have different responses, and so are located in different regions of the response space. For Animal B, there are depicted two pixels with similar pixel responses, and are thus located in the same region.

2.3.3 Across-animal Glomerulus Registration

Extending the idea of cluster analysis of pixel responses further, pixels from physiologically equivalent glomeruli of different animals, with similar response profiles, should also be found in the same region of the response space (Figure 2.4a). Thus, physiologically equivalent glomeruli from separate animals will be expected to form a single cluster. We can exploit this to automatically registrate glomeruli between animals in the same process as the identification of glomeruli. To test this method, cluster analysis was

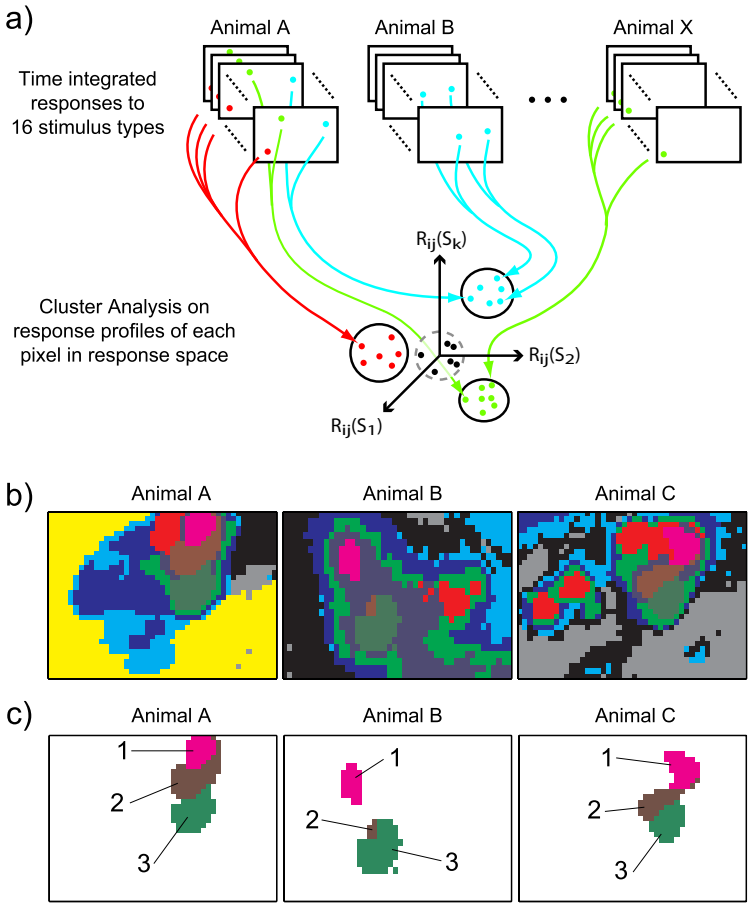

Figure 2.4: Identification of functionally equivalent glomeruli. (a) Schematic showing the response profiles (see text) extracted for each pixel and placed into the response space. In this space, pixels that have similar response profiles are located in the same region. A threshold can be set (grey dotted line) to omit pixels from non-responding regions. (b) The clusters derived from cluster analysis mapped onto original images for animals A, B and C, as denoted in Figure 2.2. The colours differentiate between clusters, thus pixels of the same colour are of the same cluster, even across animals. Three identified glomeruli are labelled 1 to 3 corresponding in each of the animals. (c) Identified clusters that are above 50% of maximum response magnitude, leaving only the more reliable responding glomeruli.

applied to multiple animals simultaneously, to perform unsupervised identification and registration of functionally equivalent glomeruli from different animals.

Three salient clusters were obtained that were found in each of the three animals (Figure 2.4c). These clusters are spatially very well localised in each animal, and are around the correct anatomical size for a glomerulus, at around 55 μm in diameter. The exception to this is Glomerulus 2 in Animal B which is much smaller. This may be due to this glomerulus being at a different focal depth, or being partially hidden beneath other glomeruli, or perhaps it was underdeveloped in this animal. These registrated glomeruli also seem to be similarly positioned in each animal, which is tested for later.

The identification and registration of these three glomeruli suggest that, physiologically, glomeruli are consistent across animals. However, when an attempt was made to verify whether this glomerulus registration technique really gives functionally equivalent glomeruli, it was not possible to state this conclusively from these data. To test the glomerulus registration, first the response profile of each glomerulus in each animal was generated by taking the mean pixel responses for pixels within each glomerulus. Comparisons between two glomeruli were made by calculating their correlation coefficient. Comparisons between all three glomeruli from all animals are summarised in Figure 2.5. Between Animals A and C, the three highest correlations are between the corresponding glomeruli identified in these animals. This shows that the corresponding glomeruli identified in Animal A and Animal C have highly correlating response patterns and are indeed functionally equivalent. The glomeruli of Animal B, in contrast, does not support that this glomerulus

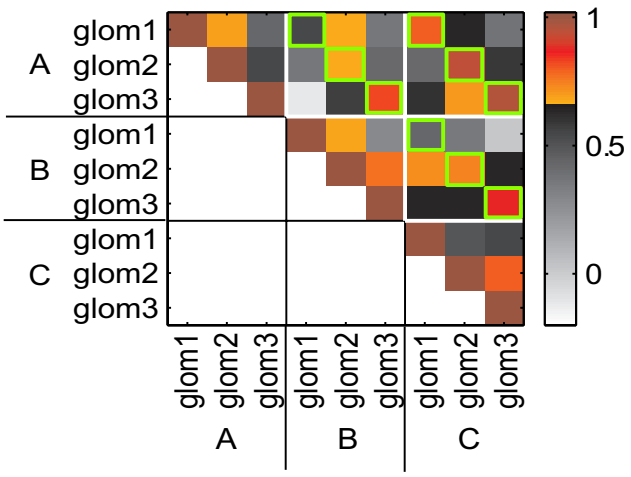

Figure 2.5: Correlation between the response profiles of all the identified glomeruli (1, 2 and 3) in all animals (A, B and C). The colour scale threshold is chosen to highlight at least three of the highest correlated pairs for each across animal comparison. Ideally, the three highest correlated pairs should be in the squares outlined in green. Between Animals A and C, such is the case. For Animal B, glomeruli 2 and 3 are correlated as expected, but glomerulus 1 of Animals A and C are more correlated with glomerulus 2 of Animal B than glomerulus 1.

registration technique matches functionally equivalent glomeruli. Glomeruli 2 and 3 show high correlation between Animals B and A, and between Animals B and C. However, Glomerulus 1 of Animal B is ambiguous. It correlates best with Glomerulus 1 of the other two animals, but in each of these cases, there are cross-glomeruli correlations that are stronger than the Glomerulus 1 to Glomerulus 1 correlation coefficient.

Principal component analysis (Rencher, 2002d) was used to help visualise the data by reducing their dimensionality, and to investigate the source for the ambiguity observed in the correlations (see Appendix A). Principal component analysis was applied to the pixel responses from all three animals. The first 4 principal components contribute to 95% of the variance in the data, so reducing to these four dimensions will retain most of the features

in the data. The first principal component captures the general activation of glomeruli to all odours and the subsequent principal components help to discriminate between activation patterns of glomeruli to different stimuli (Figure 2.6a). Plotting of the pixel responses from each of the identified glomeruli is shown in Figure 2.6b. Since we already know the location of areas of high activation, the first principal component is not informative, so the data points are plotted using coefficients of principal components 2, 3 and 4.

The data plotted in the reduced principal component space shows that the cluster analysis has categorised the pixels according to their proximity in the response space as expected. However, it is apparent that while the pixels from a single glomerulus from one animal are all tightly clustered together, pixels from corresponding glomeruli (as registrated by the cluster analysis) in other animals do not necessarily overlap. This indicates variability between animals in these data, which lowers the correlation in the glomerular response profiles between corresponding glomeruli. Applying multivariate analysis of variance (Rencher, 2002c) on the dimensionally reduced data shows that pixels of Glomerulus 1 are not significantly distinct between animals, with a p-value of 0.415, while Glomerulus 2 and 3 from each animal are statistically separate, with p-values of 0.001 and 0.002 respectively. There may be many factors creating such inter-animal variability in the optical imaging data. Likely causes are differences in the absorption of the calcium sensitive dye into the glomeruli, actual physiological differences between animals, and variability of the responses within each animal. Such variability makes the cluster analysis unreliable for registration of glomeruli between animals, and a more robust technique is needed such as singling out glomeruli for which odorants induce the greatest response (Carlsson & Hansson, 2003).

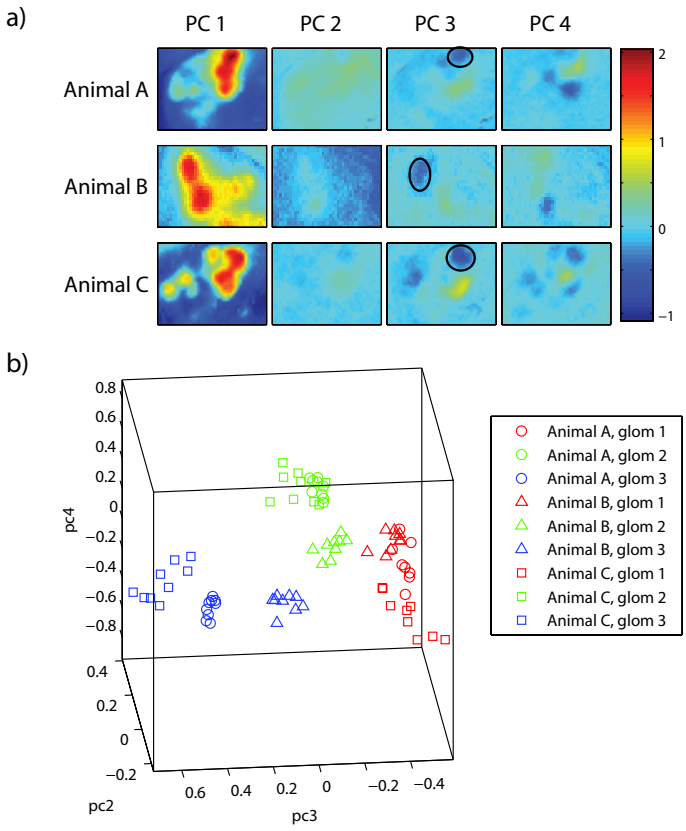

Figure 2.6: Principal component analysis of pixel responses. (a) The coefficients of the pixel responses for the first four principal components (PC). The first principal component shows the areas of high activation, and so highlights the activated glomeruli for all stimuli. The next three principal components distinguish between the glomeruli. The black circles indicate an example of where equivalent glomeruli show similar coefficients in the same principal component. (b) The pixel responses from each of the registrated glomeruli in each animal. The data are represented with the dimensions reduced to PC 2, 3 and 4. PC 1 is omitted since it provides little more information once glomeruli have been located. Equivalent glomeruli are localised in the same region of this space as expected, but it is apparent that glomeruli of separate animals form distinct clusters, despite being identified as equivalent by the cluster analysis.

2.4 Consistency of Glomerular Positioning

Due to variability of the apparent activity patterns between animals, it was not possible to confirm that our cluster analysis technique will correctly registrate glomeruli across animals in general. However, the high correlation of the activity patterns between registrated glomeruli of Animal A and Animal C (Figure 2.5) gives us confidence that it has given the correct result in this case (for completeness, the ambiguous Animal B is also included). Furthermore, this technique has registrated the glomeruli without using morphological measurements, and so this allows us to investigate the consistency of glomerular morphology between animals in physiologically identified glomeruli.

2.4.1 Perspective Correcting Linear Transformations

To assess the differences in glomerular positioning between individual animals, first the differences in camera view need to be negated. Also it is necessary to take into account the differences between the physical sizes of the antennal lobes, so that comparisons can be made of the relative positioning of the glomeruli across animals. These corrections are calculated using standard matrix algorithms as follows. The centroids of glomeruli identified using the clustering methods become points of reference. First, a coordinate grid is defined that is centred at the mean of the glomeruli locations, and the centroids of glomeruli are given coordinates relative to this. Let $\mathbf{X}$ and $\mathbf{Y}$ be two $2\times N$ matrices containing the coordinates of N identified glomeruli in two animals. We want a transformation $\mathbf{T}$, a 2×2 matrix, that maps the coordinates in $\mathbf{X}$ onto those in $\mathbf{Y}$, giving $\mathbf{TX} - \mathbf{Y} = 0$. However since $N >$

2, $\mathbf{X}$ is not a square matrix. Therefore, this equation is overdetermined with no exact solution for $\mathbf{T}$, and we instead calculate a least-squares solution. In other words the transformation $\mathbf{T}$ is calculated so that the norm of the matrix $\mathbf{TX} - \mathbf{Y}$ is minimised (Figure 2.7a). $\mathbf{T}$ is calculated using standard matrix techniques, namely Householder reflections for an orthogonal-triangular factorisation of non-square matrices (Stewart, 1998). The transformation $\mathbf{T}$ is affine (preserves parallel lines and ratios along lines) and is geometrically equivalent to a specific sequence of rotations, reflections, shears and scales that minimises the square of the differences between the coordinates of corresponding glomeruli of two animals. Note that this transformation is linear and so any nonlinearities in perspective introduced by nonlinear lens properties would need to be removed prior to this step – however such information is usually supplied by the manufacturer and can be applied to any data produced by the camera. Any remaining differences between $\mathbf{TX}$ and $\mathbf{Y}$ cannot be explained by change of camera view or size differences, and must be due to morphological differences between the two animals other than size. This provides a lower bound estimate for the size of the difference in relative glomerular positioning across animals.

2.4.2 Glomerular Positioning is Consistent

Using camera view negating transformations, we compared the positioning of the identified glomeruli within the ALs of the different animals. The camera views for each animal were transformed to conform with that of another animal such that all combinations were covered. The results are collated in Table 2.1. The errors shown for the transformation represent the amount

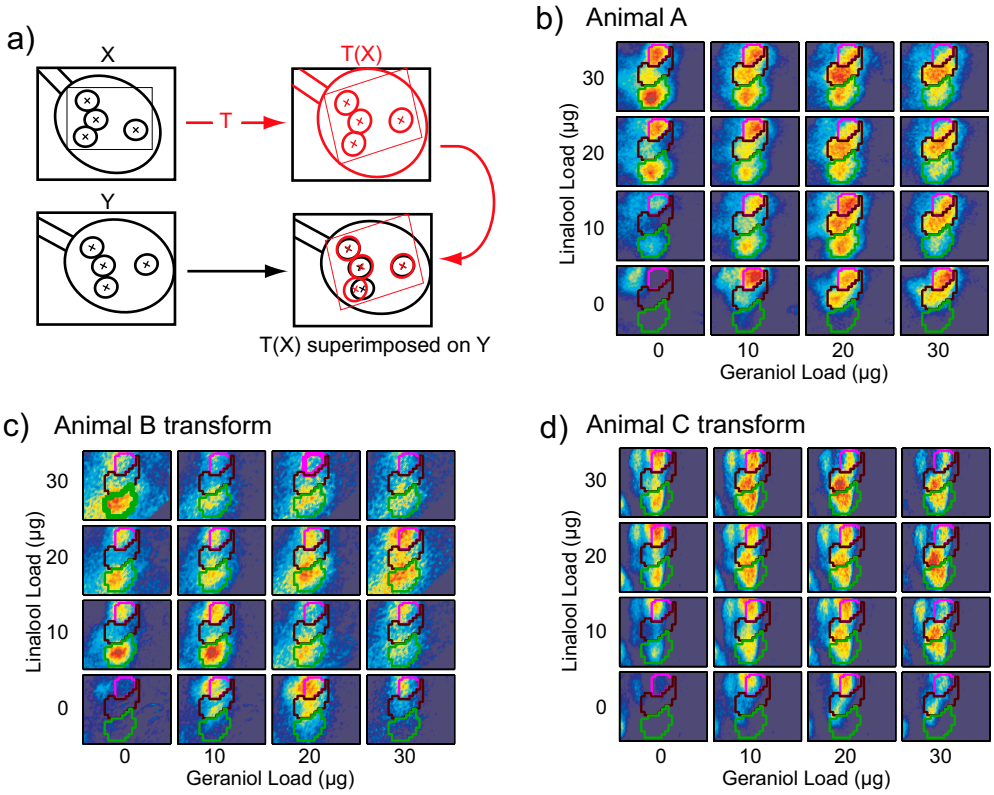

Figure 2.7: Consistency of glomerular positioning. (a) An illustration showing the action of the view-correcting transformation T. The AL outlines and glomerular positioning of two hypothetical animals X and Y are shown. Householder reflections are used to determine T, which, once applied to X, minimises the difference between the glomerular positioning X and Y. The rectangle in X is a reference to show how T transforms the glomeruli of X onto those of Y. (b) The glomerular boundaries of Animal A superimposed onto its responses. Only the region around the glomeruli is shown. (c) and (d): Glomerular boundaries superimposed onto the responses from Animal B and C, respectively, after camera view correction, indicating how consistent the glomeruli locations are across animals. There is consistency between the responses of the identified glomeruli of Animals A and C, with the glomeruli responding coherently to different stimuli.

of variability in the glomeruli positioning that cannot be accounted for by linear transformations alone. This error has also been transformed back to the original space so that it may be compared with the known anatomy of the animal. When Animal A was the target for view-corrections of the Animals B and C, it was found that the total distance between the glomeruli of Animals A and B was 30 μm in the transformed space (37 μm in the original space) and between A and C was 37 μm (50 μm in the original space). This was the highest distance for all transformations. Considering that the diameter of a glomerulus is around 55 μm, this indicates that glomerular positioning is indeed consistent across individuals of this species. This is true even for Animal B, for which glomerular responses were not unambiguously consistent with the other animals.

Figure 2.7b, c and d show the responses of the three animals, with c and d showing the responses of Animals B and C adjusted to align with the camera view for Animal A. The glomerular boundaries identified for Animal A in Figure 2.4 are superimposed and colour coded as in Figure 2.4c. The transformed regions of activity predominantly fall within the glomerular boundaries of Animal A. Morphological differences will mean that there cannot be a perfect match. The activity within these glomerular boundaries seems to correspond very well between Animals A and C. The activity patterns of the corresponding glomeruli seem to match very well for this stimulus set. Whenever a glomerulus responds strongly to a stimulus for Animal A, the corresponding glomerulus in Animal C also responds strongly and vice versa. This confirms the high correlation between glomeruluar activity of these two animals.

	Transformed animal					
	Animal A		Animal B		Animal C	
Target animal	**Targ**	**Orig**	**Targ**	**Orig**	**Targ**	**Orig**
Animal A						
Glom 1	-		9	11	11	15
Glom 2	-		15	19	19	26
Glom 3	-		6	7	7	9
Animal B						
Glom 1	5	5	-		4	8
Glom 2	17	16	-		13	27
Glom 3	12	11	-		9	18
Animal C						
Glom 1	6	11	5	10	-	
Glom 2	14	24	12	22	-	
Glom 3	5	9	4	8	-	

Table 2.1: Glomerular positions. Distances (in μm) between identified glomeruli of two animals after view correcting transformations in the target view and original view.

However, Animal B has glomeruli that respond incongruously with the other two animals. For example, glomerulus 3 (green in Figure 2.7c) responds strongly to the 0 μg geraniol/10 μg linalool blend, and to the 10 μg geraniol/10 μg linalool blend, but in the other two animals, there is not such a strong response; and glomerulus 1 (pink) in Animal B does not respond strongly for any blends containing 30 μg of linalool, which contrasts with the strong activation of this glomerulus in the other two animals for these stimuli.

2.5 Discussion

An algorithm was developed that was based upon unsupervised cluster analysis to automatically locate glomeruli using only their responses to stimuli. Each pixel location is associated with a vector of response magnitudes to a set of stimuli. It was shown that pixels, from which the image of a glomerulus is composed, have coherent pixel profiles since each glomerulus acts as a single unit for this method of optical imaging. This was exploited to successfully locate glomeruli with standard cluster analysis methods in the response space. Moreover, this novel technique has no requirement of any morphological staining, which can be problematic and not always attainable. Nor does this rely on the judgement and experience of the experimenter to identify glomeruli.

An attempt was made to extend this idea to also automatically registrate glomeruli from separate animals in the same algorithm. Since physiologically equivalent glomeruli from separate individuals should respond in the same way to the same stimuli, pixels of these equivalent glomeruli should have pixel

response profiles that are found in the same region of the response space, just as pixel responses within a glomerulus are found in the same region of the response space. However, while this is broadly true, inter-animal variation in the measured responses can cause pixels from equivalent glomeruli of different individuals to form statistically distinct clusters. Thus, it is not possible to say that this method will registrate glomeruli in general. A further test of the correlation showed that in two particular individuals the correct glomerulus registration was achieved.

High correlation between all identified glomeruli in two individuals gave confidence that these two animals had physiologically matching glomeruli. Importantly, since nothing was assumed about the morphological positioning of the glomeruli in order to identify them, it was possible to test and confirm that the positioning of the functionally identified glomeruli is consistent across animals. With this method, it was shown for the first time that physiologically equivalent glomeruli identified across animals are consistently positioned relative to each other within the antennal lobe. Although this was only shown for two animals, it helps to verify that the consistency in the location of odour-dependent activity within the AL (Carlsson *et al.*, 2002) is due to the consistency of glomeruli across individuals. Also, this result helps to validate the notion of a functional atlas with which to identify glomeruli morphologically (Galizia *et al.*, 1999), as has been created for the honeybee (Galizia & Menzel, 2000, 2001).

In conclusion, the algorithm developed here will systematically identify glomeruli in optical imaging data from the physiological responses to stimuli, and I will use this technique in the next chapter for studying the odour

code in the antennal lobe. It can registrate glomeruli between animals when inter-animal variation is low. High correlation between glomeruli of different individuals indicates a good match of identified glomeruli. This technique allowed confirmation that glomeruli are organised in the antennal lobes consistently between animals.

Chapter 3

Glomerular Responses to Binary Odour Mixtures

3.1 Introduction

Natural odour stimuli rarely occur as single compounds but are very often complex mixtures of different molecular components. Behaviourally relevant compound and mixture information often drives chemically mediated behaviour of both aquatic and terrestrial animals (Laing, 1989). These odours are often present against a background of irrelevant and interfering compounds. Despite the chemical complexity and low signal to noise ratio the olfactory apparatus can filter out relevant information, for example about food acceptability, presence of predators and sexual status of the opposite sex. Yet, little is known about how mixtures are encoded within the olfactory pathway to support this type of processing.

Mixtures of odours are often perceived as having unique synthetic qualitative properties and it is generally difficult to distinguish the individual components of the blend (Laing & Livermore, 1992; Laing & Francis, 1989; Moskowitz & Barbe, 1977). Hence, the neural representation of individ-

ual components within the context of a mixture is believed to interact non-trivially along the olfactory pathway, in a manner that may hinder the deconvolution of component information from mixture responses. When the neural response to a blend is not the simple sum of the responses to its constituents then a nonlinear mixture interaction has occurred. Such nonlinear interactions can contribute to the synthetic perception of a blend which include: suppression, where the blend response is weaker than that of one or more of the components at the same concentration; and synergy, where the blend response is higher than that of the most strongly responding component at the same total concentration (Duchamp-Viret *et al.*, 2003). Neural representations of odour components within a mixture may start to interact non-trivially even at the olfactory receptor neuron (ORN) level, with individual ORN responses to odour mixtures that exhibit suppression or synergy: in invertebrates, such as insects (Carlsson & Hansson, 2002; Akers & Getz, 1993; Ochieng, Park, & Baker, 2002) and crustacean (Steullet & Derby, 1997); and in vertebrates, such as fish (Kang & Caprio, 1991, 1997) and mammals (Oka, Omura, Kataoka, & Touhara, 2004; Duchamp-Viret *et al.*, 2003). More commonly, mixture interactions have been observed in second-order neurons in vertebrates as well as invertebrates (Christensen, Mustaparta, & Hildebrand, 1991; De Jong & Visser, 1988; Tabor, Yaksi, Weislogel, & Friedrich, 2004).

Nonlinear coding of mixtures at the periphery would seem to make identifying the individual components of a blend from the mixture representation a difficult task, and yet information relating to the components can persist in the perception of odours, as has been observed in rats (Linster & Smith, 1999) and honeybees (Hosler & Smith, 2000). This suggests a so-called non-configural, elemental aspect to odour perception, in addition to

the synthetic paradigm. This together implies that neural representations of complex odour mixtures comprise both configural and elemental properties. It is, however, unclear where and how mixture interactions take place in the olfactory pathway and its neural representation.

The insect antennal lobe (AL) and the mammalian olfactory bulb consist of a species-specific number of glomeruli, each of which represents the input from all ORNs housing a specific receptor (Mombaerts *et al.*, 1996; Vosshall *et al.*, 2000; Fishilevich & Vosshall, 2005; Couto *et al.*, 2005). Therefore, an activation across ORNs due to odour stimulation (Malnic *et al.*, 1999) translates to combinatorial patterns of activation of glomeruli. This has been confirmed in a number of optical imaging studies in vertebrates (Friedrich & Korsching, 1997; Rubin & Katz, 1999; Uchida, Takahashi, Tanifuji, & Mori, 2000; Meister & Bonhoeffer, 2001) as well as insects (Joerges, Kuttner, Galizia, & Menzel, 1997; Galizia *et al.*, 1999; Carlsson *et al.*, 2002). It has been suggested that glomerular activity patterns constitute a spatial olfactory code (Galizia *et al.*, 1999). Such a code or representation is not only dependent on the chemical structure of the odour molecule but also on the concentration (Carlsson & Hansson, 2003; Sachse & Galizia, 2003). A handful of imaging studies have tested odour blends and the results diverge. Joerges *et al.* (1997) reported strong suppressive interactions between components using optical imaging in the honeybee, while other studies have reported responses to mixtures that are simply the sum of the components' responses (Belluscio & Katz, 2001). Tabor *et al.* (2004) demonstrated that mixture interactions were weak or negligible in the ORN presynapses in the zebrafish glomeruli whereas both suppressive and synergistic interactions were observed in olfactory bulb output neurons.

In this chapter, the optical-imaging techniques developed in the previous chapter are used to identify glomeruli in a further data set. These data sets are designed in order to find and study mixture interactions. In an attempt to mimic natural conditions in which an animal may realistically find itself, plant odours were used in a narrow range of biologically realistic concentrations (Carlsson & Hansson, 2003). Also, these data sets include more ratios of mixture between components than have been studied before.

3.2 Stimuli in a Linear Grid

3.2.1 Experimental Design

Combinations of activated glomeruli are used for encoding the identity of single component odours (Malnic *et al.*, 1999; Galizia *et al.*, 2000; Galizia & Menzel, 2001; Carlsson *et al.*, 2002) and also their concentration (Johnson & Leon, 2000; Carlsson & Hansson, 2003). This implies that the perceived identity of an odour may change depending on concentration. How, then, does this system encode for both of these properties when presented with multiple odours simultaneously, and how can they both be represented by such a glomerular spatial code? The pooling of responses allows us to address such questions, since they are generalised across individuals within a species.

In Chapter 2, a set of concentration loads that linearly increased with regular intervals were used: 0 μg, 10 μg, 20 μg and 30 μg. Geraniol and linalool, both host-plant odours, were chosen to produce the matrix of binary odour blends. This matrix of stimuli covered all combinations that were possible with these four concentration loads. These stimuli were used to develop and test the automatic glomerular identification algorithm, but also

allow some analysis of the glomerular response to these binary blends. The linear grid of odour blend stimuli allows comparisons between the responses to blends against the responses to the components of those blends.

To assess the representation of odour blends from the data from Chapter 2, the response profiles of the three identified glomeruli for the three animals were computed as the mean of the pixels contained in the respective glomerulus. The labelling of the animals (A, B, C) and glomeruli (1, 2, 3) are kept consistent with the previous chapter. Although the responses were shown to vary between animals, for completeness, all the data are kept in consideration for this chapter. These data are plotted in Figure 3.1. The data for each glomerulus were pooled by taking the mean response for each blend across the three animals.

3.2.2 Response Surfaces

The pooled responses shown in Figure 3.1 are less variable and form more uniform surfaces than the responses for each animal as physiological noise in the recordings and individual variability were partly averaged out. This is an immediate advantage to pooling the data, since the shape of the response curves become more apparent, which would otherwise be obscured by variability across trials in any single animal. Thus, mechanisms employed by the glomeruli for their coding scheme can be more reliably elucidated. Also, pooling of responses over many animals allows us to investigate general properties of the olfactory code in this species as opposed to that of an individual.

The matrix of stimuli allows the plotting of responses as a two-dimensional surface. One can observe the effect that gradually adding more

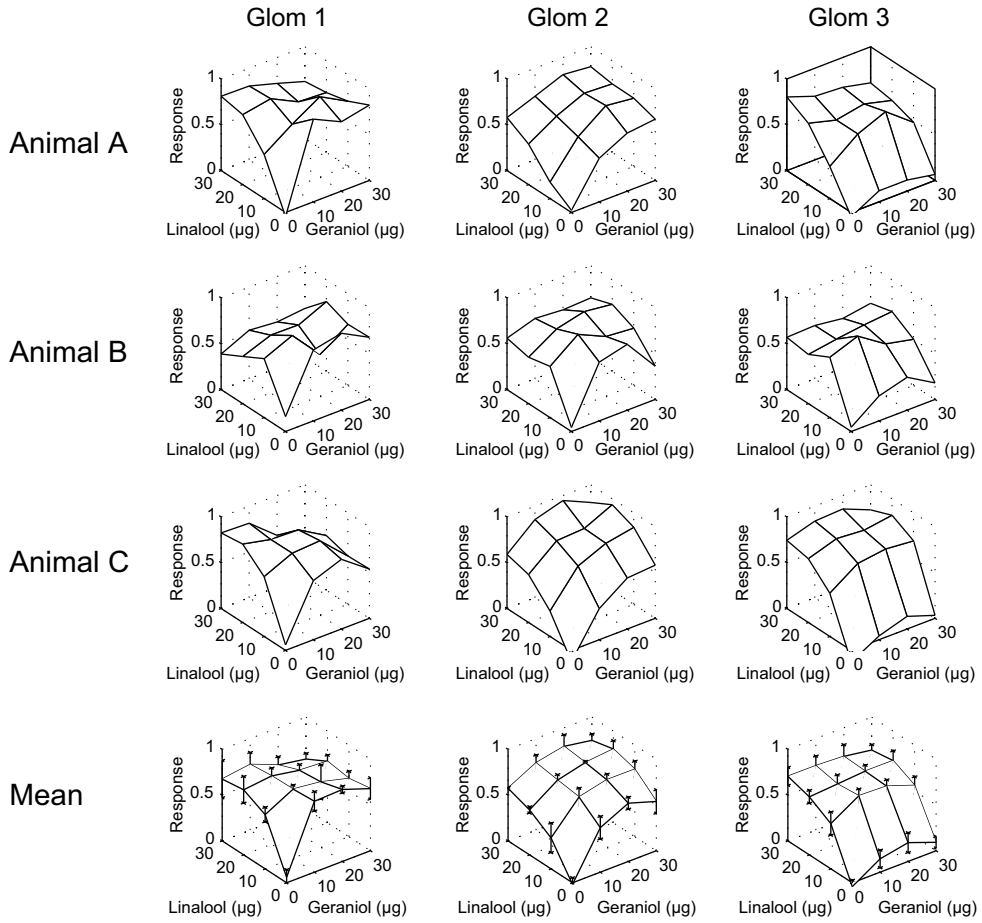

Figure 3.1: The glomerular responses to different mixtures. These are the response curves to the blends for each registrated glomerulus (columns); for Animal A, B and C, and the subsequent mean value once all animals are pooled together (rows). The x- and y-axes give the geraniol and linalool loads, respectively, and the z-axis gives the normalised response to these blends. Glomerulus 1 is highly activated by everything except blank. Glomerulus 2 also responds to both components, but displays a gradual increase in activation as total stimulus load increases. Glomerulus 3 responds only to linalool, and so does not vary its response in the geraniol direction at these concentrations. The pooled responses have standard deviation across the animals plotted at each point. The pooled data has some of the variability of the individual animal responses averaged out, giving much smoother response curves, making it easier to determine the response characteristic of each glomerulus.

of one odour has to the concentration curve of the other odour. Also, one can see the linearity (or otherwise) of the blend responses. In other words, to what degree the blend responses are the summation of the responses to their components at the appropriate concentrations.

We see that Glomerulus 1 responds in a binary manner: giving either a full response if either component is present at any concentration tested; or no response for the blank. This is highly nonlinear in the sense that the response to blends is far from the summation of the responses to the components. This glomerulus shows a plateau of activity even for the lowest stimulus load. Glomerulus 2 has what seems to be a very symmetric response shape, indicating that the receptor type innervating this glomerulus does not distinguish greatly between the two odorants in the stimuli. Unlike that of Glomerulus 1, its response to these stimuli changed in magnitude gradually as the concentration changed. Because of this, the response to blends is higher than to any single component stimulus. Glomerulus 3 responds predominantly to linalool only, and varies little with increasing geraniol concentration. Like Glomerulus 2, it has a graduated response curve, but almost entirely only to linalool. This curve is only slightly affected by the geraniol load. Thus, it provides a readout for the linalool concentration load, and shows very little effect of blend interactions.

These three glomeruli provide an encoding scheme from which it is possible to identify the stimulus from the glomerular responses. Each blend elucidates a unique pattern of glomerular activation. This unique representation of each blend is possible primarily due to Glomerulus 3, which encodes for linalool concentration almost independently of geraniol concentrations.

Glomeruli 1 and 2 are more ambiguous in their responses, giving a mixture (synthetic) response dependent on the combined concentration of both components, and for these glomeruli, many different blends would give rise to the same response. However, when combined with Glomerulus 3, it is possible to decipher better the individual component concentrations from the mixture. Once the linalool concentration is known, the response of Glomerulus 2 becomes an independent measure for geraniol concentration.

3.2.3 Limitations

Simply adding together two odours at different concentrations seems a logical first step to testing blend responses. The resulting response surfaces are not flat and linear surfaces, instead displaying a nonlinear relationship with the concentration and nonlinear response summation between odours. However, it is thought that glomerular responses are sigmoidal with logarithmic concentration scales (Carlsson & Hansson, 2003). In other words, the response is at zero for low concentrations and at a saturated plateau for high concentrations, but between these extremes there is a range of concentrations for which the response curve is monotonically increasing in a linear way, given a logarithmic concentration scale. Therefore, the nonlinear concentration curve observed in these data is, at least in part, due to having non-logarithmic concentration intervals. Also, there is the problem that any apparent mixture interactions may simply be concentration effects since adding together two components will inevitably increase the total stimulus load. Without data to show what these concentration effects are, we cannot separate genuine mixture interactions from these effects. These issues are addressed in the following set of experiments.

3.3 Logarithmic Concentrations and Blends

3.3.1 Preparation of Animals

We recorded neural activity optically in the antennal lobe of male *S. littoralis* by imaging Ca^{2+} dynamics by bathing the lobe in calcium sensitive dye as before. These experiments were designed by the author in collaboration with Mikael A. Carlsson (Swedish University of Agricultural Sciences). The dissection of the animals were performed by Carlsson. The author assisted in the preparation of stimuli and operating the recording equipment during experiments. All processing of the data was done by the author with custom programs using Matlab. Analysis and interpretation of the results was collaborative.

Only animals with a complete or near complete stimulus panel (see Odour stimuli) that could be tested were further analysed. Out of 28 animals with recorded responses, 13 animals were used in the analysis. Animals usually failed because they stopped responding after just a few odour presentations, despite a strong response initially. Many more animals (uncounted) were dissected, but gave no response and so no recording was attempted.

3.3.2 Odour Stimuli

Each animal was tested with a set of binary blend stimuli consisting of mixtures of two particular compounds. Three host-plant compounds with known physiological and behavioural significance were used (Anderson *et al.*, 1993; Anderson, Hansson, & Lofqvist, 1995) - geraniol, linalool and phenylacetaldehyde (PAA). Previous electrophysiological and optophysiological studies have shown that these odorants evoke strong responses in ORNs and glomeruli

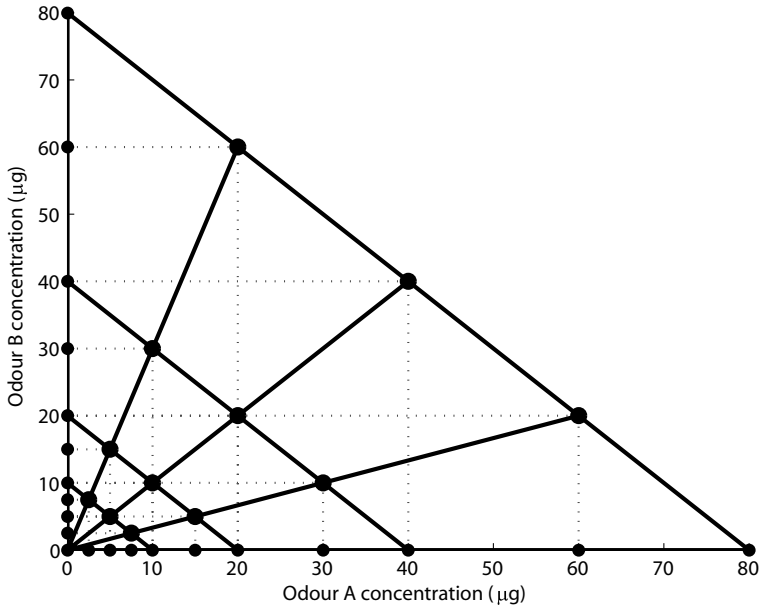

Figure 3.2: Schematic diagram showing the odour blends. The dots represent odours that were used for the experiments. The axes show the loading of each odour component (labelled generically A and B, but were actually two of geraniol, linalool and PAA) and blends are plotted according to the concentration loadings of each odorant. The binary blend ratios used in the experiments are represented by the radial lines emanating from the origin, showing loci of equal ratios. These ratios ranged from purely A to purely B, with the composition ratios of 75% A, 25% B; 50% of each; and 25% A, 75% B. The parallel diagonal lines depict lines of equal total concentration loading. These doubled at each step at 10 μg, 20 μg, 40 μg, and 80 μg. This produced 12 different binary blends and 8 different single odorants. Additionally, stimuli were created of each pure odorant at the loadings that were used to create the binary blends for comparison purposes. At the origin is the control, with neither odorants present.

(Anderson *et al.*, 1995; Carlsson *et al.*, 2002; Carlsson & Hansson, 2003). In addition, both larvae and adults could be trained to respond behaviourally to these compounds (Fan & Hansson, 2001; Carlsson, Anderson, Hartlieb, & Hansson, 1999).

Our model animal, the noctuid moth *Spodoptera littoralis*, is a broad generalist species found on at least 84 different host-plant species (E. Brown & Dewhurst, 1975). Anderson *et al.* (1993) demonstrated that *S. littoralis* is strongly deterred by a complex mixture (but not by submixtures) of odorants induced by larval feeding. This indicates that synergistic blend interactions occur along the olfactory pathway in this species. In the present study we exposed the animal to 3 plant-related compounds (and their binary mixtures) common to many of the moth's host-plants. Odorants were chosen as they have previously been shown to activate either overlapping or non-overlapping subsets of ORNs and glomeruli depending on the binary combination (Anderson *et al.*, 1995; Jönsson & Anderson, 1999; Carlsson *et al.*, 2002; Carlsson & Hansson, 2003). Thus, mixture phenomena due to either agonistic or antagonistic interactions could potentially occur.

Odorants were dissolved in paraffin oil, which does not evoke a detectable response in the antennal lobe (Carlsson & Hansson, 2003). 10 μl of the solvent containing the respective odorant were applied on a filter paper (5 $\times$ 15 mm). For the control stimulus, paraffin oil solvent was applied alone onto filter paper. Two filter papers were inserted in a Pasteur pipette attached to a plastic pipette tip at the proximal end (total volume $\sim$4.5 ml), each containing an odorant or pure paraffin oil. As before, blends were constructed and mixed only in the headspace. The pipettes were sealed with Para-film

(American National Can., Chicago, USA) and stored in a freezer until the start of an experiment. Odorants were delivered in a randomised order. We allowed at least 60 seconds between stimulations to reduce potential adaptation effects.

The total concentration loads of the blends were doubled at each step: 10 μg, 20 μg, 40 μg, and 80 μg. This gave regular dyadic steps on a logarithmic scale. While this enabled comparisons between blends and their components at the same total concentration load, also needed were comparisons between blends and their components at the concentrations of which the blends consisted (Figure 3.2). With these extra concentration loads for the individual components, mixture interactions can be distinguished from concentration effects. Altogether, 10 different stimulus loads were used of each compound (2.5–80 μg) and 12 different binary mixtures. In addition, the third compound that was not included in the binary mixtures was tested at 4 doses in order to physiologically identify the corresponding glomerulus. Thus, including a control stimulus, in each experiment we used 37 different stimuli (Figure 3.2). The concentrations were chosen to lie between the threshold of optophysiological detection and saturation (Carlsson & Hansson, 2003).

3.3.3 Criteria for Mixture Interactions

We used a definition for suppression, where the blend response is weaker than that of either of the responding components (same concentration singly or in mixture); and synergy, where the blend response is stronger than that of the most strongly responding component at the same total loading as the blend. The following criteria were used:

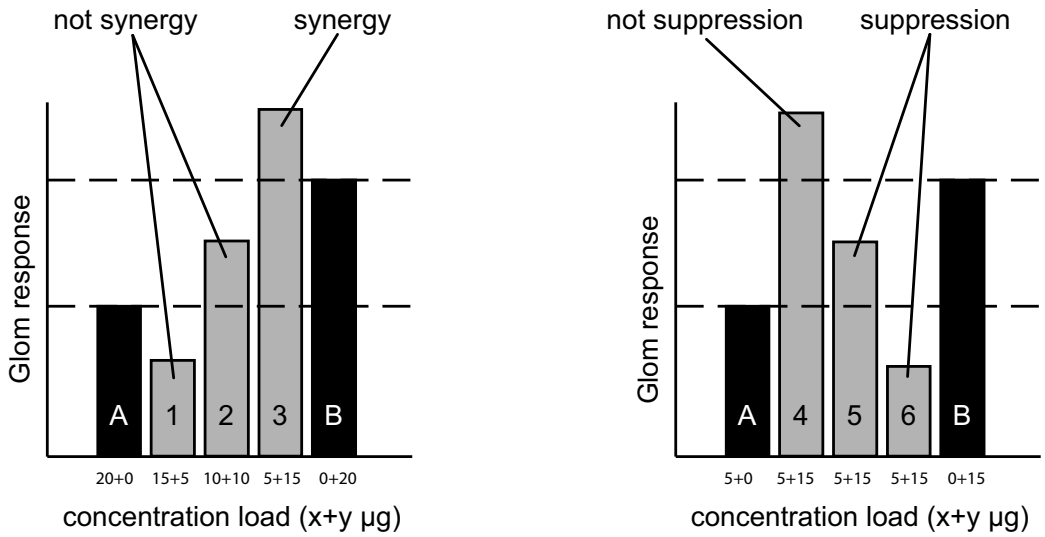

Figure 3.3: Synergy and suppression criteria. The bars show hypothetical responses from a glomerulus to some stimulus examples. The stimuli are of binary odour blends of two components A and B. Blends are denoted by $x + y$ where the blend is composed of x μg of A and y μg of B. In each panel, the black bars show pure compounds against which to compare the grey bars of blends. In the left panel, all stimuli have the same total concentration, so from this diagram it is possible to see when the synergy criterion is not met (as in bars 1 and 2) and when it is met (such as bar 3). Bar 2 is not synergistic even though it exceeds bar A since it is not greater than bar B. The layout of the bars in Figure 3.6 is identical to this layout. This can only show synergy and not suppression. For example, although bar 1 is less than bar A, this does not necessarily indicate suppression is present since this depends on the slope of the concentration response curve.
In the right panel, hypothetical responses to just one particular blend are shown. These are compared with the responses to pure components at the same load as found within the blend. This is necessary to depict the suppression criterion. Bar 4 displays no suppression, but is not necessarily synergistic since here the comparison is with pure component responses of different total concentrations. Bars 5 and 6 show situations where suppression is apparent. Bar 5 shows suppression even though it exceeds bar A because it is only necessary to be less than one component response: in this case bar B. No equivalent of Figure 3.6 for the test for suppression is shown since there is no compact way of displaying all comparisons.

Synergy: $R(A_x + B_y) > \max[R(A_{x+y}), R(B_{x+y})]$

Suppression: $R(A_x + B_y) < R(A_x)$ or $R(A_x + B_y) < R(B_y)$

where R is the normalised response, A and B are the 2 components used, x and y the doses, and $\max[\,\cdot\,,\,\cdot\,]$ gives the largest of the two values. It is important to take note of the subscripts x and y, which indicate the concentration loads that are compared. A graphical illustration of these criteria is shown in Figure 3.3. For statistical comparisons we used a one-way ANOVA or Student's t-test.

3.3.4 Response Curves and Blend Interactions

In each animal, glomeruli were located from localised and coherent regions of activation using the method developed in Chapter 2. This new method allowed the automatic detection of glomeruli without the need to manually decide the location of glomeruli by viewing activity maps to all stimuli. From these glomeruli, three were identified in each animal based on the respective physiological response. Since the across-animal glomerular registration algorithm was affected by inter-animal variability, a more robust registration technique was applied that has already been used in a previous study (Carlsson & Hansson, 2003). The 3 compounds we used (geraniol, linalool and PAA) each activated a single glomerulus most strongly, and we refer to the glomerulus that gave the greatest response magnitude for a compound as the 'best' glomerulus for that component. With the different stimulus sets it is not directly possible to match the identified glomeruli from the two studies in this chapter. A likely estimate from the overall responses and locations of the glomeruli would be that the 'geraniol-best' glomerulus is Glomerulus 2,

and the 'linalool-best' glomerulus is Glomerulus 3. The 'PAA-best' glomerulus has no counterpart in the first data set since that set did not include stimulation with PAA. Glomerulus 1, which was responsive to both geraniol and linalool, would not have been identified in the logarithmic data set since this glomerulus would not be the one with the greatest response to either components.

The 'PAA-best' glomerulus, with strongest activity for PAA, was located in the medial part of the AL, whereas the other two glomeruli were located more laterally. The 'linalool-best' glomerulus was located ventral of the 'geraniol-best' glomerulus. This morphology agrees with the locations that have been previously observed in other studies (Carlsson *et al.*, 2002; Carlsson & Hansson, 2003). The latter glomerulus actually responded similarly to geraniol and linalool, but during geraniol stimulation this glomerulus was the one with the greatest response magnitude. During linalool stimulation, this glomerulus gave only the second strongest response of all the glomeruli. These 3 glomeruli could be unambiguously identified in all animals and allowed us to pool data across individuals. Figure 3.4 shows a typical example of false-colour coded responses to geraniol, linalool and the binary mixtures of these in a single animal. In all images identical intensity scales were used for ease of comparison.

Dose-response curves for individual components and their binary mixtures were constructed based on the total stimulus load (Figure 3.5). In almost all cases there is an upward trend by way of response magnitude increasing with stimulus load. The 'geraniol best' glomerulus was strongly activated by both geraniol and linalool and only weakly by PAA at the highest concentrations. It responded to geraniol and linalool indifferently, and

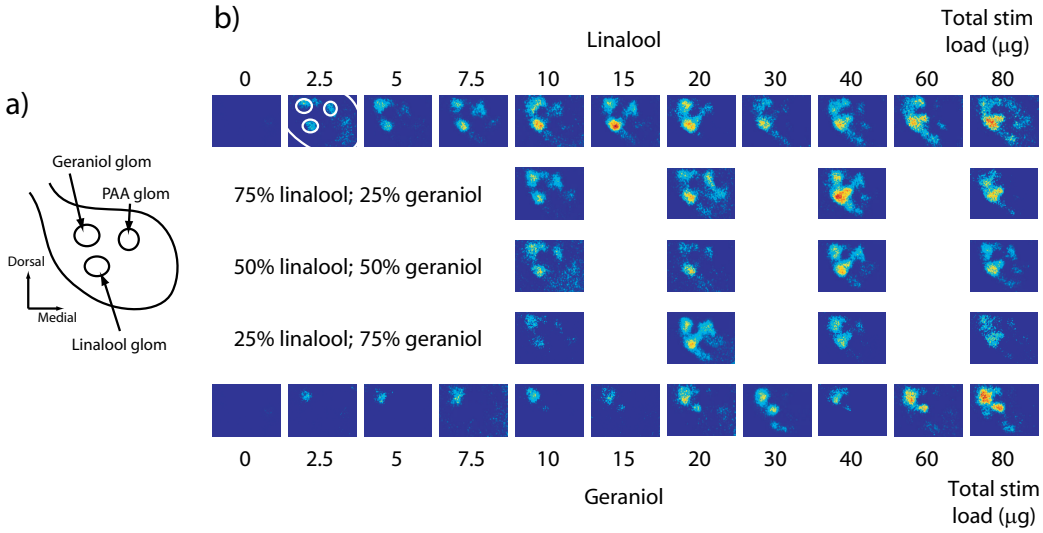

Figure 3.4: Example of responses recorded in a single animal. a) A map of the antennal lobe indicating regions which were used to attain glomerular activity, with an estimated outline for the antennal lobe. To indicate the relative positioning of these glomeruli against the activity images, the map has been superimposed onto the response to linalool at 2.5 μg stimulus load. b) After initial image processing, we attain spatial activity maps for each of the odours tested in one binary combination of odorants. In this case the binary combination was of linalool and geraniol. Generally in this diagram, columns represent the total stimulus load (μg), increasing form left to right, and rows represent different ratios, from pure linalool at the top, to pure geraniol at the bottom. In this diagram, we can see the regions of activity develop in the series as loading increases, particularly for the pure odorant stimuli. The increase in activity and the spatial spreading of activity in the recruitment of more glomeruli can be observed. Also evident is the progression of the spatial activation as the odour ratios move between one pure odorant to the other. There appears to be a smooth transition in general.

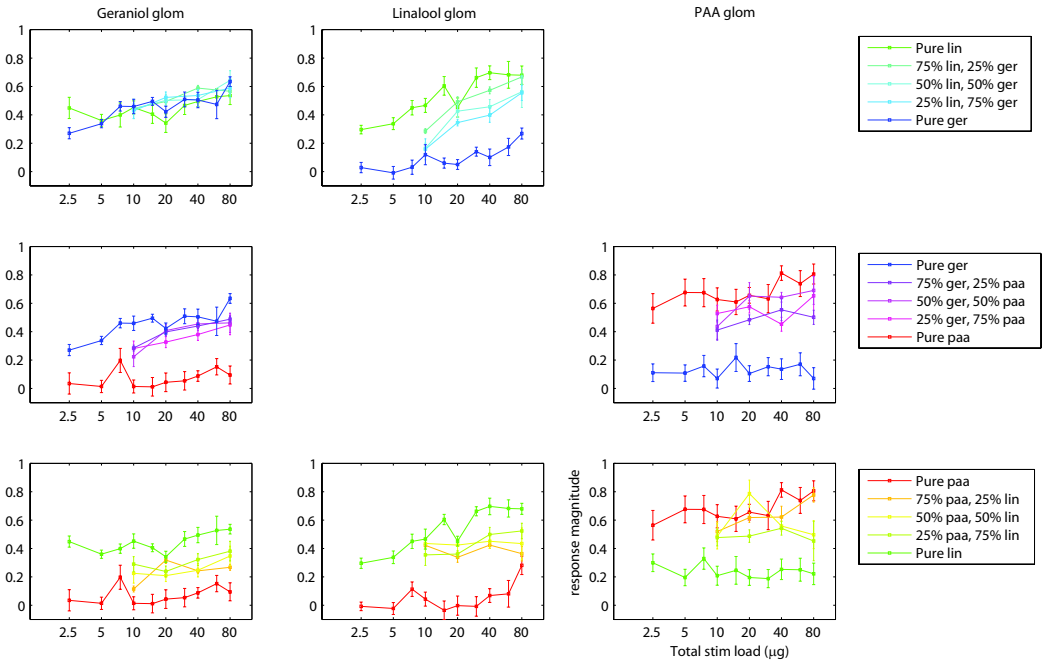

Figure 3.5: The responses to all odours pooled across animals. The graphs show the concentration curves for each ratio, mean averaged over identified glomeruli across animals, with error bars showing the standard error. The colours are chosen to represent the different pure odorants and their mixtures. Linalool is assigned green, geraniol assigned blue, PAA assigned red, and the colours for the binary blends are the colours of the respective constituent components mixed in the corresponding ratios (see legends). Each panel shows the response of an identified glomerulus (columns) to binary blends of one pair of odorants (rows). The glomeruli, identified in each animal as the one responding strongest to a pure odorant, show different response strategies. Responses were normalised between zero and one before pooling. The responses for the linalool glomerulus to geraniol-PAA blends and for the PAA glomerulus to linalool-geraniol blends have been omitted since these glomeruli did not respond to these blends.

the response magnitude changes according to concentration, discriminating only the total stimulus load. The 'linalool-best' glomerulus, on the other hand, was strongly activated only by linalool, with geraniol and PAA evoking detectable responses only at much higher concentrations. Finally, the 'PAA-best' glomerulus was only activated by PAA within the concentration range used. Figure 3.5 shows only dose-response curves for blends with at least one potent compound. The dose-response curves for the blends all lie between the curves for the individual components, except for blends of geraniol and linalool in the 'geraniol-best' glomerulus, which elicit equal responses to either of the components or to the blend. It is also apparent that the responses to the varying ratios are roughly in the order one would expect as they graduate from one pure stimulus to another. For a clearer view, the responses are shown in a bar chart (Figure 3.6). In each section the bars show responses to stimuli with the same total load. The ratio responses generally fall on the slope connecting the responses of the pure odorants. The differences between the mean responses within each section were tested with an ANOVA. These tests show that the difference between these responses overall are statistically significant. However, the geraniol glomerulus response to geraniol-linalool blends (top left panel) are not statistically different for blends of the same load, and this is noticeable in the lack of slope within each five-bar group since the responses are all of the same magnitude ($p=0.226$–0.997). All other combinations were, however, highly significantly different ($p=0.014$–0.000).

To test for synergistic interactions according to the criterion (Figure 3.3a), the blend response was compared to single component responses where the

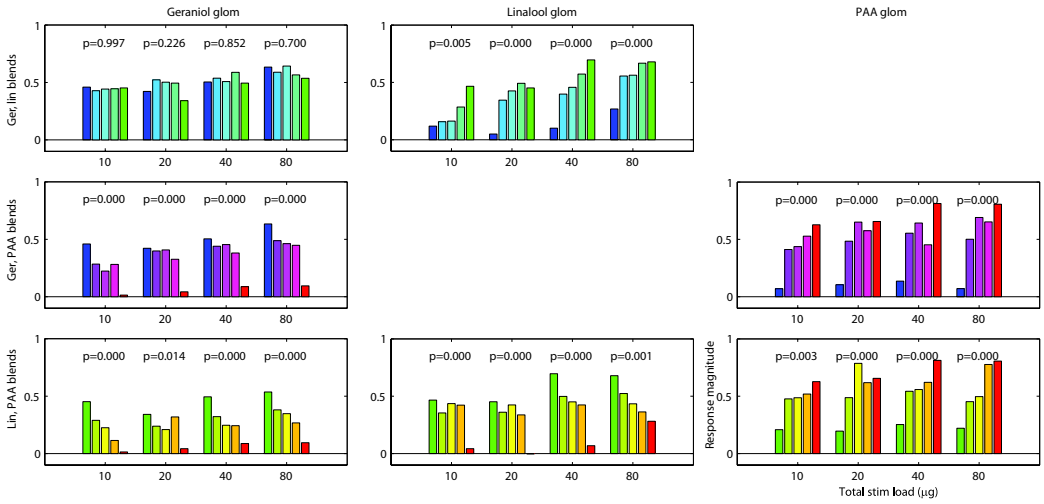

Figure 3.6: Comparisons of the blend responses to the pure stimuli response. These bar graphs are colour coded as in Figure 3.5, with green depicting pure linalool stimuli, blue geraniol, and red PAA. The panels are organised as in Figure 3.5, with different identified glomeruli arranged into columns and each odorant pair arranged into rows. Each small group of five bars are the responses to the odours of the same total stimulus load but at different ratios. These bars are organised such that left- and right-most bars of each five-bar grouping are the pure odorants, and the three bars in between are the ratios graduating from one odorant to the other. The p-values quoted for each group is of an ANOVA to test if the bars are statistically different. This arrangement allows one to observe two things: 1) whether the glomerulus responds differentially to the two odorants and 2) whether there are any cases of synergy (see Figure 3.3). For all responses except for the geraniol glomerulus response to geraniol-linalool blends, it is apparent that each glomerulus can distinguish between any two pure odorants at each concentration load. Synergy can be seen here if the ratio responses exceed both the pure odorant responses at the same load. On the bar charts, this would mean any of the middle three bars being greater than the left- and right-most bars (see Figure 3.3 for details). One obvious example is the PAA glomerulus response to the blend 10 μg linalool plus 10 μg PAA (bottom right panel, 20 μg total stimulus, central bar) which exceeds both the pure linalool response at 20 μg and the pure PAA response at 20 μg. However, no responses to blends were significantly stronger than a response to the strongest component alone ($p>0.05$).

single component is at the same concentration load as the total concentration load of the blend. This ensured that we did not identify a synergistic effect when an increase in response was merely due to an increase in concentration load as two components were added together. We statistically tested all pairs (strongest responding versus mixture) containing identical total loads (Table 3.1). No responses to the blends were significantly stronger than the responses to the corresponding single components (84 comparisons, all $p>0.05$, Student's t-test). That is, no synergistic effects were observed. Finally, we tested the occurrence of suppressive interactions (Table 3.2). In this test, we compared the blend responses to the component responses such that the components were at the same concentration load as that from which the blend was comprised. In this way, any decrease in the response to the individual components compared to the response to the blend cannot be the result of lowering the concentration load of either component. A graphical illustration of the suppression criterion can be seen in Figure 3.3b. Every combination where the key component had the same concentration singly or in a mixture was compared. Out of 168 comparisons, we found that 62 meet the suppression criterion, and only in 4 cases did we find a mixture that evoked a significantly weaker ($p<0.05$, t-test) response than the component alone. The observed suppressions were not dependent on mixture, concentration or ratio (see Table 3.2). Furthermore, when a Bonferroni correction for multiple tests was applied, a $p<0.05$ threshold level for the whole suppression experiment required individual tests to give a p-value less than $0.05 \div 62 \approx 8 \times 10^{-4}$. This only took into account the cases where the criterion was met and Student's t-test was performed, yet none of the individual tests were significant to this level.

	Ger:Lin						Ger:PAA						Lin:PAA					
	1:3		1:1		3:1		1:3		1:1		3:1		1:3		1:1		3:1	
	p	n	p	n	p	n	p	n	p	n	p	n	p	n	p	n	p	n
Geraniol-best Glom																		
10 μ**g**	-	5	-	4	-	4	-	5	-	4	-	4	-	5	-	4	-	4
20 μ**g**	0.33	4	0.30	4	0.23	5	-	4	-	4	-	5	-	4	-	4	-	5
40 μ**g**	0.46	3	0.97	5	0.71	5	-	3	-	5	-	5	-	3	-	5	-	5
80 μ**g**	-	5	0.92	3	-	5	-	5	-	3	-	5	-	5	-	3	-	5
Linalool-best Glom																		
10 μ**g**	-	4	-	4	-	4							-	4	-	4	-	4
20 μ**g**	0.73	4	-	4	-	3			n/a				-	3	-	4	-	3
40 μ**g**	-	4	-	4	-	4							-	3	-	4	-	3
80 μ**g**	-	4	-	4	-	4							-	3	-	3	-	4
PAA-best Glom																		
10 μ**g**							-	4	-	4	-	4	-	4	-	4	-	4
20 μ**g**			n/a				-	3	-	4	-	3	-	3	0.17	4	-	3
40 μ**g**							-	3	-	4	-	3	-	3	-	4	-	3
80 μ**g**							-	3	-	3	-	4	-	3	-	3	-	4

Table 3.1: Tests for synergy. Responses satisfying the criterion for synergy, with p-values showing significance of the observed synergy where a Student's t-test was performed. Dashes are used where the responses do not satisfy the criterion for synergy. n-values show the number of animals that provided data for each comparison. n/a is used where there is a mismatch between the responsive compounds for a glomerulus and the compounds of the stimulus.

	Ger:Lin						Ger:PAA						Lin:PAA					
	1:3		1:1		3:1		1:3		1:1		3:1		1:3		1:1		3:1	
	Ger	**Lin**	**Ger**	**Lin**	**Ger**	**Lin**	**Ger**	**PAA**	**Ger**	**PAA**	**Ger**	**PAA**	**Lin**	**PAA**	**Lin**	**PAA**	**Lin**	**PAA**
Geraniol-best Glom																		
10 μ**g**	-	-	-	-	0.59	0.84	-	-	0.08	-	**0.04***	-	0.14	0.56	0.29	-	0.65	-
20 μ**g**	-	-	-	-	-	-	0.87	-	0.57	-	0.25	-	0.73	-	0.15	-	0.38	-
40 μ**g**	-	-	-	-	-	-	0.40	-	-	-	0.45	-	0.20	-	0.65	-	0.41	-
80 μ**g**	-	-	-	-	-	-	-	-	0.68	-	-	-	0.72	-	0.24	-	0.36	-
Linalool-best Glom																		
10 μ**g**	-	0.15	-	**0.03***	-	0.13							-	-	-	-	0.26	-
20 μ**g**	-	0.32	-	0.68	-	-			n/a				1.00	-	0.66	-	0.08	-
40 μ**g**	-	0.52	-	-	-	0.37							0.73	-	1.00	-	0.20	-
80 μ**g**	-	0.90	-	0.16	-	-							0.53	-	**0.02***	-	0.28	-
PAA-best Glom																		
10 μ**g**							-	0.15	-	0.08	-	0.28	-	0.15	-	0.32	-	0.55
20 μ**g**			n/a				-	0.83	-	-	-	0.26	-	-	-	-	-	0.24
40 μ**g**							-	0.24	-	0.89	-	0.38	-	0.94	-	0.34	-	0.34
80 μ**g**							-	0.36	-	0.15	-	0.10	-	-	-	**0.00***	-	0.07

Table 3.2: Tests for suppression. Responses satisfying the criterion for suppression, with p-values showing significance of suppression using t-tests, and dashes showing no suppression. * indicate significant t-tests ($p<0.05$). For n-values, see Table 3.1. Again, n/a is used where there is a mismatch between the glomerulus and the stimulus.

3.4 Discussion

Using the methods developed in Chapter 2, it is possible to quantify a glomerular odour code that is not specific to a single animal. These methods permit the pooling of large stimulus sets over many animals, providing a generalised quantification of the glomerular odour code in a particular species.

Non-trivial interactions between components within odour blends have been observed in moths, both in behavioural studies (Arn *et al.*, 1980; Lofstedt *et al.*, 1982; Wu, Hansson, & Lofstedt, 1995) and in electrophysiological recording from antennal lobe interneurons (Christensen & Hildebrand, 1987; Christensen, Hildebrand, Tumlinson, & Doolittle, 1989; Christensen *et al.*, 1991; Christensen, Mustaparta, & Hildebrand, 1995; Anton & Hansson, 1995; Wu, Anton, Lofstedt, & Hansson, 1996; Anton, Lofstedt, & Hansson, 1997; Hartlieb *et al.*, 1997). However, it is as yet unclear from how far along the olfactory pathway these interactions originate. It is possible that interactions happen at each and every stage of olfactory information processing. In the antennal lobes, this would be from the peripheral receptor cells, computational processes in the AL, and even feedback from higher brain regions. The responses in single glomeruli represent the convergent input from hundreds of ORNs likely housing identical receptor proteins (Vosshall *et al.*, 2000; Gao *et al.*, 2000; Fishilevich & Vosshall, 2005; Couto *et al.*, 2005). Therefore, the glomerular responses in this chapter actually reveal the interactions at the very first stages of the olfactory pathway, at the ORNs.

Generally, olfactory receptor neurons are broadly tuned to a wide range of odour stimuli and have overlapping receptive fields. Thus, we might expect that chemically dissimilar odorants that stimulate non-overlapping subsets of

receptors should display elemental properties, while similar odorants stimulating highly overlapping subsets of receptors would induce more interaction between the odorants, giving rise to configural properties in the representation. This is supported by behavioural studies that demonstrate the effects of odour component similarity on the ability of rats to distinguish blends from their components (Kay, Lowry, & Jacobs, 2003; Laing *et al.*, 1989; Wiltrout *et al.*, 2003). However, our results indicate that blends of either similar (geraniol and linalool) or dissimilar (geraniol and PAA; linalool and PAA) odorants are linearly represented at the first stage of olfactory processing.

With the matrix of blend stimuli, it was possible to observe the encoding which, despite overlapping glomerular receptive sensitivities, conserved information of the components for higher processing in the sense that component information could be deconvolved from the blend responses. However, it was still not clear from these data what the interactions entailed. One could not tell if there were synergistic or suppressive interactions, or even concentration effects altering the blend responses from a simple addition of component responses. In the logarithmic data set, these issues were addressed.

Two conservative approaches were used to identify possible mixture interactions. Suppression was defined as a response to a blend that was significantly weaker than the strongest responding component alone, applied at the same concentration as in the mixture. Synergy, on the other hand, was defined as a blend response that is stronger than that of the most strongly responding component at the same total loading as the blend. Using this approach, no identifiable synergistic interactions were found, and only few and

weak suppressive interactions, irrespective of concentration or ratio. However, it is entirely possible that less pronounced interactions may have been overlooked with this approach.

The nearly complete lack of suppressive interactions (and complete lack, after the Bonferroni correction) in this study as opposed to the study by Joerges *et al.* (1997), using the same imaging technique, can be explained by the differences in stimulus loads used. The doses in our study were chosen to be well below saturation level (Carlsson & Hansson, 2003) to mimic naturally occurring concentrations. Joerges *et al.* (1997) used non-diluted substances, which in the moth *S. littoralis* would elicit responses above saturation level (Carlsson & Hansson, 2003). It has been shown that suppression in pheromone-sensitive ORNs in the moth *Agrotis segetum* only occur at very high concentrations of mixtures (Carlsson & Hansson, 2002). When there is a very high concentration of odour molecules, it is likely that there is significant competition for receptor sites. Thus, a molecule that does not elicit a response from ORNs may act as a competitive antagonist and block the action of a responsive compound, inhibiting an otherwise strong response. Such a dual function of ORNs has been observed in the pheromone detecting subsystem in moths (K. E. Kaissling, Meng, & Bestmann, 1989; Hansson *et al.*, 1990). Competition between odour molecules may occur even before reaching the receptor sites of ORNs. Upon entering a sensillum, having passed the hair surface cuticle via a pore, odour molecules are thought to be transported to receptor sites by odorant binding proteins (Stengle, Ziegelberger, Boekhoff, & Krieger, 1999). Odorant binding proteins are necessary to carry the mostly hydrophobic odorants through the aqueous sensillum

lymph. Potentially, there may be competition for these odorant binding proteins, especially if high odour concentrations deplete their numbers.

Strong mixture interactions have been observed in the pheromone processing subsystem in moths. Some PNs, from the pheromone specific cluster of glomeruli, the macroglomerular complex (MGC), have been reported to have blend-specific properties and respond exclusively to a species-specific blend and not to its individual components (Christensen & Hildebrand, 1987; Christensen, Hildebrand, *et al.*, 1989; Christensen *et al.*, 1991, 1995; Anton & Hansson, 1995; Wu *et al.*, 1996; Anton *et al.*, 1997; Hartlieb *et al.*, 1997). However, no such interactions have been reported from studies of ORNs (Akers & O'Connell, 1988, 1991; Almaas & Mustaparta, 1990; Berg & Mustaparta, 1995; Carlsson & Hansson, 2003). Thus, blend-specific responses in the pheromone sub-system are likely to be a result of interglomerular computation within the MGC. Responses to mixtures of plant-related compounds in insects have been less well studied and the results diverge. De Jong and Visser (1988) showed that extracellular responses in certain ORNs in the Colorado potato beetle were suppressed when stimulated with binary mixtures containing general green leaf volatiles. Likewise, suppressive interactions were observed in single cockroach ORNs (Getz & Akers, 1997). Akers and Getz (1993) found that responses to binary mixtures of aromatics and octyls in the honeybee were often stronger than would be predicted.

In honeybees, a blocking paradigm was used to show that conditioning could alter the perception of blends (Hosler & Smith, 2000). In their experiment, preconditioning to one odorant diminished the strength of association

between a reward and another odorant when animals were conditioned to associate the reward with the blend of both odorants. In order to associate the unconditioned stimulus with components of a blend rather than only the blend in full, the components must be identifiable from the blend. This shows that mixture interactions can be altered by prior experience, so that components are recognised within a mixture. Therefore, it may be possible that an animal can exploit both configural and elemental coding paradigms depending on what it has learned from its environment. Associative learning of odours alters the synapses that drive PNs of the antennal lobe (Yu, Ponomarev, & Davis, 2004). With such plasticity at this level, it may be possible for animals to alter the role of these neurons between configural and elemental coding. For such a system, it would be necessary to preserve elemental information up to this stage of processing, as indicated by our data. The weak mixture interactions observed at the ORN level may be necessary for plasticity in the olfactory system. Information should be reliably transferred to second order neurons where collateral processes or efferent feedback may alter responses to emphasise particular mixtures that an animal has learnt to be important in previous experiences.

In summary, no strong mixture interactions between common plant compounds, at biologically realistic concentrations, were present in the data. This means that the second component of a mixture, regardless of whether it is excitatory or neutral, did not alter the response to the mixture in a highly nonlinear manner. Instead, the interactions were between the extremes of synergy and suppression, in an additive regime. It is likely that mixture interactions occur downstream of the ORNs, during computation by

interneurons in the antennal lobes and beyond. If the processing of olfactory information really starts in the antennal lobe, then it is important that the ORNs reliably report component information. In order to preserve the encoding of quality up to the second order neurons, blend interactions in ORN should be weak or negligible.

Chapter 4

Ratio Encoding in the Macroglomerular Complex

4.1 Introduction

The macroglomerular complex (MGC) is a structure within the antennal lobe (AL) of some insect species (including moths and cockroaches) that processes pheromone information. It is composed of a group of specialised glomeruli located where the antennal nerve first enters the antennal lobe. It is almost entirely functionally separate from the general odour system. As such, it is like the antennal lobe in miniature, but with the very specific task of identifying the presence of one behaviourally significant odour: the species-specific pheromone blend (Hansson, 1999). This system is highly important for reproduction. During chemotaxis for seeking a mate, detecting and identifying the correct sex pheromone of a calling female is vital for enabling male moths to fly up the pheromone plume to locate the female (Murlis, Elkinton, & Carde, 1992; Baker & Haynes, 1996; Hartlieb & Anderson, 1999).

The olfactory receptor neurons (ORNs) responsible for relaying pheromone information to the MGC are very specifically tuned to pheromone

components (Akers & O'Connell, 1988). Furthermore, each component is detected by just one receptor type, and each glomerulus receives convergent axons from just one receptor type (Hansson *et al.*, 1992; Carlsson *et al.*, 2002). Thus, information of each component is integrated to a different glomerulus, separating the information about components before entering the glomeruli. This makes the MGC a good starting point for modelling since it offers a much simplified system, with a specific task. However, as I describe below, it is still not a simple task.

Behavioural evidence shows that male moths prefer the full pheromone extracted directly from female glands (Valeur & Lofstedt, 1996). In wind tunnels experiments, male oriental fruit moths, *Grapholita molesta*, can distinguish between the full pheromone blend and scents composed of incomplete blends of major pheromone component agonists (Valeur & Lofstedt, 1996). This moth will usually complete chemotaxis to the source of the full pheromone extract, even when another plume is simultaneously presented composed of an incomplete blend. Also, there are examples of species of moths that live in overlapping habitats, and also use overlapping pheromone components. However, these sympatric species do not interbreed since males are attracted only to the conspecific pheromone blend (K. Kaissling & Kramer, 1990). In electrophysiological studies, MGC interneurons were found that responded to all pheromone stimuli or selectively to just one pheromone component, or even to a particular blend or ratio (Wu *et al.*, 1996; Christensen, Mustaparta, & Hildebrand, 1989; Christensen, Hildebrand, *et al.*, 1989; Heinbockel, Christensen, & Hildebrand, 2004). For *S. littoralis* in particular, interneurons were found that responded to one, two,

three or all four pheromone compounds, and some just to the mixture of all four. This all indicates that moths can detect ratios of pheromone blends very precisely. This is a difficult task since it not only requires detection of the presence of specific components, but also their relative concentrations. In terms of overlapping information channels, differentiating between different ratios of the same components would completely overlap, and therefore be the most difficult to achieve.

While there have been a few previous efforts to model different aspects of the AL, only a handful have been specific to the MGC (Av-Ron, 1994; Av-Ron & Rospars, 1995; Av-Ron & Vibert, 1996; Linster *et al.*, 1992, 1993; Linster, Kerszberg, & C, 1994; Linster & Dreyfus, 1996), and only Linster *et al.* (1994) and Linster & Dreyfus (1996) consider ratio detection. Linster *et al.* (1994) describes a highly abstracted oscillatory model, showing that by balancing numbers of inhibitory and excitatory neurons in a network receiving two-component input, a system can be made to oscillate when a particular ratio is presented. Linster *et al.* (1996) build a more biologically constrained model including local interneurons (LNs) that mediate information to projection neurons (PNs). Again, the balance between inhibitory and excitatory elements is investigated, this time to show that PN response patterns can be made dependent on the input ratio. The model can be tuned such that PNs will display both inhibitory and excitatory influence from the LNs when a particular ratio is presented. As such, PNs will respond with a pattern of activation, which includes mixed periods of excitation and inhibition, only for input that is close to a particular ratio.

In the few studies that model the MGC, and those that model the AL for general olfaction, focus has been on generating PN response patterns that are

biologically realistic. In some previous studies, high-detailed neurons exhibiting bursting behaviour have been connected into different neuronal circuits of four-or-less interneurons (Av-Ron, 1994; Av-Ron & Rospars, 1995; Av-Ron & Vibert, 1996). It was shown that these circuits can be designed such that the computer-simulated PNs display excitation or inhibition depending on which components are present in a simulated pheromone blend input. This replicated some responses observed in the activity of PNs in the Sphinx moth, *Manduca sexta*, when pheromone components are presented (Christensen, Mustaparta, & Hildebrand, 1989; Christensen, Hildebrand, *et al.*, 1989). In other studies, using the Winnerless Competition (WLC) theoretical framework (Afraimovich *et al.*, 2004), AL models were created, largely based on locust physiology, that utilised a spatiotemporal PN code to encapsulate odour identity information for downstream neurons (Rabinovich *et al.*, 2000, 2001). These spatiotemporal codes emulated very well the temporal patterns of PN responses (Rabinovich *et al.*, 2000, 2001; Laurent *et al.*, 2001). WLC involves inhibitory neurons that have asymmetric interconnections, which allow the focus of activity to continually switch between different PN ensembles and never settle on one spatial pattern of PN activity. Thus, unlike a Hopfield-like attractor network with multi-stable attractor points, a WLC network has input-dependent attractive limit-cycles, with the continual switching behaviour generating the spatiotemporal PN output.

The models created in this chapter extend the work of Linster *et al.* (1996,2005) in terms of the modelling of two distinct classes of AL interneuron, PNs and LNs, in glomerular structures (Linster & Dreyfus, 1996). Afferent input to inhibitory LNs and excitatory PNs, and the interconnection

between these interneurons, was determined according to their glomerular innervation patterns (Linster *et al.*, 2005). The models in this chapter also build on the work of Rabinovich *et al.* (2000,2001) and Afraimovich *et al.* (2004) in terms of the WLC framework, which I investigate further by application to LN subnetworks in some models.

Although a lot is known of the morphology of interneurons in the MGC, the precise circuitry and connectivity is unknown, and mathematical modelling can provide an insight into the form these connections may take. In this chapter, I model the MGC to investigate spatial and temporal coding of odour ratios. In these simulations connections are, as much as possible, biologically constrained to known morphological details of moth MGC. Two types of models are created, and the neural connectivity remains the same between the two model types except for the LN-to-LN inhibitory connections. The two inhibition schemes I consider are those of Winner-Takes-All (WTA) networks, and WLC networks. These competitive networks provide the framework for the mutually inhibitory interconnections between the LNs. WTA networks employ symmetrical inhibition between competitive elements, and the resulting neural network encodes stimulus with the spatial identity of neurons, while WLC networks have asymmetrical inhibition as described above, and the output is spatiotemporal. In this way, the PN output can be shaped to give very different dynamical properties: one that is predominantly spatial with relatively simple dynamics, and one that is temporally rich. In this chapter, I develop and investigate two types of MGC model using these two different inhibition schemes, and compare and contrast their ability to encode binary odour ratios.

4.2 Construction of MGC Models

4.2.1 Modelling of Neurons

All neurons are modelled as firing-rate neurons using a first order differential equation that describes the evolution of the firing-rate activation of a neuron over time,

$$\tau \frac{da_i}{dt} = -a_i(t) + \mathrm{S}\left(\sum_{j \in \mathrm{P}} w_{i,j} a_j(t) - \sum_{k \in \mathrm{L}} w_{i,k} a_k(t) + R_i(t) \right) \qquad (4.1)$$

where a_i is the activation level of the ith interneuron; P is the subset of interneurons that are PNs, and L the subset of interneurons that are LNs; $w_{i,j}$ is the strength of synaptic influence of j on the activity of i (similarly for $w_{i,k}$); $R_i = v_{i,1} r_1 + v_{i,2} r_2 = \mathbf{v}_i \cdot \mathbf{r}$ is the afferent input from receptor neurons to the ith interneuron, which is the sum of glomerular inputs from the two receptor neuron types, $\mathbf{r} = (r_1, r_2)$, weighted by the strength of connections, $\mathbf{v}_i = (v_{i,1}, v_{i,2})$; S is a sigmoidal squashing function; and τ (= 10 ms for all interneurons) is the time constant governing the speed of neuronal dynamics. $\mathrm{S}(x) = x^3/(0.5^3 + x^3)$, rectified such that $\mathrm{S}(x) \geq 0$ for all x, is a sigmoid function (Wilson, 1999b) that limits the neuronal activity to values between 0 and 1 while still allowing a linear-like response to a range of input levels between non-activation and saturation. Note that synaptic influence from projection neurons, $j \in \mathrm{P}$, is excitatory and therefore positive, while local interneurons, $k \in \mathrm{L}$, are inhibitory and negative. More details for the determination of the the connection weights $w_{i,j}$ and $w_{i,k}$ are given in section 4.2.2.

Simulation of these neurons was carried out on a PC running MATLAB using customised code. The evolution of the neuronal firing-rates over time

was calculated using integration by a Runge-Kutta algorithm with fixed time-steps of 1 ms. A Guassian noise (mean = 0, standard deviation = 5×10^{-4}) was added to this algorithm at each time-step to create non-deterministic firing-rates. This value was chosen such that the neuronal activity was not completely dominated by noise, but still generated variability between repetitions to allow a comparison of the robustness to noise between different models.

4.2.2 Network Connectivity

The general connectivity of the networks was determined according to known morphological principles of the moth MGC. Pheromone sensitive ORNs are highly specifically sensitive to just one pheromone component, with each ORN type relaying information for one pheromone component to one particular glomerulus (Akers & O'Connell, 1991; Hansson *et al.*, 1992; Carlsson *et al.*, 2002; Carlsson & Hansson, 2002). This detail is translated to the models in this chapter by having glomeruli that each receive an excitation from just one component. Since the encoding of blend ratio is investigated here, a two-component 'pheromone blend' and, accordingly, two glomeruli are simulated. The input to each glomerulus is taken to be the aggregated activity of ORNs activated by the respective component, which is taken to be a scalar value. Thus, the input to the simulated MGC is a two element vector (r_1, r_2).

30 projection neurons and 30 local interneurons were modelled in each network. Projection neurons, which are mostly uniglomerular in moth MGC (Homberg *et al.*, 1989), therefore each receive input from just one receptor

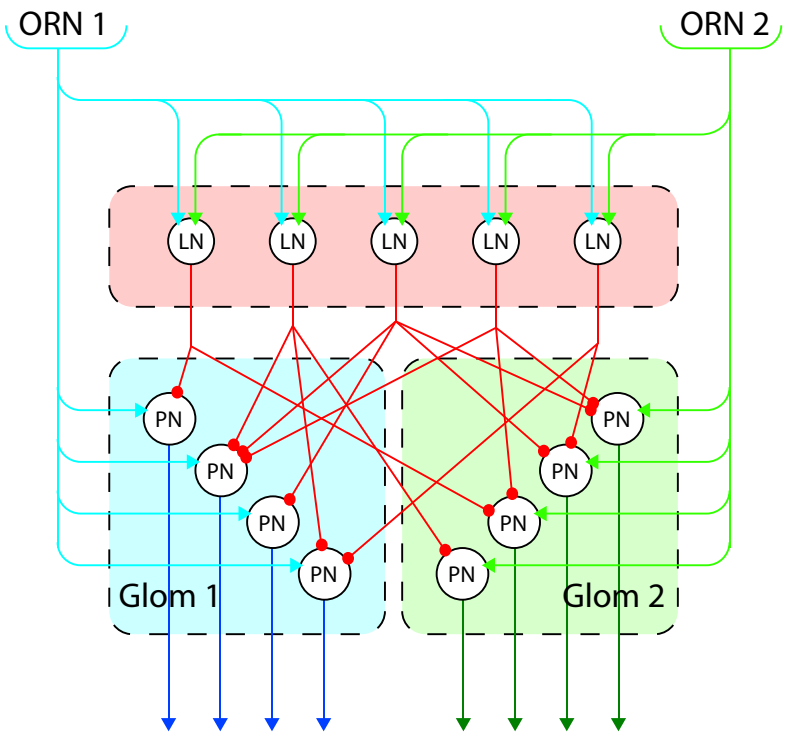

Figure 4.1: Neuronal connectivity schematic. Connections between neurons of different classes are shown. Just two glomeruli are modelled, the convergent sites for the axons of two olfactory receptor neuron types, one glomerulus for each ORN type accordingly. The receptor neurons provide afferent excitation (arrowheads) to the both classes of antennal lobe interneurons. Projection neurons, being uniglomerular, receive excitation from just one type of receptor, while local interneurons, being multiglomerular, can receive excitation from both receptor types. Local interneurons form random inhibitory connections with projection neurons. Interconnections between interneurons of the same class are not shown explicitly, but possible interconnections are indicated by the shaded regions. Interneurons of the same class can form interconnections only within each shaded region enclosed by dashed lines. In the blue and green shaded areas are projection neurons that have random excitatory interconnections. In the red shaded area, local interneurons are shown that either have all-to-all inhibitory connections to produce WTA networks, or random inhibitory connections to produce WLC networks.

type (either $v_{i,1}$ or $v_{i,2} = 0$, for all $i \in \mathrm{P}$) via a randomly weighted connection (in order to give most PNs direct afferent excitation, weights were drawn from a normal distribution, mean = 1, s.d. = 1, negative values rectified to 0), and has random excitatory interconnections with other projection neurons of the same glomerulus. Projection neurons have a 0.8 chance of synapsing to another projection neuron, with connection weight 0.3. These values have been chosen so as to not cause runaway excitation. With the connection strength kept below and not near 1, the system is not sensitive to the exact values. Multiglomerular local interneurons receive input from both receptor types, so receiving information of both pheromone components. Each local interneuron is tuned to be most sensitive to a particular ratio. This tuning to a particular ratio $\mathcal{R} = r_1/(r_1+r_2)$ is achieved by setting the receptor type-to-interneuron connection strengths to the same ratio, $v_{i,1}/(v_{i,1} + v_{i,2}) = \mathcal{R}$ for all $i \in \mathrm{L}$, whilst keeping the length of the vector $\mathbf{v}_i$ constant for all $i \in \mathrm{L}$. To ensure that the local interneurons cover all input ratios as evenly as possible from purely one component to purely the other, the local interneurons are tuned to evenly spaced ratios.

Inhibitory connections from the local interneurons to the projection neurons were chosen randomly. A local interneuron had a probability of 0.2 to connect to any projection neuron, irrespective of the glomerulus to which the projection neuron is associated, and a high strength weighting for that connection ($15 >> 1$). The high strength of connection ensured that any post-synaptic PN would be completely inhibited, and as such, any value much greater than 1 would suffice. Relatively sparse connectivity from LNs to PNs was required to ensure that not all PNs were completely inhibited

during odour presentation. Although the exact value was not important, 0.2 provided a balance that allowed LNs to influence but not overwhelm PNs.

WTA network and WLC network models differed by how interconnections between local interneurons were determined. For WTA networks, competition between cells is created through mutual inhibition, so local interneurons were given all-to-all connections with a high inhibitory connection strength ($15 >> 1$). For WLC networks, cells are connected asymmetrically with high connection strength, leading to uneven competition that prevents a long-term winner, and therefore prevents a stable equilibrium point. To generate this asymmetry, connections between local interneurons were chosen randomly with a probability of 0.25 for any local interneuron connecting to any other. For this value, the subnetworks of LNs would generate switching behaviour. Any value between 0.2 and 0.4 could also generate switching behaviour. However, for values less than this, the subnetworks would lack LN interactions; and for values greater, subnetworks would become largely symmetrical. In either case, switching behaviour would not occur.

20 networks were created for each type of network, following the above rules. All of these connections are summarised in Figure 4.1. Connections from PNs to LNs were not included in the models since any randomly selected feedback excitation would also cause asymmetries in the LN sub-networks. Thus, fo consistency between the WTA and WLC models, PN-to-LN excitation was omitted. The behaviours of the MGC models created are illustrated by an example response of a WTA network, and one of a WLC network in Figure 4.2.

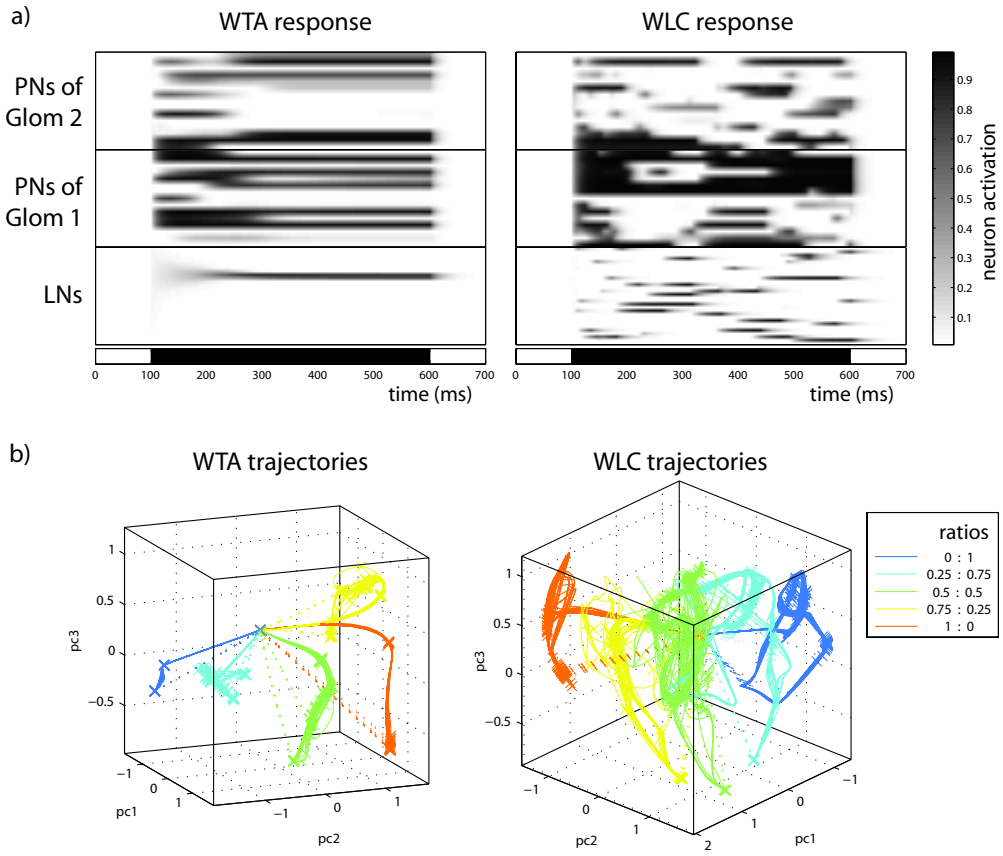

Figure 4.2: Examples of modelled responses. a) These two panels show examples of the response to stimulation from a Winner-Takes-All model (left) and a Winnerless Competition model (right). The bar in the horizontal abscissa indicates stimulus duration and timing. For illustrative purposes, a 0.75:0.25 ratio stimulus was used. In the sub-panels, the rows are the activity for each neuron. The top two sub-panels show projection neuron activity in the two glomeruli, while the bottom sub-panel shows local interneuron activity. The WTA model displays transient activity patterns before settling to a stable spatial pattern around 200 ms after stimulus onset, while the WLC model displays complicated temporal patterns throughout stimulation. b) Trajectories of the projection neuron responses to different input ratios, each with 20 repeats. The first three principal components have been taken to produce 3-dimensional plots (see Appendix A). Solid lines indicate the trajectories during stimulation, while dotted lines indicate return trajectories after stimulation. The crosses are plotted at regular time intervals of 100 ms, and thus indicate the speed of the trajectories and the variability of trajectory speed between trials. The different network behaviours are also apparent in these plots.

4.2.3 Network Behaviours

The LNs in the WTA network compete directly with one another, with symmetrical all-to-all inhibitory connections between them. The factors that break this symmetry are random variability and the stimulus input. The LNs were organised such that for any ratio, there would be some LNs that received greater excitation from afferent input than all others. This allowed these LNs to inhibit their competitors and become dominant. In Figure 4.2a, this WTA competition can be seen in the LN responses. Initially at stimulus onset many LNs were weakly activated, but as time progressed two adjacent LNs became dominant, and the network settles into a stable spatial pattern of activity. This is reflected in the PN responses, with changing spatial patterns in the transient activity immediately after stimulus onset until a stable pattern is established. In contrast, the LNs in the WLC network never settled to a stable spatial pattern, and instead continually changed, driving the PN activity to do the same. This resulted in a sequence of PN activation patterns, and forms the spatiotemporal response.

The transient PN responses can also be seen in the trajectory plots of Figure 4.2b. Principal component analysis was used to reduce the dimensions of the PN responses. A point in these plots represents a spatial response pattern. The WTA model responses have fast onset transients that travel towards stable attractors, near which the system stays until the return transients after stimulation. These uncomplicated transients lead to stable attractors in a repeatable manner, despite the addition of random variability in the firing-rates. The WLC model also displays a fast transient from rest at stimulus onset. These transients either then enter into limit cycles

of repeated temporal patterns, or chaotically never settle. These trajectories are also quite consistent over repeated trials. Even where there appears to be more variability in these paths, in particular for the 0.5:0.5 ratio (green trace), the trajectories largely follow a repeatable path and are localised within a bounded region.

The trajectories also show how the responses differ across input ratios in each network. In both networks, the responses to different ratios are separated. In the WTA model, trajectories never cross for different ratios. In the WLC model, the trajectories are localised in different regions that do not appear to overlap. In the WTA model, the separate stable attractors indicate that the fixed spatial PN response patterns are different for each ratio. For the WLC model, the separated paths indicate that the spatiotemporal patterns are composed completely of different spatial patterns as well. Theoretically, it would not matter if these paths overlapped since the sequence of spatial patterns would also be important. The trajectories also show that responses that are closest together are induced by neighbouring ratios, suggesting that the responses change smoothly with changes in the input ratio.

It is worth noting that the non-trivial temporal behaviours are network phenomena that are not due to any intrinsic neuron properties. Except for the addition of a monotonically increasing sigmoidal transfer function, all neurons are first-order equations. All the simulated neurons have simple intrinsic dynamics, without any oscillatory behaviour. Also, the different behaviours between WTA and WLC models are due entirely to the way that LN inhibitory interconnections are chosen, since everything else is constructed in the same way.

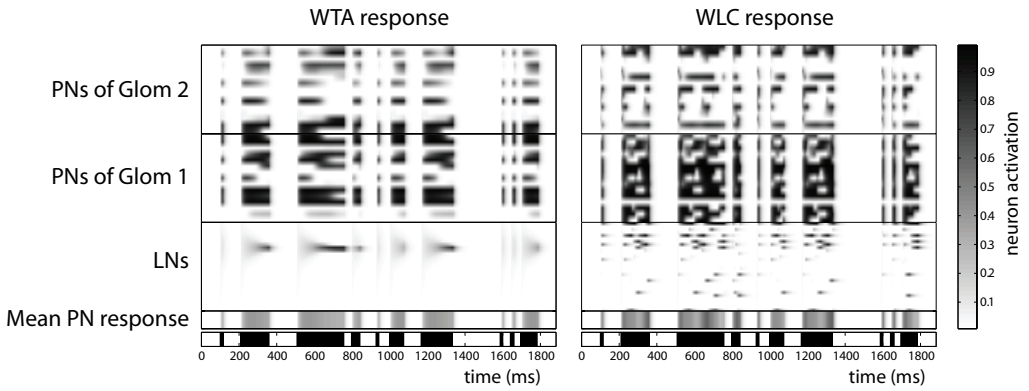

Figure 4.3: Responses to randomly timed pulses. The WTA model (left) and the WLC model (right) were presented with the same randomly timed stimulus. This illustration shows that the models were able to follow the odour pulses very well. At each onset of stimulus, the initial transients appear to start anew. The averaged PN activity shows that both models follow the odour pulses very closely and this averaged activity accurately relays the timing information of the stimulus.

4.3 Conflict between Stimulus Dynamics and Code Dynamics

4.3.1 Spatiotemporal Output

An issue with using time as a coding dimension for odour quality is that this temporally structured code may become confounded with the dynamics of the stimulus. This is especially problematic for animals, such as the moth, that perform chemotaxis in odour plumes where the stimulus dynamics can be very complex and have been shown to be behaviourally relevant (Vickers *et al.*, 2001; Balkovsky & Shraiman, 2002). Both WTA and WLC models can preserve and accurately pass on the stimulus dynamics to down stream neural processes, as illustrated in Figure 4.3. The smallest pulse in Figure 4.3 is around 40 ms, which is realistic for odour plumes (Balkovsky & Shraiman, 2002). However, does this interfere with the encoding of odour

identity, namely the blend ratio, in WTA and WLC models? To assess the spatiotemporal odour code, first I need to define it.

For each test, the spatiotemporal output of the MGC models is taken to be the activity of the projection neurons partitioned into time-bins. The mean activity for each projection neuron was found over each time-bin, $\Delta t = t_j - t_{j-1} = 10$ ms, for each time-step j. This produced a matrix, A_{ij}, composed of a time series of activity for each projection neuron, $i \in$ P:

$$A_{ij} = \frac{1}{\Delta t} \int_{t_{j-1}}^{t_j} a_i(t) dt. \tag{4.2}$$

4.3.2 Correlating PN Responses

The similarity between projection neuron responses at different times was measured using a correlation method. The correlation coefficient between any two vectors $\mathbf{x}$ and $\mathbf{y}$ is taken to be

$$c = \frac{\langle \mathbf{x}, \mathbf{y} \rangle}{\|\mathbf{x}\| \, \|\mathbf{y}\|} \tag{4.3}$$

where $\langle \cdot, \cdot \rangle$ is the scalar product and $\|\cdot\|$ is the euclidean length norm. To assess the evolution of the projection neuron code over time, the spatiotemporal output was broken into a set of vectors, each describing the instantaneous spatial activation pattern of the PNs at the jth time-bin. Then, to calculate the correlation between spatial patterns for two time-bins, say j_1 and j_2, equation 4.3 was applied to the vectors A_{i,j_1} and A_{i,j_2}. This is applied to assess the effect of inter-pulse intervals in Figure 4.4.

The different network behaviours are clearly evident in the cross correlation diagrams of Figure 4.4. The stable spatial patterns of the WTA models

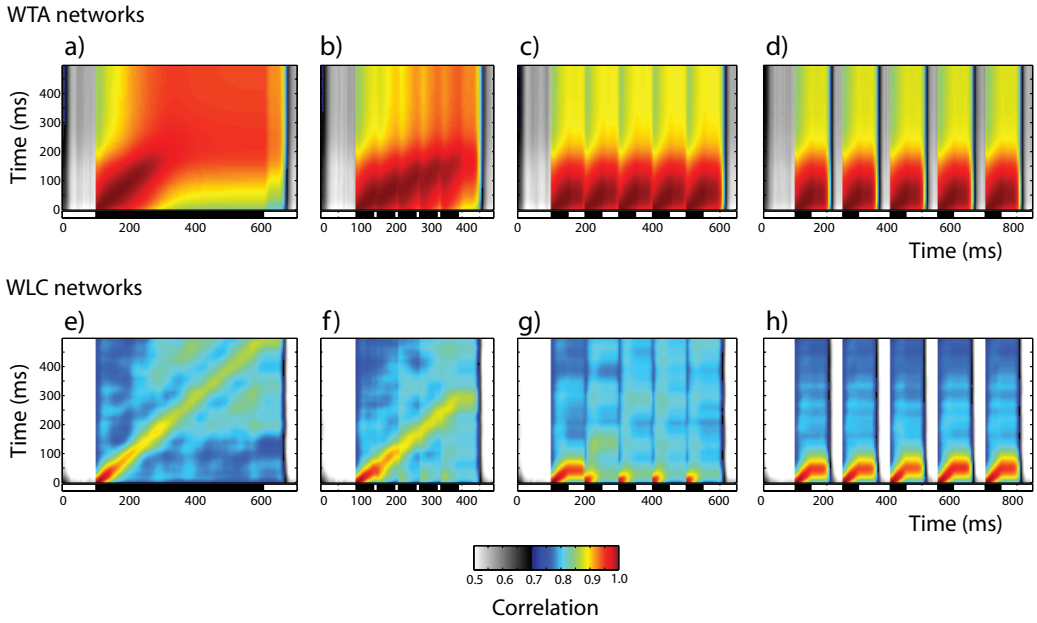

Figure 4.4: Cross correlation and stimulus timing. Time-binning the projection neuron responses results in a series of instantaneous spatial activity patterns. The spatial activity patterns for a 500 ms duration stimulus (vertical axis) were correlated with the spatial patterns from differently timed pulsed stimuli (indicated by bars on horizontal abscissas). This was done for WTA networks (a–d) as well as for WLC networks (e–f). The pulse patterns are: a) one 500 ms pulse and; b) five 50 ms pulses with inter-pulse intervals of 10 ms, c) 50 ms and d) 100 ms. The same patterns were used for WLC (e–f). The correlation coefficients shown are mean values taken from 400 random input ratios and 20 networks. The different network behaviours between WTA and WLC networks result in very different cross correlation maps for the 500 ms pulse results (a and e). WTA networks show high correlation throughout periods of stimulation, indicating that the spatial patterns are very similar across time-bins (a). WLC networks display lower correlations, with highest values in a thin region along the diagonal (e). For both WTA and WLC networks, very short inter-pulse intervals of 10 ms have little affect except to slow the progression of the sequence of spatial patterns (b and f). The pulses with long intervals of 100 ms do not interfere, and each pulse elicits a separate response that is almost identical to each other pulse (d and h). However, for 50 ms intervals, the tail of the previous pulse overlaps with the next response (c and g). This has no apparent effect on WTA models, but WLC models show a marked difference in the shape of pattern of correlation for pulses following the first.

result in high correlation coefficients between all time-steps for the 500 ms single pulse (Figure 4.4a). For the first 200 ms after stimulus onset (during the initial transient period), there is a wide band on the upward diagonal of almost perfect correlation showing that: 1) the responses were highly consistent between two stimulations and, 2) the transients are slow changing. In contrast, the temporally rich behaviour of the WLC models results in relatively low correlation except for a narrow band on the upward diagonal (Figure 4.4e). This narrow diagonal shows that the changes in spatial patterns happen smoothly but quickly, with the width being no greater than 50 ms, the spatial pattern must be switching within this time.

When 10 ms intervals are introduced to break up the single long pulse, in both the WTA and WLC models (Figure 4.4b and f), the systems begin to return to rest at each interval, but these return transients have not enough time to get established. Thus, the progression of responses is temporarily halted at each interval, but then resumes at the onset of the next pulse.

The long inter-pulse intervals of 100 ms (Figure 4.4d and h) allow enough time for these networks to fully reset and start responses afresh, and so each pulse produces the same spatiotemporal response. For WTA models, there is still the block of high correlation for each pulse (Figure 4.4d), and for WLC models, there is the same diagonal for each pulse (Figure 4.4h). For both networks, the correlation pattern during the pulse is the same as the first 50 ms of the 500 ms pulse. In the next 50 ms after each pulse, the correlation pattern does not change from that at stimulus offset. This indicates that the spatial response patterns do not change during the return transients. However, they do reduce in strength until the randomness in the firing-rate destroys them.

In the case of 50 ms inter-pulse intervals, this intermediate time length allows overlap between the return transients after one pulse and the initialising transients of the next pulse (Figure 4.4c and g). With low temporal complexity in the responses of WTA models, these responses again display high correlation for each pulse as for the 100 ms interval pulses (Figure 4.4c). However for WLC networks, 50 ms intervals do not allow a full reset as for longer intervals, nor a continuation of the temporal neural sequence as for shorter intervals (Figure 4.4g). Instead, except for the first 20 ms after stimulus onset the spatial patterns appear to be completely altered. This will have a profound effect on the encoding of identity of odours by the spatiotemporal PN responses, as can be seen next.

4.3.3 Identifying Ratios from PN Responses

In order to investigate how well WTA and WLC models encode blend ratios, an assessment is made of the separability of the spatiotemporal code between ratios and its robustness to noise. This is done by discriminant analysis (Rencher, 2002b), observing how well the input ratio can be identified from the projection neuron responses. Stimuli were created by randomly selecting ratios from a uniform distribution in the interval $[0, 1]$. These were partitioned into five ratio groups $\mathcal{R} = 0,\ 0.25,\ 0.5,\ 0.75,\ 1$ corresponding to 0:1, 0.25:0.75, 0.5:0.5, 0.75:0.25, 1:0 respectively. The randomly selected ratios were categorised according to whichever of the five ratios were the closest.

In the same way as for correlation analyses, the spatiotemporal output was taken to be the time-binned projection neuron responses. Thus, for each

odour presentation, a time series of instantaneous PN activity patterns was used for this analysis. A training set of 100 stimuli gave 100 instantaneous PN responses for each time-step. A 500 ms pulse was used for generating the training set, and the time-steps for this are set on the vertical axis of the plots in Figure 4.5. A data set from 400 stimulations (the time-steps of which are on the horizontal axis) was then classified using discriminant analysis.

To understand this analysis, first consider one time-bin on the vertical axis. This represents the instantaneous spatial activity patterns generated by the training set of stimuli for this time-bin. This was used to classify the instantaneous spatial patterns at each of the time-bins on the horizontal axis, which represents the instantaneous patterns generated by the data set. This will show the times at which the data set is coherent with the training set, and thus allow correct classification. Figure 4.5 shows the success rate for correctly classifying the ratio blend from the instantaneous PN response for all times. This was performed on 20 instantiations of each model type.

As part of the calculations involved in discriminant analysis, the covariance matrix of the variables has to be inverted. As such, linearly dependent dimensions in the training set that are completely redundant caused failures in the calculations. So principal component analysis (PCA) was applied beforehand to retain only the principal dimensions reflecting 90% of variance before classification was attempted.

Figure 4.5 confirms the underlying behaviours of the WTA and WLC models seen in Figure 4.4. Classifying the PN responses of the 500 ms pulse WTA models show a large square region of almost perfect classification from 200 ms to end of stimulus on both axes (Figure 4.5a). This is indicative of

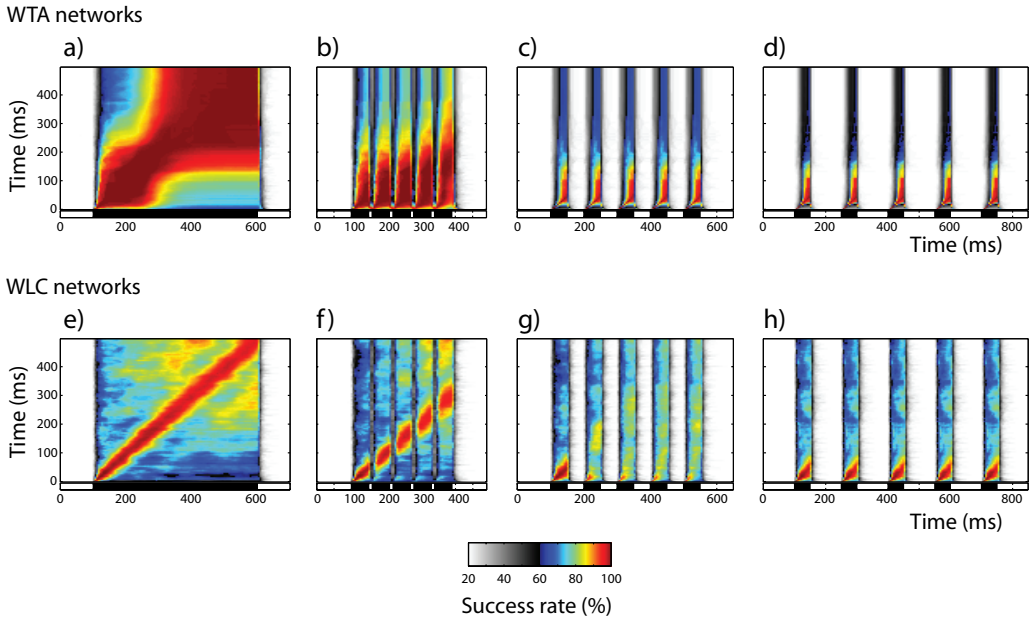

Figure 4.5: Cross classification and stimulus timing. Again, we use the series of instantaneous spatial patterns as in Figure 4.4. WTA and WLC networks were repeatedly stimulated with 500 ms pulses of five different ratios. The subsequent projection neuron spatial patterns for each time-bin was used to train a statistical model. The networks were also stimulated with the differently timed pulses of the same 5 ratios, generating spatial patterns which were then classified by the statistical model, estimating which ratios generated each spatial pattern (see methods). The data shown is of mean success rate for multiple trials and networks. 20% is the chance success rate. The colour scale is the same for all panels. For the single pulse of 500 ms, there is high accuracy along the diagonal for both WTA and WLC networks. WLC networks have a thin region around the diagonal of high accuracy, indicating a smooth transition between spatial patterns, which are constantly switching. WTA networks have a much wider region around the diagonal, indicating slower change of patterns. After 200 ms, there is a block of high accuracy, indicating that the spatial patterns no longer change here.

the constant spatial code generated by the stable attractor that the WTA networks attain after initial transients. The slow changing transients leading to the stable attractor are evident in the wide band of high classification rates along the diagonal immediately after stimulus onset. WLC models show a slim band where the accuracy is greater than 90% (Figure 4.5e). The narrow width indicates the fast switching behaviour of the spatiotemporal PN code. This diagonal is pronounced for the whole stimulus duration in this analysis, showing that temporal code spans the whole stimulation. There are also elevated success rates on two off-centre diagonals during the last half of the stimulation. This is evidence of the WLC models entering limit cycles, repeating spatiotemporal output. However, these regions do not seem well defined since the properties of these limit cycles would be different for each model instantiation and stimulus ratio. These features were also evident in the correlation analysis, but the colour scale of the diagram made it more difficult to see, and also the correlation analysis was more affected by the variability of the neural activity, which would accumulate over time, gradually weakening the correlation.

The effect of short 10 ms intervals can be seen to momentarily halt the progression of the response dynamics, which resume at the next pulse (Figure 4.5b and f). During these intervals the drop in classification rates can be seen clearly. The 100 ms intervals provide enough separation for each pulse to start a completely new response for both WTA and WLC models (Figure 4.5d and h). The most interesting case of the intermediate length 50 ms intervals shows that WTA responses allow classification in each pulse just as if they were presented individually (Figure 4.5c). However, WLC models suffer a

big drop in classification accuracy as the tail of the first pulse is confounded with the spatiotemporal responses of subsequent pulses (Figure 4.5g). This shows that this spatiotemporal encoding scheme cannot reliably convey odour identity for certain dynamical stimuli, when the stimulus dynamics are at a similar time scale, and can interfere with, the intrinsic dynamics of the WLC network.

4.4 Time as an Encoding Dimension

4.4.1 Measure of Ratio Specificity

The advantage of using time as an extra encoding dimension is that, theoretically, it can greatly increase the potential encoding space available. No longer is the information confined to just a static spatial activity pattern, but can entail a sequence of spatial patterns, multiplying the possible representations with each time step. Here, I compare the spatiotemporal PN codes for the WTA and WLC models to investigate if the more temporally complex output of WLC models utilises this advantage.

In this section, analyses are performed on the spatiotemporal code including time, not just instantaneous 'snapshots' as before. Here, the response to stimulation is taken to be a vector produced by all the elements of the matrix A_{ij} (as defined by equation 4.2), giving

$$(A_{11}, A_{12}, ..., A_{1m}, A_{21}, ..., A_{nm})$$

if A_{ij} is an $n \times m$ matrix. This makes a vector space with a dimension for each time-step for each PN.

When the response to one input ratio is correlated with other ratios, the closest ratios have highly correlating neuron responses while very different ratios have low correlating responses. This creates a bell-shaped curve (Figure 4.6a). Using the mathematics for calculating standard deviation as inspiration, one can calculate a measure for the width of this bell-shaped curve, and thus the specificity of the projection neuron code. Let the input ratio be denoted by the proportion of the input composed of type 1 receptor input, $\mathcal{R} = r_1/(r_1 + r_2)$, then the curve width, $\sigma_{\mathcal{R}_\mu}$, for a particular ratio, $\mathcal{R}_\mu$, is defined to be

$$\sigma^2_{\mathcal{R}_\mu} = \int_p^q (\mathcal{R} - \mathcal{R}_\mu)^2 \, c(\mathcal{R}_\mu, \mathcal{R}) \, d\mathcal{R} \tag{4.4}$$

where $p = \mathcal{R}_\mu$ and $q = \mathcal{R}_\mu + 0.5$ for $0 < \mathcal{R}_\mu \leq 0.5$, and $p = \mathcal{R}_\mu - 0.5$ and $q = \mathcal{R}_\mu$ for $0.5 < \mathcal{R}_\mu \leq 1$. p and q are defined to ensure that the integral is always over an interval of the same length, even if $\mathcal{R}_\mu$ is near 0 or 1. $c(\mathcal{R}_\mu, \mathcal{R})$ is the correlation coefficient for the spatiotemporal responses to the two ratios. The average width for a network was taken to be the mean width over ratios.

This bell-curve width is indicative of the specificity of the PN output to ratios. Since the correlation between the spatiotemporal output to different stimuli gives a measure for the similarity of these outputs, a narrow bell-curve with very steep sides would be produced by a spatiotemporal code that changes greatly across ratios. The sharper the bell-curve, the better the differentiation can be of the input ratios from the spatiotemporal output.

This measure for ratio specificity was used to assess the importance of time to WTA and WLC models. The time-length from stimulus onset of the spatiotemporal PN responses was changed, and the analyses were carried out

for each time-length. In this way, I tested the effect of the time-length of the code on the ability of PN responses to encode ratios.

The temporal simplicity of the PN responses from WTA models means that the ratio specificity is not enhanced by taking longer time-lengths of PN responses. The fixed spatial response patterns do not allow any more information to be conveyed once the steady state has been reached. Therefore for WTA models, one would not expect that ratio specificity is dependent on code length once the stable attractor has been reached, and this is indeed the case (Figure 4.6b). Interestingly, specificity is not dependent on code length even during the transient phase before a stable spatial pattern is fully established, as depicted in Figure 4.6b by a horizontal plot for code lengths of over 50 ms.

In contrast, WLC models have improved ratio specificity as time allowed for encoding is increased. The largest drop in bell-curve width is within the first 100 ms, after which the change is more shallow, though it is still falling at 500 ms (Figure 4.6b). This drop in bell-curve width corresponding to an increase in ratio specificity of the PN code demonstrates that the spatiotemporal activity of PN responses in WLC models does indeed utilise time as a coding dimension. Furthermore, although the WLC models have slightly larger widths than WTA models for very short response lengths, the situation is quickly reversed within the first 25 ms. This suggests that a spatiotemporal code can and does carry more information than spatial-only code, allowing a more precise determination of the input ratio.

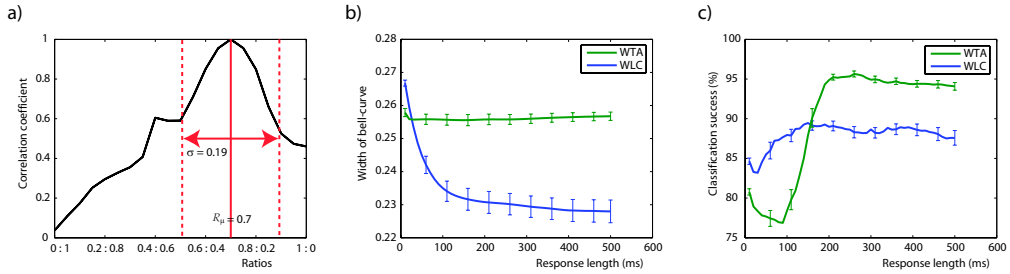

Figure 4.6: Ratio specificity, output reliability and code length. a) An example illustrating the bell-shaped correlation curve. Correlating the projection neuron response for a particular ratio, $\mathcal{R}_\mu$, against all other ratios gives this bell-shaped curve, which peaks at $\mathcal{R}_\mu$ with a correlation coefficient of value 1. The more specific the projection neuron response to a ratio, the sharper and thinner the bell-shaped curve. Thus, the width of the bell-curve, σ, marked by the dotted lines (see text for definition) indicates the specificity of the projection neuron response. b) The effect of response length on code specificity. This shows the specificity of the spatiotemporal projection neuron responses as the response length taken into account is changed, indicating how the ability of the models to encode ratios is dependent on the temporal dynamics. For WTA networks, the curve widths are not affected by the response length over 50 ms, before which there is a slight initial drop. This is expected of a spatial code where time is not an encoding dimension. Increasing time length does not add more information once the system starts settling into a spatial pattern. For WLC networks, there is a sharp drop in widths up to 100 ms, and thereafter a gradual decline. This shows that the ratio specificity of the spatiotemporal code increases as time length of the code is increased, with specificity rising mostly in the first 100 ms. For response lengths longer than 25 ms, the bell-curve widths for WLC models are less than for WTA models, meaning that spatiotemporal output of WLC models is more ratio specific. The error bars show standard error. c) The effect of response length on reliability. Discriminant analysis was used to predict the input ratios from projection neuron responses according a training set of responses (see text). The accuracy of this classification indicates the reliability of the projection neuron responses for the identification of input ratios. This test was applied to different response lengths as in b). The accuracy of both types of networks plateaus after 200 ms, with WTA networks at around 95% and WLC networks at around 88%. Before 200 ms, WTA networks start with lower accuracy but quickly increase and exceed that of WLC networks, which have a more uniform accuracy level throughout. Again, error bars are of standard error.

4.4.2 Response Length and Reliability

The final analysis was to take the idea of the spatiotemporal code over limited time-lengths as above in section 4.4.1, and apply it to the training and data set responses from section 4.3.3 and perform the discriminant analysis on this spatiotemporal output, not the instantaneous spatial patterns (Figure 4.6c). Surprisingly, the WTA models display a strong time dependence for classification accuracy, while the WLC models show much less.

Classification accuracy is dependent on the consistency of the PN responses as well as separability between responses to different input ratios. The PN output of WLC models have increasing separability for the first 100 ms since the ratio specificity increases (Figure 4.6b). However, this is only partly reflected in the classification accuracy. Accuracy only slightly increases before levelling out at around 88%. WTA models start with relatively low accuracy, but between 100 ms and 200 ms accuracy increases sharply, after which accuracy stays at around 95%. This coincides with the time that stable spatial patterns are established. This indicates that the stable spatial patterns of WTA models must be highly reliable. Importantly, they are more reliable than the spatiotemporal responses of WLC networks at 200 ms and above. However, WLC models are better during the early transient phase.

4.5 Discussion

The obvious advantage of a spatiotemporal code over a spatial code is the increase in potential information carrying capacity, with no additional neural components needed (ignoring what may be needed in downstream decoding

neurons). However, it is not as yet known how the AL interneurons in moths use time to augment the odour code from the PNs, if at all.

In locust physiology, the spatiotemporal code may take the form of precise spike timing against a background oscillation (Laurent *et al.*, 2001), as has previously been analysed in a model of the locust AL (Bazhenov, Stopfer, Rabinovich, Huerta, *et al.*, 2001; Bazhenov, Stopfer, Rabinovich, Abarbanel, *et al.*, 2001). Activity oscillations of the AL as a whole indicate a general synchronisation of spiking activity. Each oscillatory cycle creates a time epoch. Within these regular time epochs the timing of a PN spike can be taken as a phase variable relative to the cycle at which the spike occurred. During stimulation, PN spikes would transiently synchronise at certain epochs, and from this it is possible to discriminate input odour identity from the spatiotemporal PN output (Bazhenov, Stopfer, Rabinovich, Huerta, *et al.*, 2001). On a slower timescale, it was also possible to discern odour identity from observing the epochs in which PN spikes occurred (Bazhenov, Stopfer, Rabinovich, Abarbanel, *et al.*, 2001), which demonstrated another possible spatiotemporal mechanism.

However, locust and moth have notable differences in morphology and physiology. For instance, locust local interneurons are non-spiking, and interact by graded potentials and oscillatory membrane potentials (MacLeod & Laurent, 1996; Laurent & Davidowitz, 1994). Morphologically, the locust AL consists of many more glomeruli that are smaller than for most other insect species (Anton & Homberg, 1999). Importantly, glomeruli of locust AL receive overlapping receptor input from multiglomerular receptor neurons (Hansson, 1999). Thus, the functional distinction between glomeruli

and the chemotypic structure is not clear, as it is for other insect species. Perhaps it is for these reasons that the glomerular structures did not feature in these locust AL models (Bazhenov, Stopfer, Rabinovich, Huerta, *et al.*, 2001; Bazhenov, Stopfer, Rabinovich, Abarbanel, *et al.*, 2001).

In moth physiology, it is unclear what role spike synchronisation plays. It is possible that different coding strategies have been adopted by moths since odour stimuli for the moth are naturally found as odour plumes, and as such are themselves highly dynamic (Vickers *et al.*, 2001; Balkovsky & Shraiman, 2002). Studies have shown that precise synchronisation of PN spikes may be dependent on the temporal dynamics of the odour stimulus rather than the odour identity (Christensen *et al.*, 2000; Christensen, Lei, & Hildebrand, 2003; Christensen, 2005). This would mean that such spike timing properties cannot be used for encoding of odour quality. Hence, it is not clear what mechanisms the AL of moths use to encode olfactory information. Indeed, it is not clear whether the moth uses time as a coding dimension at all.

In the models I created in this chapter, many details of MGC morphology and physiology were included. Most importantly, these models included glomerular structure, which determined the afferent input to the two classes of AL interneuron, PNs and LNs, and their interconnections, according to what has been observed experimentally in the MGC of moths. Although it is known that LN dendritic arborization is multiglomerular, more precise connectivity is not known, and this modelling effort tests two possible connection schemes and their respective consequent encoding schemes. Namely, the two connection schemes are those of WTA networks with symmetrical inhibition and a predominantly spatial code, and WLC networks with asymmetrical inhibition and a spatiotemporal code (Figures 4.4 and 4.5).

The theoretical framework of WLC has been proposed as a suitable principle by which an AL model can be created with a spatiotemporal output (Laurent *et al.*, 2001; Afraimovich *et al.*, 2004; Rabinovich *et al.*, 2000, 2001). Rabinovich *et al.* (2000,2001) created an AL model based on WLC networks involving nine interneurons with FitzHugh-Nagumo spiking dynamics, but are limited with little biological detail. An upper limit of the information carrying capacity was calculated for WLC networks, and it was shown by applying mutual information measures that several switches in interneuron response patterns were necessary to successfully relay odour identity. Notably, despite the few biological details, the output of these models resembled PN responses from real biological systems.

Without using any special intrinsic neuron properties, so that as few as possible assumptions are made, WTA and WLC models in this chapter generated spatiotemporal outputs that were purely network phenomena depending only on connectivity. Except for LN interconnections, WTA and WLC networks were statistically identical, and so could be compared. Despite, their similarity, WTA and WLC networks behave very differently to generate a spatial code and a spatiotemporal code respectively. Interestingly, the WTA models exhibit very similar dynamics to glomerular dynamics (Galan, Sachse, Galizia, & Herz, 2004). The odour-specific trajectories in Figure 4.2 appear to follow similarly shaped paths to trajectories of glomerular activity observed in the honeybee. Although glomerular activity is at a different functional level, being the combined activity of many neurons, it is not mathematically far removed from these neuron models. Thus, this indicates that the total strength of inhibition between glomeruli should be symmetrical.

Returning to the PN spatiotemporal output of the WTA and WLC models at a neuronal scale, the output from the WTA models resembled real PN activity during the transient phase with continually switching behaviour, but the stable phase with unchanging spatial patterns is not realistic. In this sense, WLC inhibition performs better than WTA, and suggests that WLC networks were closer to the actual inhibitory connectivity between LNs. The fact that real PNs do indeed display a mixture of excitation and inhibition during an odour stimulation suggests that there is a temporal aspect to the odour code, at least at this level. Further evidence for WLC networks is the resemblance of the progression of the PN responses over time shown in Figures 4.4 and 4.5 with that seen in a similar treatment of intracellular recordings from AL interneurons of locust (S. L. Brown, Joseph, & Stopfer, 2005). However, WTA connectivity still cannot be ruled out since there may be other mechanisms in the biological AL, such as adaptation or slower timescale neurotransmitters, that could interact and prevent the stable phase. This may be what creates the spatiotemporal PN responses.

One problem with using time as a coding dimension is that a temporally structured odour code may become convolved with the temporal structure of the stimulus. This is particularly a problem for moth olfactory coding since odours in a plume have temporally rich dynamics, and furthermore, this temporal structure may be significant to the moth for chemotaxis (Vickers *et al.*, 2001; Balkovsky & Shraiman, 2002). Figure 4.3 shows that the dynamics of the stimulus is relayed for both WTA and WLC models. This is achieved, in both cases, by the overall activation levels on the glomeruli so that the individual PNs responses can change during stimulation without losing the

stimulus dynamics. This allows individual PNs the flexibility for a temporally structured code for more than just the stimulus dynamics. However, Figure 4.5 shows that WLC models can confound temporal code for odour identity with stimulus dynamics in certain cases, whereas the spatial code of WTA models is unaffected. This breakdown of the WLC system occurs for inter-pulse intervals of 50 ms which is a quite typical value found in odour plumes (Balkovsky & Shraiman, 2002). Relative to the intrinsic dynamics of the WLC models, 50 ms is almost enough time for the systems to return to rest. Thus, the dynamics of the stimulus and the intrinsic dynamics are closely matched in this case. In spite of this, the WLC models deal well with other inter-stimulus intervals, and so the real MGC may be able to deal with this by having neurons with a range of different time constants. The models here all have identical time constants, which would not allow a triphasic (inhibition-excitation-inhibition) response pattern observed in *M. sexta* MGC-PNs (Heinbockel, Christensen, & Hildebrand, 1999), except as a random network behaviour. Having a triphasic response pattern would also help separate the pulse responses by resetting the responses before coding of the next odour pulse, preventing interference.

The use of time by the WLC models to encode odour identity can be seen in Figure 4.6b. Here, the advantage of having a temporal aspect for coding becomes apparent, with the increase in ratio specificity over WTA spatial codes. It seems that WTA models provide a more consistent representation once stable spatial patterns are established (Figure 4.6c), but surprisingly, WLC spatiotemporal codes are more reliable when there is less time available. This is because the WTA models only have higher consistency when the stable spatial pattern is established.

In summary, I have created two MGC models to compare and contrast spatial encoding against spatiotemporal encoding. These were created by using two different principles for connecting competitive networks of inhibitory LNs: symmetrical connectivity for WTA networks, asymmetrical for WLC networks. These networks were able to drive the dynamics of the PN responses to have either low temporal complexity (WTA) or rich temporal structure (WLC). These models were tested on their ability to encode ratio information. The spatiotemporal output of WLC models better resembled genuine MGC-PN responses, and therefore present a more realistic organisation of the MGC connections. I demonstrate the advantage of this spatiotemporal code over the spatial code in holding more information by its improved specificity between ratios. The spatiotemporal code also has an advantage in terms of identifying the ratio for brief timeframes from stimulus onset, beating the slow dynamics of the WTA models. The disadvantage for spatiotemporal codes in the confounding of consecutive odour pulses is also demonstrated for WLC models, but this may not be a problem in the real MGC system. These reasons may provide some explanation for the apparent use of a similar spatiotemporal code in the MGC.

Chapter 5

Blend Encoding in the General Antennal Lobe

5.1 Introduction

Evidence from studies in olfactory perception shows that, in certain cases, an odour blend can be perceptually distinct from the component odours of which the blend is comprised. Psychophysical studies in humans demonstrate that perceptually, odour mixtures can take on configural or synthetic properties, where qualities perceived in the mixture are very different from the constituent odour components (Laing *et al.*, 1989; Laing, Panhuber, Willcox, & Pittman, 1984). Invertebrates, too, have a configural perception of odour blends. For instance, behavioural studies show that honeybees can be taught by classical conditioning to recognise and distinguish between binary blends (Chandra & Smith, 1998), even when those blends are created such that each component is equally rewarded and punished across different blends. Thus, in this scenario, component information is ineffectual and what is important is configural information of blends taken as a whole.

The degree to which odour mixtures have configural properties is thought to be dependent on the similarity between the odour components, and there-

fore, the overlap in the neural representation of these odours. Similar odours use overlapping information channels, and such odours may elicit interactions between their neural representations as mixture components. This has been confirmed, for example, in behavioural experiments in rats (Kay *et al.*, 2003), where animals were trained to recognise binary odour mixtures. These animals did not also recognise the components of the mixtures when the mixtures were created from similar odours, whereas for non-similar odours the opposite was true, with animals recognising one or both components. The significance of odour similarity for synthetic mixture perception has also been shown with olfactory blocking experiments on honeybee where, during associative learning for an odour mixture with an unconditioned sucrose reward, the association of one odour component with the reward is 'blocked' by a prior association with the other component that was already learned (Hosler & Smith, 2000).

However, such high-level behavioural studies cannot explain the neural mechanisms responsible for configural blend perception. For this, one must look at data from neurons along the olfactory pathway. The configural encoding paradigm implies non-trivial interactions between neural representations of odours along the olfactory pathway, as opposed to the competing elemental paradigm, which implies few interactions other than simple summation. This is because an elemental olfactory code encapsulates blend information such that information of the components can be easily deconvolved, whereas a configural code generates a representation of the blend which is completely different from that of the components. As such, highly nonlinear interactions that convolve component information along the olfactory pathway could explain configural mixture perception.

In Chapter 3, I discussed how other studies have shown nonlinear interactions beginning at the receptor neurons, with suppression and, to a lesser extent, synergy occurring at the very first step of olfactory coding. However, in Chapter 3, no cases of synergy or suppression were found. This contradiction with other studies was likely to be due to the unnaturally high odour concentrations used in those studies. Nonetheless, when the odour information reaches the PN responses, the output stage of the antennal lobe, some nonlinear mixture interactions have occurred. Pheromone blend specific PNs in the MGC of moths, so-called specialists (Christensen, 2005; Anton & Hansson, 1995; Christensen & Hildebrand, 1987), are an example of a nonlinear response that can give rise to a synthetic sense of the blend, albeit in a very specialised system. More generally, second-order neurons have commonly been found to exhibit synergy and suppression in response to mixtures of general odours, in invertebrates (Christensen *et al.*, 1991; De Jong & Visser, 1988) and vertebrates (Tabor *et al.*, 2004). Given that, as described in Chapter 3, receptors reliably transfer odour information to the antennal lobe without strong nonlinearities, some nonlinear synthesis must originate from within the AL glomeruli. The AL certainly has the potential for such synthesis, with interactions in the neural representation mediated by inter-glomerular inhibition from multiglomerular LNs.

It is possible that the aforementioned blocking effect could arise purely from AL neural interactions, as demonstrated by a model of honeybee AL (Linster & Smith, 1997). In terms of the neural representation of odours, a blocking effect was reproduced by changing the modulatory influence of a centrifugal interneuron on PN activity. This centrifugal interneuron introduced into the AL information of the 'sucrose reward', which was used to

train the system with a Hebbian learning process (Dayan & Abbott, 2001). The blocking effect was reproduced by altering the synthetic representation of the mixture to become more similar to the representation of a pre-trained component. This illustrated a non-trivial summation of component responses that can occur in the AL.

In this chapter, I extend the spatiotemporal MGC model from Chapter 4 into a general odour system. The same WLC framework of competitive LNs is used to induce underlying temporal dynamics of the neural system. This WLC temporal attribute drives the spatiotemporal odour code of the PNs. In the general model more glomeruli are added, corresponding to more receptor types. However, instead of responding exclusively to particular pheromone compounds, these receptor types have broader receptive fields, as inspired by the biological evidence (Galizia *et al.*, 2000; Carlsson *et al.*, 2002; Sadek, Hansson, Rospars, & Anton, 2002; Sachse *et al.*, 1999; Galizia & Menzel, 2001). Thus, odour stimuli induce combinatorial glomerular activation patterns with which to represent different odours. Accordingly, stimuli are created that provide excitation to a distributed pattern of glomeruli. I investigate the encoding of these odours by this spatiotemporal code of WLC networks. In particular I verify whether the spatiotemporal code in this general odour model causes configural effects when changing the stimulus concentration. Moreover, I investigate whether the spatiotemporal code generates configural coding for blends, and how it might be affected by the similarity of the odour components and overlapping glomerular activation.

5.2 Construction of General Odour Model

5.2.1 Hexagonal Network Architecture

As an extension of the MGC model, this general odour model has neuronal dynamics that are governed by the same differential equation as the MGC model in Chapter 4 (equation 4.1 on page 92). However, for ease of the analyses the Guassian variability was not added at each time-step of simulations. This is since adding variability would then require taking some average path of trajectories from repetitions, which may not be appropriate since this average may not actually be attainable. Without the variability, the model still produces the same dynamics as seen in Chapter 4, and so is still biologically realistic. Another advantage of omitting the variability is that any synthetic blend responses that may be found will certainly not be due to random flukes.

There are also many differences in the network architecture. Instead of just two glomeruli aggregating information for two pheromone components, this model employs twelve glomeruli. In the AL, general odour glomeruli, like MGC glomeruli, each receive input from one receptor type (Vosshall *et al.*, 2000; Fishilevich & Vosshall, 2005; Couto *et al.*, 2005). However, unlike pheromone specific receptors, the general odour receptor neurons are broadly tuned, and each receptor type is receptive to a range of compounds (Galizia *et al.*, 2000; Carlsson *et al.*, 2002; Sadek *et al.*, 2002; Sachse *et al.*, 1999; Galizia & Menzel, 2001). The receptive ranges also overlap between receptor types, and so each odour activates a combination of glomeruli, giving rise to spatial patterns of activation at the glomerular level.

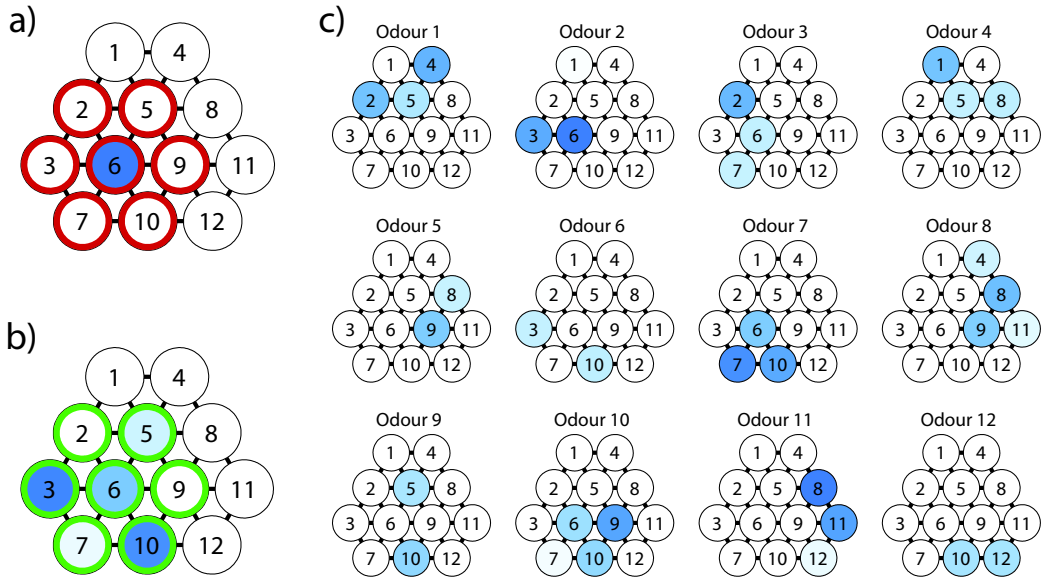

Figure 5.1: Hexagonal glomerular organisation. a) LN inhibitory connectivity. Twelve glomeruli are arranged with a hexagonal layout, with circles indicating glomeruli and black lines between neighbouring glomeruli. LNs receive synaptic input within one glomerulus, from ORNs and interneurons that innervate that particular glomerulus. LNs can form inhibitory connections to other interneurons that receive synaptic input from within the same glomerulus, and also interneurons from the surrounding glomeruli. This schematic indicates the innervation pattern of one LN. For the LN in the diagram, the input glomerulus is indicated by the blue-filled circle, number 6, and the output glomeruli are indicated by red-outlined circles. b) Glomerular activation by an odour. The green-outlined glomeruli indicate those which have overlapping receptive field with number 6 glomerulus, creating a hexagon of potential activation of glomeruli. However, not all glomeruli are excited by this odour, and those which are excited receive varying degrees of excitation from the ORNs. The degree of excitation is indicated by the intensity of the blue colour fill. c) Twelve odours centred at each glomerulus in turn. For glomeruli on the edge of the hexagonal arrays, only neighbouring glomeruli within the array can receive excitation. These odours are used to create binary blends used in the analysis.

For convenience, the glomeruli in the model are spatially organised into a hexagonal arrangement such that adjacent glomeruli have overlapping receptive fields (Figure 5.1). In ALs, glomeruli are not necessarily morphologically organised like this. Inter-glomerular inhibition that is proportional to the overlap in receptive fields, rather than morphological proximity, produces glomerular activity that most closely resembles observed AL activity (Linster *et al.*, 2005). By arranging the glomeruli in the fashion shown in Figure 5.1, the spatial proximity reflects the functional overlap. Therefore, to produce functionally organised inhibition in this general odour model, LNs each receive input from within one glomerulus and provide inhibition to the local hexagonal region, including that glomerulus and all neighbouring glomeruli (Figure 5.1a). In the glomeruli for which a LN provides inhibition, that LN will have a 0.25 probability of forming an inhibitory connection to each LN receiving input in any of those glomeruli. The LNs also have a 0.25 probability of connecting to each PN receiving input in those glomeruli.

5.2.2 Odour Stimuli

As mentioned above, each receptor type should be broadly tuned to be receptive to a range of odour molecules. Therefore, each odour molecule should activate a collection of glomeruli. In the functional scheme for glomeruli in this model, this translates to each odour activating a local combination of glomeruli within a hexagonal neighbourhood (Figure 5.1b). Each odour was designed to activate on average three glomeruli. This corresponded with what was observed in the data from Chapter 3. These 2–4 glomeruli were chosen from seven that together formed a hexagon, since this reflects a set

of glomeruli with overlapping odour receptivity (Figure 5.1b). Hexagons were permitted to overhang from the twelve glomeruli, in which case the 2–4 glomeruli were chosen from the glomeruli that intersected the hexagon. These chosen glomeruli were then activated to varying degrees, to complete the spatial activation pattern. In this way twelve odour stimuli were created from hexagonal neighbourhoods centred on each of the twelve glomeruli, each activating a different combination of glomeruli (Figure 5.1c). These odour stimuli can each be represented by the vector $\mathbf{r}^j = (r_1^j, r_2^j, ..., r_{12}^j)$ where r_i^j is the input to the ith glomerulus for Odour j. Finally, these twelve odours are taken to be presented at the same concentration here, which becomes important for defining concentration curves later.

5.2.3 Uniglomerular and Multiglomerular PNs

The PN connectivity in the general odour model is the same as in the MGC model. In the MGC, PNs are thought to be all uniglomerular, but in the general odour system, there are multiglomerular PNs as well as uniglomerular (Homberg *et al.*, 1989). The PNs in the general odour model have been left as uniglomerular during simulations. Then to assess the effect of multiglomerular PN connections, PNs were randomly grouped together, and the responses were summed for each group. The responses were then limited between 0 and 1 by a sigmoid function. In this way, multiglomerular PNs were created from the uniglomerular PNs. These multiglomerular PNs integrated their responses from different glomeruli before each PN generated a single output.

Throughout this chapter, the spatiotemporal PN response output of the general odour model was taken to be the concatenation of time-binned PN responses, the same as defined in section 4.4.1 (page 108). The spatiotemporal

PN response output was defined to be the vector

$$(A_{11}, A_{12}, ..., A_{1m}, A_{21}, ..., A_{nm})$$

with elements taken from the matrix of time-binned PN responses A_{ij} with projection neurons $i = 1, ..., n$ and time-bins $j = 1, ..., m$. In this way, the response for every PN and every time-step to a stimulus presentation is encapsulated in a single vector.

Using the correlation calculation in equation 4.3 (page 101), the first analysis performed is to verify that similar odours produce similar PN responses. The similarity between responses was taken to be the correlation between spatiotemporal output vectors. The similarity between odours, j and k, was taken to be the correlation between the stimulus vectors $\mathbf{r}^j$ and $\mathbf{r}^k$. Figure 5.2 plots the odour similarity against response similarity for many pairs of random odours, and shows that these are closely linked. The responses were those of one network instantiation of the general odour model. For uniglomerular PNs, only similar odours produce similar responses, and the degree of correlation between odours determines very well the correlation of the responses. This is indicated by all the points lying close to the diagonal.

The effect of integrating PN responses into multiglomerular responses can also be seen in Figure 5.2. For multiglomerular PNs, there is still a close relationship between odour similarity and responses similarity. However, the more glomeruli each PN innervates, the more similar the PN responses become between odours. This is an interesting result since it would seem to lessen the information capacity of the spatiotemporal code, and yet multiglomerular PNs are found in invertebrate ALs in addition to

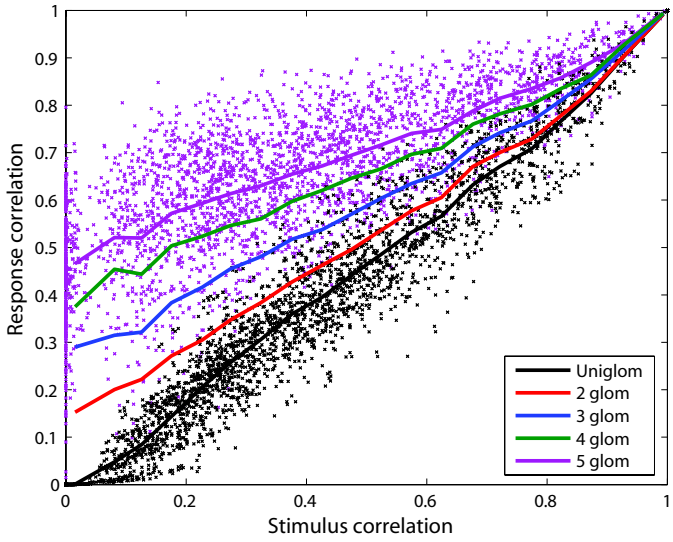

Figure 5.2: Odour similarity and response similarity. There is a strong relationship between odour similarity and the similarity of the responses that those odours elicit. For uniglomerular PNs (black) all the points lie close to the diagonal, showing that stimulus correlation roughly equates to response correlation. This systematic response does not preclude a configural effect, but indicates that if a configural effect is present here, there is continuity in the mapping from stimulus to response. The averaged response correlation for multiglomerular PN responses were also plotted for comparison. As PNs arborise into more glomeruli, the responses become more similar across all odours. For clarity, only the points for responses from PNs innervating 5 glomeruli (purple) have been plotted.

uniglomerular PNs. This may indicate that multiglomerular PNs are using an entirely different encoding scheme, which this model may not be able to capture.

In the remainder of this chapter, I will investigate the spatiotemporal code further. Since the effect of having multiglomerular PNs is just to increase the similarity between responses for all odours, the analyses continue with uniglomerular PNs only. This enables the investigation into the configural effects due to the spatiotemporal code, without the confounding effects of multiglomerular PNs.

5.3 Changing Concentration

5.3.1 Sigmoidal Concentration Curves

Before assessing odour blend responses, first the way stimulus concentration alters the input to the glomeruli must be defined. This is important in order to enable summing together odours to create blends. Also, it is important to verify that changing concentration does not itself cause configural effects on the responses.

The data in Chapter 3 was of the cumulative presynaptic ORN activity in each glomerulus. As such, it reflected the magnitude of input entering the glomeruli. These data confirmed that concentration response curves for each glomerulus, at this stage, is sigmoidal for a logarithmic concentration scale, as has been observed in another study (Carlsson & Hansson, 2003). That is, if a glomerulus responds at all to an odour, there is no glomerular activity until a response threshold concentration is reached, then there is a linear response for a concentration range, before a plateau is reached for a certain

concentration after which the response increases no more since the response has reached saturation. The data in Chapter 3 show that over 5 dyadic logarithmic steps of stimulus concentration, some sigmoidal response curves were within their linear range. This informs the model of the steepness of the sigmoid, that the range of glomerular activation can happen when doubling the concentration 5 times.

For the model, sigmoidal concentration curves in the glomerular input were approximated by piecing together three straight lines: a zero response line up to response threshold, a linear response increase, and a horizontal line from plateau threshold (Figure 5.3a). For each odour, a response threshold and a plateau threshold were chosen randomly, relative to the implicit concentration of the odours depicted in Figure 5.1c. The condition for the response threshold concentration was that it was between 5 and 2 dyadic steps below the concentration, and the plateau threshold was between 2 and 5 dyadic steps above. In combination with the activation level for a glomerulus by an odour, these determine the slope of the linear portion and the maximum response of the sigmoid. This sigmoid was chosen since it is easier to combine such sigmoids to generate blend activation levels, since there is as yet no generally accepted method to sum sigmoids in olfactory responses.

In order to attain the activation of one glomerulus for a blend of two odours, it is not enough to simply sum the glomerulus activation levels for the two odours because the upward slope of the sigmoid is linear only with logarithmic concentration steps. For instance, doubling the concentration would not double the glomerulus activation, but only increase the activation by the equivalent for one dyadic step.

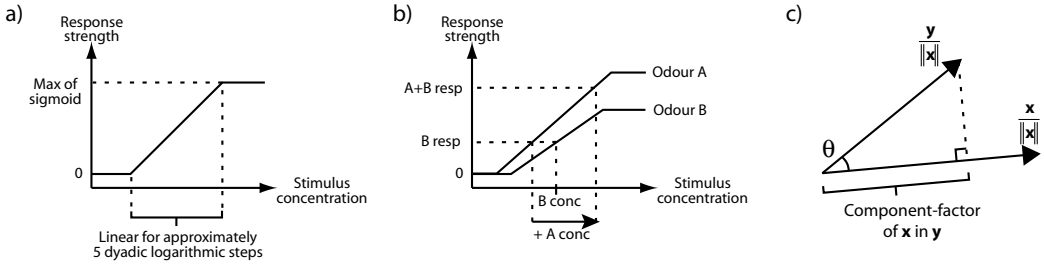

Figure 5.3: Sigmoidal response curve and component-factor definitions. a) The sigmoidal concentration curves are approximated by three lines. The activation level is zero for low concentrations, and a constant plateau for saturation concentrations. Between these extremes, for around 5 dyadic steps, there is a linearly increasing response curve. b) Calculating the glomerulus activation for a blend. For two odours A and B, first take the glomerular activation for the odour with the least plateau response (B in this case). Find the concentration for A that gives the same glomerular activation, and add this to the concentration of A in the blend. The blend activation of the glomerulus is taken to be equivalent to the activation by Odour A at this concentration total. Generally, the specific definition does not greatly affect the resultant responses as long as the activation levels are generally additive, as was seen in Chapter 3. c) Geometric illustration of the component-factor. Vectors $\mathbf{x}$ and $\mathbf{y}$ are normalised by $\|\mathbf{x}\|$, then the component-factor is the $\hat{\mathbf{x}}$ component in $\mathbf{y}$.

For the glomerular activation by the blend of two odours, the sigmoidal response curve of the odour with the highest response plateau is used (Odour A in Figure 5.3b). The equivalent concentration that produces the same activation as the other odour (Odour B, Figure 5.3b) is added to the concentration of the first odour (A). Then the blend activation is taken to be that of the first odour (A) at this total concentration.

5.3.2 Component-Factor

Now I define a measure for how much one vector is composed of another vector. This will be useful for determining how one response (for instance, to a component odour) may be preserved and used in the construction of other responses (the blend responses). For two vectors $\mathbf{x}$ and $\mathbf{y}$, I define the component-factor of $\mathbf{x}$ in $\mathbf{y}$ to be,

$$\frac{\langle \mathbf{x}, \mathbf{y} \rangle}{\|\mathbf{x}\|^2} = \frac{\|\mathbf{y}\|}{\|\mathbf{x}\|} \cos\theta \tag{5.1}$$

where θ is the angle between the vectors, $\langle \cdot, \cdot \rangle$ is the scalar product and $\|\cdot\|$ is the euclidean length norm. It is closely related to the correlation measure defined by equation 4.3. Geometrically, it is the same as normalising $\mathbf{x}$ and $\mathbf{y}$ by the length of $\mathbf{x}$, then finding the orthogonal projection of $\frac{\mathbf{y}}{\|\mathbf{x}\|}$ onto $\frac{\mathbf{x}}{\|\mathbf{x}\|}$ (Figure 5.3c). The length of this projection is the component-factor.

There are two ways to interpret what the component-factor signifies. The first is that it is a scalar for how much of $\mathbf{x}$ can be found as a component in $\mathbf{y}$. The second is that it is the proportion of $\mathbf{x}$ that is comprised of $\mathbf{y}$. In both interpretations, the scalar is relative to the length of $\mathbf{x}$. The component-factor is useful because it indicates how much of a response can

be found to be 'within' another response, or how much a response is 'made up' of another response. This can be used to indicate whether any interactions occur between blend components. For instance, if two odour responses were completely independently encoded (giving perpendicular spatiotemporal response vectors) such that the response to their blend is the linear sum of the odour responses, then the component factor for the odour response in the blend response would be equal to 1. Furthermore, so long as the odours remain perpendicular, one could be changed without changing the component-factor of the other odour in the blend.

5.3.3 Concentration Effects

The effect on the spatiotemporal PN responses of concentration changes in the stimuli was assessed for configural effects. Figure 5.4 shows how the spatiotemporal code changes with concentration. The concentration of the odours in Figure 5.1 would be at 4 times the lowest concentration level in Figure 5.4. Figure 5.4a shows the correlation between responses to varying concentrations. Generally for the twelve odours, there is a band of high correlation (>0.9) around the upward diagonal. This indicates a smooth change in the PN spatiotemporal responses as stimulus concentration changes. For some odours, Odour 3 for example, this region of high correlation is wide and evident across all the concentrations, indicative of only a small change in spatiotemporal response over this concentration range. Other odours, Odour 1 in particular, appear to have concentrations for which the region of high correlation is pinched towards the diagonal. This is a consequence of the sigmoidal concentration input to the glomeruli. Since the sigmoidal response

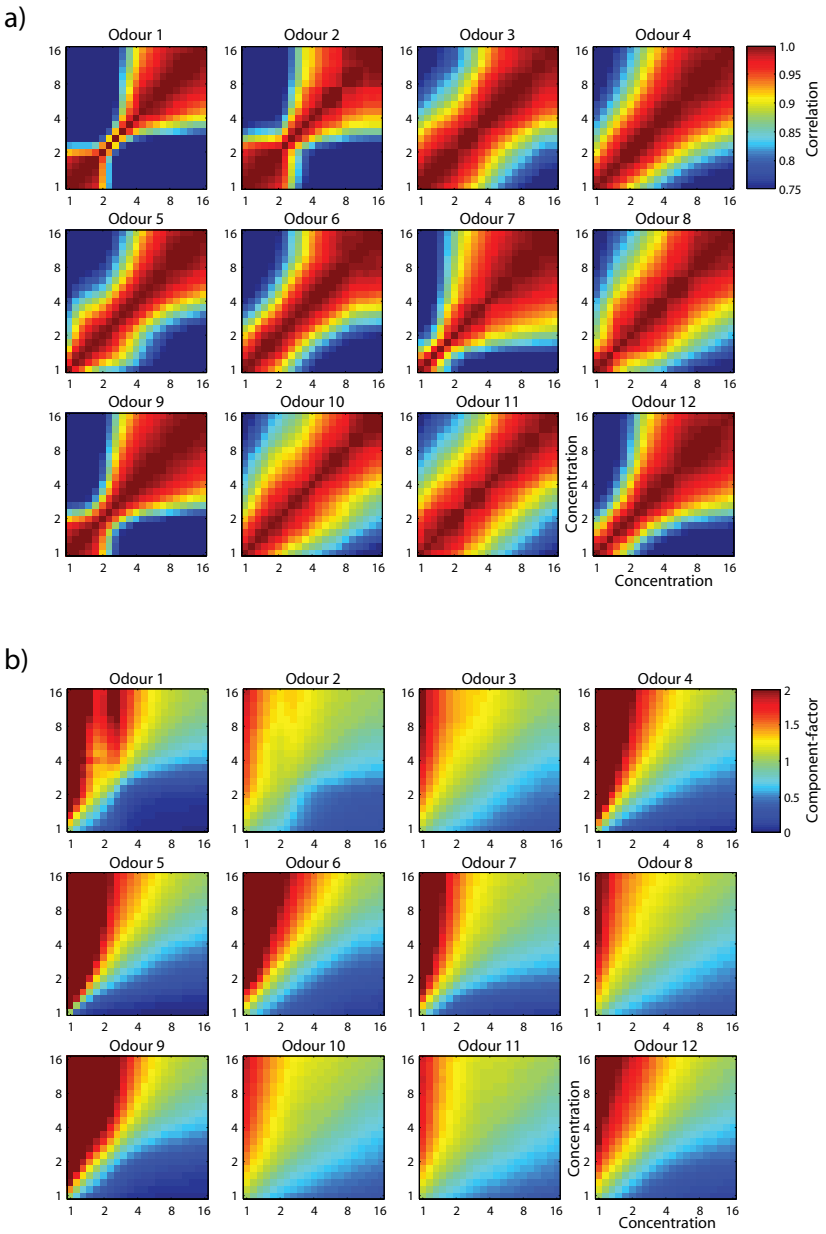

Figure 5.4: Consistency over concentration changes. a) For each odour as defined in Figure 5.1, the spatiotemporal responses for a range of stimulus concentrations were correlated against each other. The concentrations increase on a dyadic logarithm scale. The correlation coefficients depicted here are the mean values for 20 network instantiations of the general odour model. b) For each odour, the component-factor of one response in another was calculated for responses to different concentrations. $\mathbf{x}$ of equation 5.1 is the spatiotemporal PN response to concentrations on the x-axis, and $\mathbf{y}$ is that on the y-axis. These are also mean values over 20 networks.

to an odour has different gradients and thresholds for each glomerulus, the relative input activation levels between the glomeruli will change over concentration. For instance, the dominant input may change from one glomerulus to another, and thus alter the spatial activity pattern. This, in turn, changes the spatiotemporal PN code accordingly.

Overall, it appears that the PN spatiotemporal responses for odours change according to concentrations. This might suggest a configural code for concentrations, leading to perceptually distinct qualities for the same odour at different concentrations. However, one can see from Figure 5.4b that this is not necessarily the case. Figure 5.4b shows the component-factor of $\mathbf{x}$ in $\mathbf{y}$ where $\mathbf{x}$ is the spatiotemporal response vector for concentrations along the x-axis, and $\mathbf{y}$ along the y-axis. Along the upward diagonal, the component-factor is equal to 1, as expected. However, above and left of the diagonal, the component-factor is greater than or equal to 1, signifying that the response to low concentrations are within the responses to higher concentrations. In fact, where the component-factors were greater than 1, this meant that low concentration response vectors were augmented by increasing their magnitude. Correspondingly, below and right of the diagonal the component-factor is less than or equal to 1 but greater than 0, indicating that low concentration responses are an integral part of high concentration responses. And thus, increasing the concentration does not create a completely new configural neural representation, but one that is built upon the representation for lower concentrations.

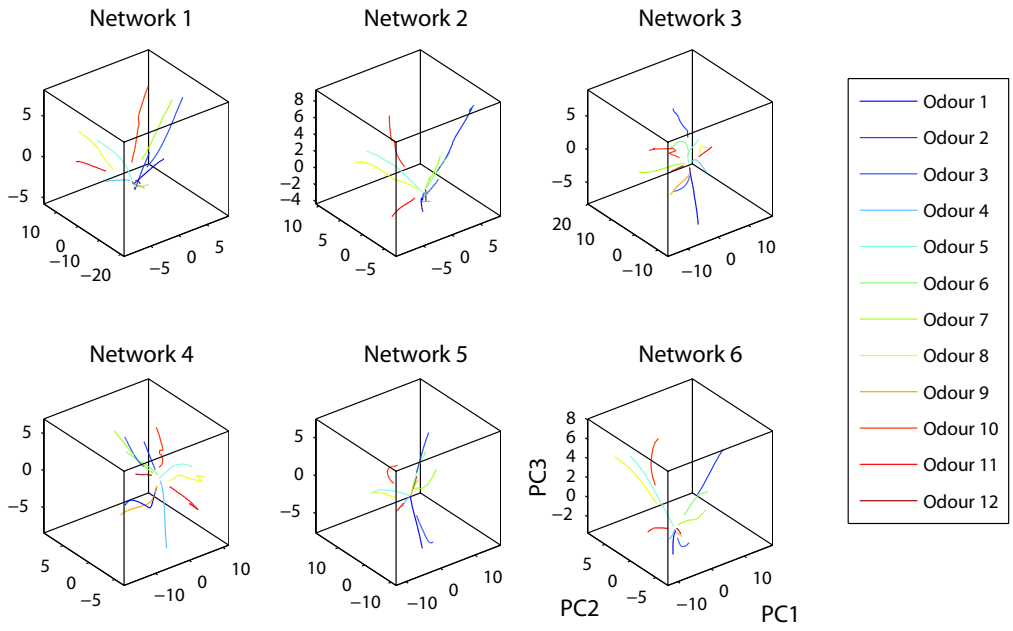

Figure 5.5: Spatiotemporal response vectors for changing concentration. The vectors for the spatiotemporal responses to the twelve odours at each concentration (the same range of concentrations as in Figure 5.4) are plotted. Principal component analysis was used for dimension reduction to allow the plotting of the vectors using the first three principal components. Points of the same odour are connected in order of increasing concentration, showing the paths the responses make in this spatiotemporal space as odour concentration changes. Here the response vectors for six network instantiations of the general odour model are plotted as examples. One can see that the paths are mainly smooth and continuous, and also the paths do not cross.

5.3.4 Varying Concentration for Different Odours

For each of the twelve odours in Figure 5.1, the spatiotemporal PN responses are plotted as concentration is increased in Figure 5.5. This confirms the smooth transition of the odour code between concentrations as indicated in Figure 5.4. Each odour forms a path in the spatiotemporal response vector space that starts near the middle and moves outward as concentration increases. This repulsion between the odours may be emphasised by the principal component analysis, but mainly indicates the underlying differences between odour responses that increase as concentration increases. The paths from increasing odour concentration are smooth and continuous, with very few sharp changes in direction. Moreover, the paths for different odours never cross. Importantly, this shows that the spatiotemporal representation of the odours are never the same between any two of the odours, irrespective of the concentration of either odour. In this spatiotemporal code, none of these odours could be mistaken for another odour at a different concentration.

5.4 Spatiotemporal Responses to Blends

5.4.1 Interactions due to Stimulus Properties

A configural perception of odour blends may in part be explained by nonlinear interactions of odour component responses during processing by the AL. Since the general odour model in this chapter converts a purely spatial input into spatiotemporal output, it is a highly nonlinear process. Therefore, the spatiotemporal code generated here may be the source of some configural effects. In this section, an investigation is made to find evidence of any configural neural representations of binary blends in the PN spatiotemporal

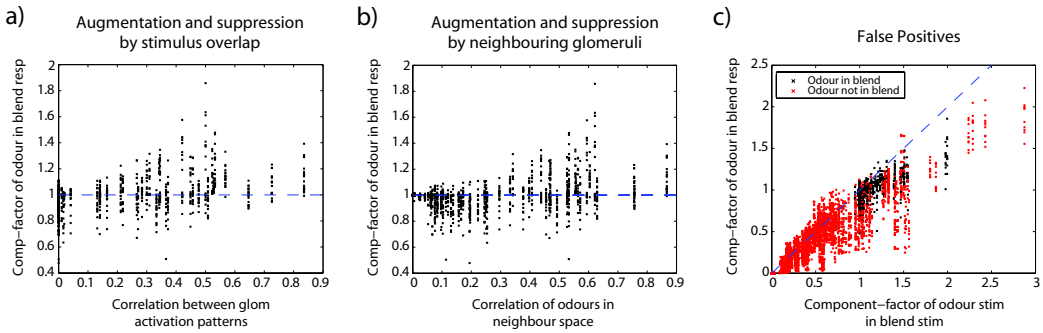

Figure 5.6: Nonlinear odour summation. These plots show if the PN representation of an odour component is kept within the PN representation of the blend (component-factor = 1), is augmented within the blend (> 1), or is suppressed within the blend (< 1). a) Augmentation and suppression by stimulus overlap. Glomerular input vectors are correlated to measure the overlap between odours that are components in blends. The data plotted are PN responses from 20 network instantiations. This shows only a slight general dependence of component-factor on stimulus overlap. For all extents of stimulus overlap there are examples of odour responses exactly preserved within the blend response. Suppressive effects, where the odour response is not fully present within the blend response, are mainly restricted to overlaps below 0.5 correlation. Strong augmentation effects, where the odour response is greater within the blend, are found around overlaps of 0.5 correlation. b) Augmentation and suppression by neighbouring glomeruli. Input vectors in the neighbour space are correlated. When the correlation between two odours is 0, there are no nonlinear interactions. For higher correlations, the graph is very similar to part (a). c) False positives. The component-factor of an odour stimulus in the blend stimulus is plotted against the component-factor of the responses. For stimulus vectors, odours that are components within a blend (black) have a component-factor value of greater than or equal to 1. Odours that are not components of a blend (red) generally follow the diagonal. False positives occur when an odour not in a blend has a response that appears to be contained within the blend response.

responses. Also investigated is how any interactions are dependent on the overlap in the glomerular input patterns of the component odours. To avoid confusion, hereafter a binary odour blend will be referred to as a 'blend', and any of the odours (as defined in Figure 5.1c) used to create these blends will be referred to as an 'odour'.

For spatiotemporal PN responses, in order to assess how the blend response compares to component odour responses, the component-factor is used (equation 5.1). It is thought that nonlinear interactions are a consequence of overlapping information channels (Hosler & Smith, 2000). To test this, the stimulus overlap was plotted against the component-factor for odour responses in blend responses (Figure 5.6). The stimulus overlap for two odours is taken to be the correlation (equation 4.3) between the glomerular spatial input vectors for those odours (as for Figure 5.2). The component-factor is that of the odour response in the blend response. In other words, this revelas how much the response for a component odour (presented singly) is kept as a component of the blend response. However, Figure 5.6a shows that stimulus overlap has only a limited effect on augmentation and suppression of component odour PN code within the blend PN code.

Another possible explanation for these nonlinear summations of responses is inter-glomerular inhibition. LNs only have the opportunity to influence interneurons in neighbouring glomeruli. To measure the potential for such inter-glomerular interaction, I define the neighbour space. For an odour, take each pair of neighbouring glomeruli (equivalently, each black bar between glomeruli in Figure 5.1) and take the sum of the inputs to the two glomeruli. This creates a 24-dimensional vector in the neighbour space for each odour.

Figure 5.6b shows that correlating the vectors of odours in the neighbour space can predict more information about the response interactions. Zero correlation between two odours in the neighbour space implies that none of the activated glomeruli for one odour is next to any activated glomeruli of the other odour. Low correlation indicates low activation in neighbouring glomeruli, while very high correlation indicates a high overlap in spatial input patterns. For odours that have zero correlation in the neighbour space, blend interactions are almost completely prevented, as indicated by the collapse of all points to 1. Therefore, inter-glomerular influences from neighbouring glomeruli is one cause of nonlinear interactions in the spatiotemporal code. However, there still does not appear to be a pattern to the suppression or augmentation. In particular, suppression seems to occur at weak to medium levels of correlation in the neighbour space, meaning that even weak inter-glomerular interactions may cause suppression.

Figure 5.6c provides some insight into the augmentation of the odour responses in the blend responses. For stimulus input vectors, the component-factor of the odour in the blend starts at 1 when the odour is a component of the blend. This is indicative of the lack of complicated interactions at this stage of input to the glomeruli, as inspired by the data in Chapter 3. Overlap between stimulus vectors increases the apparent concentration of one odour within the blend at the glomerular input level and subsequently at the PN output level. Thus, augmentation in the responses is mainly due to overlap of the glomerular input patterns from component odours, which can happen even when the odour was not used to create the blend. This relationship is indicated by the upward trend in the data along the diagonal, with no points far above the diagonal. The suppressive effects cause points to fall below the diagonal.

5.4.2 Blend Responses from Component Responses

Finally, I investigate how the spatiotemporal PN responses to odours combine to form the responses to blends. To do this, the component-factor (equation 5.1) is used extensively on the vectors of spatiotemporal responses from the PNs. Both the component-factor of the odour response in the blend response and the component-factor of the blend response in the odour response are used. The former shows how much of the odour response (relative to the magnitude of the odour response vector) is contained within the blend response, while the latter shows how much of the blend response is composed of the odour response (relative to the blend response).

Figure 5.7a shows how well the odour responses are carried through to the blend responses. In this plot, a blend response that is a summation of the odour responses with no interactions gives a cross at the point (1,1). The odours must use a completely distinct set of PNs in order to avoid summation of activity in overlapping PNs. Crosses at (1,1) are all coloured dark blue, which indicates that there is no neighbouring glomerular activity between the two odours. Along the vertical line going through (1,1) there is a high density of crosses. Points along this line are indicative that the odour on the x-axis is represented faithfully in the blend response, but the odour on the y-axis suffers suppression (for values below 1) or augmentation (above 1). Symmetrically, the inverse is also true, separating the diagram into four quadrants. The top right quadrant shows augmentation of both component odours in the blend responses. This is due to the overlap in the glomerular input from the odours, as indicated by the colour of these points. The bottom left quadrant shows suppression, with the colour indicating weak

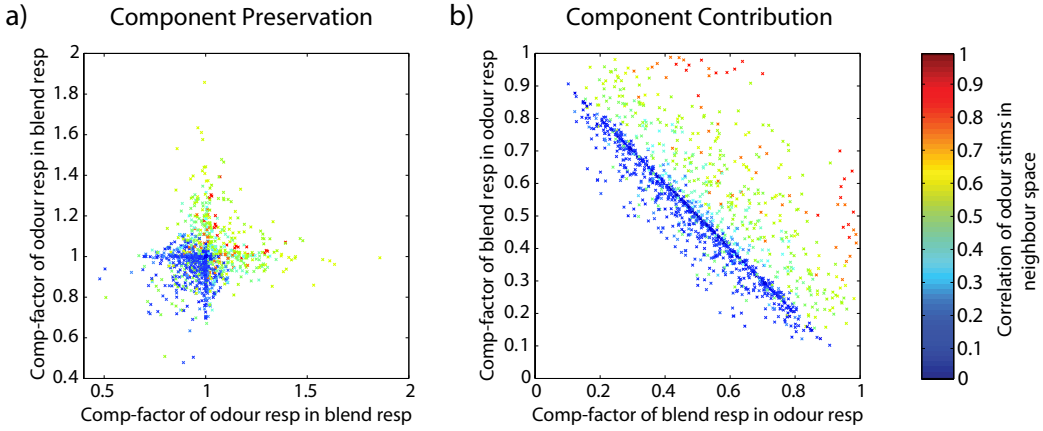

Figure 5.7: Configural code. a) Component preservation. For each binary blend, the component-factor of the odour response in the blend response is calculated for both odours from which the blend was created. This indicates how the odour responses are preserved within the responses to blends containing that odour. The two factors from the odour pair were plotted against each other, giving a cross for each blend. The colour of the crosses indicates the overlap in the neighbour space of the stimulus input to the glomeruli. The position of the data in this diagram relative to the point (1,1) augmentation of suppression of the odour response in the blend response. b) Component contribution. For each binary blend, the component-factor of the blend response in the odour response is calculated for both odours from which the blend was created. This indicates how much of the blend response is composed of an odour response. Blend responses that are just the linear combination of the component odour responses give data points along the downward diagonal. Above this line are blends that have overlapping component odour responses. Below this line are partially synthetic blend responses.

to medium neighbouring glomerular activation between the odours. The final two quadrants show augmentation of one odour, at the expense of suppression of the other.

Figure 5.7b shows the proportion of the blend responses that can be attributed to each component odour response. A striking feature of this diagram is the dense collection of data along the downward diagonal. On this line, the component-factors from both odours sum to 1, and therefore the blend response is composed exactly of the summation of the two odour responses. The crosses on this line are dark blue, indicating no activation of neighbouring glomeruli between the two odours. Above and right of this line, the component-factors sum to greater than 1, indicating that those blends must contain odours that have responses that overlap. The colours of these crosses confirm that the pairs of odours had high overlap in the stimulus vectors. Below and left of the downward diagonal, the component-factors sum to less than 1, as low as 0.8. This indicates that these blend responses are comprised of more than just the summation of the odour responses, since 0.2 of the blend response cannot be accounted for from the component odour responses. This is evidence of configural coding in these spatiotemporal AL models, with the blend response containing a synthetic component that is distinct from either single odour responses. An example of a synthetic blend representation is shown in Figure 5.8. This indicates that the synthetic nature of the blend response detected by the component-factor analysis is due to novel temporal patterning caused by interaction between the LNs.

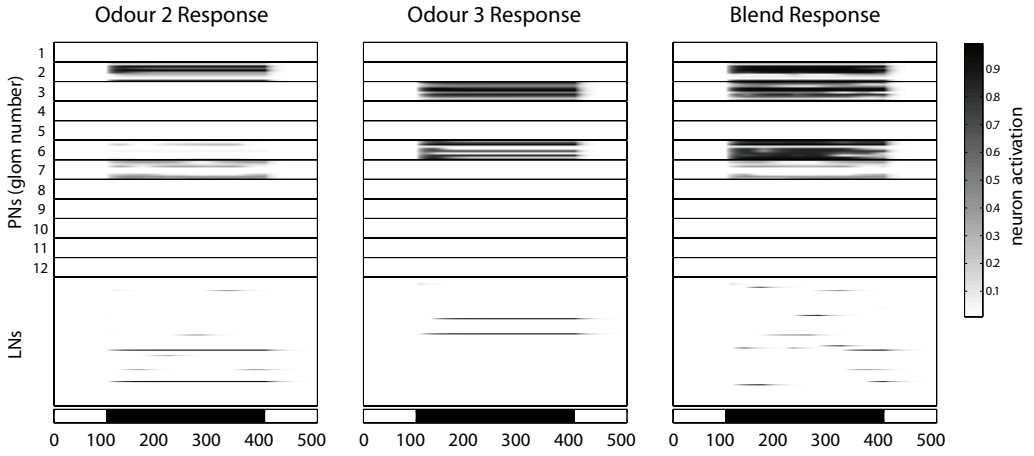

Figure 5.8: Example of Configural Responses. PN responses for the twelve glomeruli are shown for a 300 ms pulse, as indicated by the bottom abscissa. The blend response is, in some sense, a sum of the component odour responses. The set of glomeruli that have PN activity is the union of active glomeruli in the component odour responses. However, looking more closely at the temporal patterns in each glomerulus reveals very different responses in the blend. While there is some clear consistency in the blend response with the component odour responses (for example, Glomerulus 7 shows very similar temporal structure between Odour 2 and the blend), differences are also apparent (for example, Glomerulus 6). The underlying differences in dynamics are made clear by the LN activity.

5.5 Discussion

This chapter investigated the spatiotemporal output of a model of the general odour system of the AL. This model was an extension of the MGC model of Chapter 4 and generates realistic temporal patterning of PN responses (Rabinovich *et al.*, 2000, 2001; Laurent *et al.*, 2001). I analysed the spatiotemporal code from these temporally patterned PN responses to see how it reacts to changes in the stimulus concentration, and also whether this spatiotemporal code may explain some configural effects by inducing some synthetic neural representation of blends.

The model included many morphological details, including glomerular structures that determined the connectivity between interneurons. As an extension of the MGC model, the dynamics of the system were generated by the same WLC inhibitory network of LNs, which had been previously studied as a mechanism for generating a spatiotemporal AL code (Rabinovich *et al.*, 2000, 2001). However, these studies lacked any glomerular structure or even differentiated between different interneuron classes. In this chapter, the addition of these details into the general odour model allows the analysis of realistic odours and their blends and the subsequent PN output of the ALs, to investigate if this spatiotemporal model can explain any blend interactions observed at the perceptual level.

Stimuli were created with realistic input to the glomeruli, as inspired by the data from Chapter 3 and what is known from other existing studies (Carlsson *et al.*, 2002; Carlsson & Hansson, 2003). Optical imaging studies using calcium sensitive dyes show that odours elicit spatial patterns of activation of glomeruli. These patterns reflect the neural activity in the glomeruli,

particularly the ORN input to the glomeruli because presynaptic ORN activity dominates this calcium signal (Chapter 2). In Chapter 3, it was shown that this ORN input into the glomeruli lacks strong nonlinearities, whether between odours with distinct sets of activated glomeruli or overlapping sets. Chapter 3 also confirmed the sigmoidal concentration response curves for logarithmic concentration scale (Carlsson & Hansson, 2003), and indicated the range for which the sigmoids were between response threshold and plateau. All these biological details about the input to glomeruli were included in the creation of odour stimuli for the model.

Multiglomerular PNs appeared to mix the output responses from the glomeruli. Compared to uniglomerular PNs, the similarity of the odour code between different odours is increased, especially for very dissimilar odours. This model does not explain why insect ALs employ multiglomerular PNs in the general odour system. In the AL there is a mixture of PNs with dendritic branches in different numbers of glomeruli. These glomeruli then send axons to downstream brain regions via different antenno-cerebral tracts (Homberg *et al.*, 1988). In the sphinx moth *M. sexta*, these different tracts comprised of collections of PNs with different glomerular arborisation patterns. For instance, the most prominent inner antenno-cerebral tract is comprised mainly of uniglomerular PNs, while the second largest outer antenno-cerebral tract is mainly multiglomerular PNs (Homberg *et al.*, 1989). Also, these different tracts convey their PN axons to different brain regions, or the same regions in different orders (Homberg *et al.*, 1988). Thus, it may be that the different tracts convey different information from the AL and different spatiotemporal codes. Therefore, multiglomerular PNs may have a coding scheme for which

the spatiotemporal responses generated by this model are inappropriate. For instance multiglomerular PNs may employ precise spike timing more akin to the locust system (Bazhenov, Stopfer, Rabinovich, Huerta, *et al.*, 2001; Bazhenov, Stopfer, Rabinovich, Abarbanel, *et al.*, 2001). For this reason, further analyses were carried out with the uniglomerular output.

The mammalian olfactory bulb is the analogue of the insect AL, and also has glomerular structures with inhibitory connections between them. In another study, a model of the mammalian olfactory bulb has shown that lateral inhibition between glomeruli can enhance contrast between similar odours, and the same mechanism causes a configural code for odour blends (Linster & Cleland, 2004). However, this configural effect was a result of inhibition of Mitral/Tufted cells (output neurons analogous to PNs) in the overlap between activity patterns from two odours. The inhibition was to such a degree that these Mitral/Tufted cells in the overlap were completely unresponsive to the blend, displaying no activation. This is unrealistic, and one questions what would happen if an odour were to be presented at double concentration. Would this elicit no response in the Mitral/Tufted cells? The general odour model of the AL studied in this chapter has a careful treatment of concentration effects. Also, the olfactory bulb model assessed only the spatial odour code (mean activity over time), whereas I assessed the spatiotemporal code.

A danger of having a highly nonlinear transformation from the odour input to the PN output, which generates configural neural representations of odour blends, is that it may generate different configural representations for the same odour at different concentrations. Without consistency of the odour

code across concentrations, identifying an odour would be very difficult. Figure 5.4a showed that the odour code does change over concentrations. However, despite changes in the balance of relative activity between PNs and time-bins in the spatiotemporal vectors, the odour code for low concentrations is preserved and augmented within the code for higher concentrations (Figure 5.4b). The spatiotemporal neural representation over concentrations changes smoothly, and is such that no two odours ever have the same neural representation. This is true across all concentrations (Figure 5.5). Carlsson *et al.* (2003) showed that as concentration increased, more glomeruli would be recruited. Such activation of more and more glomeruli would enable the differentiation between a wide range of concentrations of the same odour. This is confirmed by the output of the general odour model. Figure 5.4a showed that the odour codes changed most at around the middle of the concentration range. This was due to the way sigmoidal concentration curves were created, meaning that the sigmoidal response curves were all increasing at around the middle of the concentration range. Thus the spatial pattern of glomerular activation would change most there, whereas there was little change once the sigmoids had reached their plateau level. Glomerular recruitment would extend the AL output to encode to a far greater concentration range.

Finally, I investigated the spatiotemporal response to odours and blends of those odours. A measure for how much a response vector is contained within another was created, and this allowed the assessment of preservation and contribution of odour responses in the responses to blends containing those odours. Suppression and augmentation of the odour responses were

detected, and these nonlinear effects in the spatiotemporal code were found to be dependent on inhibitory interactions from neighbouring glomeruli, rather than the overlap between glomerular activation patterns by odours. This may be because it is possible to separate configural effects at the receptor level from those originating from AL interactions, and to observe only the action of AL interneurons. Furthermore, synthesis of blend responses was found, which was novel to the blend and from the responses of the components. This is the first time such configural effects have been shown in a spatiotemporal general odour model of the moth antennal lobe.

Chapter 6

Conclusions

In this thesis, I have investigated the neural representation of odour blends at two stages along the odour pathway in insects, just before entering the antennal lobe (AL) and as it exits the AL. The neural representation at each stage can be thought of as an olfactory code. The input into the AL was investigated experimentally in the ALs of the moth *Spodoptera littoralis*, while the output was explored with computer simulations of antennal lobe models.

Odour blends are interesting because only a limited number of studies have considered the encoding of blends at this stage of processing, even though odours usually come as multi-component blends in the natural environment. Behavioural and psychophysical studies show that the perception of odour blends can have novel and distinct qualities compared to the odour components of those blends. In psychophysical terminology, blends can elicit synergy (increased response), suppression (decreased response), or hypoadditivity (somewhere in between). Such effects as synergy and suppression would contribute to a configural odour sense. I searched for nonlinearities in the neural representations of odour blends since nonlinearities in the odour code could be a source for configural coding.

Optical imaging of calcium dynamics in the AL was used to extract the presynaptic activity of ORNs innervating the glomeruli. However, before assessing the odour code entering the glomeruli, I had to develop some techniques in Chapter 2 to identify the glomeruli. I was able to identify glomeruli without the need of morphological staining, which can be difficult to achieve, nor a species-specific glomerular morphological map, which does not necessarily exist. The technique developed used physiological profiles from the glomerular responses to identify the glomeruli. As such, morphology details were not used, and so it was possible to show for the first time the conservation of glomerular position across animals.

The techiques developed in Chapter 2 allowed the assessment of the ORN input to the glomeruli in Chapter 3. Some studies have shown that a synthetic odour blend sense may be explicable in part to interactions between the neural representations of the odour components even at the ORN level. However, strongly nonlinear interactions were not found. This contradiction with previous studies is likely due to the very high concentration levels used in previous studies that were far above saturation levels of concentrations.

In Chapter 4 I demonstrated two alternative models of the MGC. These two alternatives differed only by the LN-to-LN competition schemes which allowed the comparison between a predominantly spatial and a spatiotemporal odour code. The spatial code was driven by dynamics of the LN subnetwork of Winner-Takes-All inhibitory connectivity, while the spatiotemporal code was driven by dynamics from a WLC subnetwork of LNs. Testing these models on their ability to distinguish between blend ratios, as a task at which the MGC is thought to be adept, I demonstrated that the more realistic spatiotemporal code was better able to encode the olfactory information in most

cases. I found one example of where the spatiotemporal code broke down due to confounding of the response dynamics for two consecutive odour pulses. However, this may not be a problem if the time-constants of the LNs were allowed to vary over the population.

Chapter 5 continues with the spatiotemporal code by extending the MGC model that was based on WLC dynamics. This model was extended to a general odour model that generated a spatiotemporal odour code. The main difference was that the number of glomeruli were increased. Data in Chapter 3 was the basis upon which realistic odours were created, which interacted without strong nonlinearities. I defined a new measure for the extent of one response within another, the component-factor, and I demonstrated that this general antennal lobe model gave a spatiotemporal odour code that exhibited some configural coding. I found that augmentation of a component response within a blend response was due to overlap in the components, whereas suppression was due to inter-glomerular interactions rather than stimulus overlap. Also suppressive effects can occur even when inter-glomerular interactions are between weakly activated glomeruli. Finally, I was able to show that, despite the lack of interactions in the input, the spatiotemporal network produced a partially synthetic code for the odour blends, with some portion of the blend response completely novel from the component responses.

Appendix A

Principal Component Analysis

Principal component analysis (PCA) is a statistical tool that finds a new orthogonal basis for the data such that the first basis vector is in the direction of greatest variance, the second basis vector is in the direction of greatest variance within the subspace perpendicular to the first, and so on. It is particularly useful for assessing high-dimensional data for redundant dimensionality since it determines how much variance is accountable in each principal component, and it enables the reducing of the dimensions to just those that can account for the variance. It is also useful for allowing visualisation of data in 3 dimensions when the first 3 principal components are plotted against each other. For more detailed information of what PCA is and how it is calculated, please see Chapter 12 of Methods of Multivariate Analysis by Rencher (Rencher, 2002d).

Bibliography

Afraimovich, V. S., Rabinovich, M. I., & Varona, P. (2004). Heteroclinic contours in neural ensembles and the winnerless competition principle. *International Journal of Bifurcation and Chaos*, *14*(4), 1195-1208.

Akers, R. P., & Getz, W. M. (1993). Response of olfactory receptor neurons in honeybees to odorants and their binary-mixtures. *Journal of Comparative Physiology A-Sensory Neural And Behavioral Physiology*, *173*(2), 169–185.

Akers, R. P., & O'Connell, R. J. (1988). The contribution of olfactory receptor neurons to the perception of pheromone component ratios in male redbanded leafroller moths. *Journal of Comparative Physiology A-Neuroethology Sensory Neural and Behavioral Physiology*, *163*(5), 641–650.

Akers, R. P., & O'Connell, R. J. (1991). Response specificity of male olfactory receptor neurons for the major and minor components of a female pheromone blend. *Physiological Entomology*, *16*(1), 1–17.

Almaas, T. J., & Mustaparta, H. (1990). Pheromone reception in tobacco budworm moth, *Heliothis-virescens*. *Journal of Chemical Ecology*, *16*(4), 1331–1347.

Anderson, P., Hansson, B. S., & Lofqvist, J. (1995). Plant-odor-specific receptor neurons on the antennae of female and male spodoptera-littoralis. *Physiological Entomology*, *20*(3), 189-198.

Anderson, P., Hilker, M., Hansson, B. S., Bombosch, S., Klein, B., & Schildknecht, H. (1993). Oviposition deterring components in larval frass of *Spodoptera-littoralis* (boisd) (lepidoptera, noctuidae)a behavioral and electrophysiological evaluation. *Journal of Insect Physiology*, *39*(2), 129–137.

Anton, S., & Hansson, B. S. (1995). Sex-pheromone and plant-associated odor processing in antennal lobe interneurons of male spodoptera-littoralis (lepidoptera, noctuidae). *Journal of Comparative Physiology A-Sensory Neural and Behavioral Physiology*, *176*(6), 773-789.

Anton, S., & Homberg, U. (1999). Antennal lobe structure. In B. S. Hansson

(Ed.), *Insect olfaction* (p. 97-124). Springer.

Anton, S., Lofstedt, C., & Hansson, B. S. (1997). Central nervous processing of sex pheromones in two strains of the european corn borer ostrinia nubilalis (lepidoptera: Pyralidae). *Journal of Experimental Biology*, *200*(7), 1073-1087.

Arn, H., Stadler, E., Rauscher, S., Buser, H. R., Mustaparta, H., Esbjerg, P., *et al.* (1980). Multicomponent sex-pheromone in *Agrotis-segetum* preliminary-analysis and field-evaluation. *Zeitschrift Fur Naturforschung C-A Journal Of Biosciences*, *35*(11-1), 986–989.

Av-Ron, E. (1994). Modeling olfactory neurons of the insect antennal lobe. In F. H. Eeckman (Ed.), *Computation in neurons and neural systems* (p. 173-178). Boston: Kluwer Academic Publishers.

Av-Ron, E., & Rospars, J.-P. (1995). Modeling insect olfactory neuron signaling by a network utilizing disinhibition. *BioSystems*, *36*(2), 101-108.

Av-Ron, E., & Vibert, J.-F. (1996). A model for temporal and intensity coding in insect olfaction by a network of inhibitory neurons. *Biosystems*, *39*(3), 241-250.

Baker, T. C., & Haynes, K. F. (1996). Pheromone-mediated optomotor anemotaxis and altitude control exhibited by male oriental fruit moths in the field. *Physiological Entomology*, *21*(1), 20-32.

Balkovsky, E., & Shraiman, B. I. (2002). Olfactory search at high reynolds number. *Proceedings of the National Academy of Sciences of the United States of America*, *99*(20), 12589-12593.

Bazhenov, M., Stopfer, M., Rabinovich, M., Abarbanel, H. D. I., Sejnowski, T. J., & Laurent, G. (2001). Model of cellular and network mechanisms for odor-evoked temporal patterning in the locust antennal lobe. *Neuron*, *30*(2), 569-581.

Bazhenov, M., Stopfer, M., Rabinovich, M., Huerta, R., Abarbanel, H. D. I., Sejnowski, T. J., *et al.* (2001). Model of transient oscillatory synchronization in the locust antennal lobe. *Neuron*, *30*(2), 553-567.

Belluscio, L., & Katz, L. C. (2001). Symmetry, stereotypy, and topography of odorant representations in mouse olfactory bulbs. *Journal of Neuroscience*, *21*(6), 2113-2122.

Berg, B. G., & Mustaparta, H. (1995). The significance of major pheromone components and interspecific signals as expressed by receptor neurons in the oriental tobacco budworm moth, *Helicoverpa-assulta*. *Journal of Comparative Physiology A-Sensory Neural And Behavioral Physiology*, *177*(6), 683–694.

Brown, E., & Dewhurst, C. (1975). The genus *Spodoptera* (lepidoptera, noctuidae) in africa and the near east. *Bulletin of Entomological Research*,

65, 221–262.

Brown, S. L., Joseph, J., & Stopfer, M. (2005). Encoding a temporally structured stimulus with a temporally structured neural representation. *Nature Neuroscience*, *8*(11), 1568–1576.

Carlsson, M. A., Anderson, P., Hartlieb, E., & Hansson, B. S. (1999). Experience-dependent modification of orientational response to olfactory cues in larvae of *Spodoptera littoralis*. *Journal of Chemical Ecology*, *V25*(11), 2445–2454.

Carlsson, M. A., Galizia, C. G., & Hansson, B. S. (2002). Spatial representation of odours in the antennal lobe of the moth spodoptera littoralis (lepidoptera : Noctuidae). *Chemical Senses*, *27*(3), 231-244.

Carlsson, M. A., & Hansson, B. S. (2002). Responses in highly selective sensory neurons to blends of pheromone components in the moth agrotis segetum. *Journal of Insect Physiology*, *48*(4), 443-451.

Carlsson, M. A., & Hansson, B. S. (2003). Dose-response characteristics of glomerular activity in the moth antennal lobe. *Chemical Senses*, *28*(4), 269–278.

Chandra, S., & Smith, B. H. (1998). An analysis of synthetic processing of odor mixtures in the honeybee (apis mellifera). *Journal of Experimental Biology*, *201*(22), 3113-3121.

Christensen, T. A. (2005). Making scents out of spatial and temporal codes in specialist and generalist olfactory networks. *Chemical Senses*, *30*(suppl 1), i283–i284.

Christensen, T. A., & Hildebrand, J. G. (1987). Male-specific, sex pheromone-selective projection neurons in the antennal lobes of the moth manduca sexta. *Journal of Comparative Physiology A-Sensory Neural and Behavioral Physiology*, *160*(5), 553-569.

Christensen, T. A., Hildebrand, J. G., Tumlinson, J. H., & Doolittle, R. E. (1989). Sex-pheromone blend of *Manduca-sexta* responses of central olfactory interneurons to antennal stimulation in male moths. *Archives of Insect Biochemistry and Physiology*, *10*(4), 281–291.

Christensen, T. A., Lei, H., & Hildebrand, J. G. (2003). Coordination of central odor representations through transient non-oscillatory synchronization of glomerular output neurons. *Proceedings of the National Academy of Sciences of the United States of America*, *100*(19), 11076–11081.

Christensen, T. A., Mustaparta, H., & Hildebrand, J. G. (1989). Discrimination of sex-pheromone blends in the olfactory system of the moth. *Chemical Senses*, *14*(3), 463-477.

Christensen, T. A., Mustaparta, H., & Hildebrand, J. G. (1991). Chemical communication in heliothine moths 2. central processing of intraspecific

and interspecific olfactory messages in the male corn-earworm moth *Helicoverpa-zea*. *Journal of comparative physiology A-sensory neural and behavioral physiology*, *169*(3), 259–274.

Christensen, T. A., Mustaparta, H., & Hildebrand, J. G. (1995). Chemical communication in heliothine moths 6. parallel pathways for information-processing in the macroglomerular complex of the male tobacco budworm moth *Heliothis-virescens*. *Journal of Comparative Physiology A-Sensory Neural And Behavioral Physiology*, *177*(5), 545–557.

Christensen, T. A., Pawlowski, V. M., Lei, H., & Hildebrand, J. G. (2000). Multi-unit recordings reveal context-dependent modulation of synchrony in odor-specific neural ensembles. *Nature Neuroscience*, *3*(9), 927–931.

Christensen, T. A., Waldrop, B. R., Harrow, I. D., & Hildebrand, J. G. (1993). Local interneurons and information-processing in the olfactory glomeruli of the moth *Manduca-Sexta*. *Journal of Comparative Physiology A-Sensory Neural and Behavioral Physiology*, *173*(4), 385–399.

Christensen, T. A., Waldrop, B. R., & Hildebrand, J. G. (1998). *Gabaergic mechanisms that shape the temporal response to odors in moth olfactory projection neurons.*

Couto, A., Alenius, M., & Dickson, B. J. (2005, September). Molecular, anatomical, and functional organization of the drosophila olfactory system. *Current Biology*, *15*(17), 1535–1547.

Dayan, P., & Abbott, L. F. (2001). Plasticity and learning. In *Theoretical neuroscience: Computational and mathematical modelling of neural systems* (p. 281-329). Cambridge, MA: MIT Press.

De Jong, R., & Visser, J. H. (1988). Integration of olfactory information in the colorado potato beetle brain. *Brain research*, *447*(1), 10–17.

Distler, P. G., & Boeckh, J. (1996). Synaptic connection between olfactory receptor cells and uniglomerular projection neurons in the antennal lobe of the american cockroach, *Periplaneta americana*. *Journal of Comparative Neurology*, *370*, 35-46.

Distler, P. G., & Boeckh, J. (1997a). Synaptic connections between identified neuron types in the antennal lobe glomeruli of the cockroach, periplaneta americana .1. uniglomerular projection neurons. *Journal of Comparative Neurology*, *378*(3), 307-319.

Distler, P. G., & Boeckh, J. (1997b). Synaptic connections between identified neuron types in the antennal lobe glomeruli of the cockroach, periplaneta americana .2. local multiglomerular interneurons. *Journal of Comparative Neurology*, *383*(4), 529-540.

Distler, P. G., Gruber, C., & Boeckh, J. (1998). Synaptic connections be-

tween gaba-immunoreactive neurons and uniglomerular projection neurons within the antennal lobe of the cockroach, periplaneta americana. *Synapse*, *29*(1), 1-13.

Duchamp-Viret, P., Duchamp, A., & Chaput, M. A. (2003). Single olfactory sensory neurons simultaneously integrate the components of an odour mixture. *European Journal of Neuroscience*, *18*(10), 2690-2696.

Ermentrout, B., Flores, J., & Gelperin, A. (1998). Minimal model of oscillations and waves in the limax olfactory lobe with tests of the model's predictive power. *Journal of Neurophysiology*, *79*(5), 2677-2689.

Ermentrout, B., Wang, J. W., Flores, J., & Gelperin, A. (2001). Model for olfactory discrimination and learning in limax procerebrum incorporating oscillatory dynamics and wave propagation. *Journal of Neurophysiology*, *85*(4), 1444-1452.

Fan, R. J., & Hansson, B. S. (2001). Olfactory conditioning in the moth *Spodoptera littoralis*. *Physiological Behavior*, *72*, 159-165.

Fishilevich, E., & Vosshall, L. B. (2005, September). Genetic and functional subdivision of the drosophila antennal lobe. *Current Biology*, *15*(17), 1548–1553.

Fonta, C., Sun, X. J., & Masson, C. (1993). Morphology and spatial-distribution of bee antennal lobe interneurons responsive to odors. *Chemical Senses*, *18*(2), 101-119.

Friedrich, R. W., & Korsching, S. I. (1997). Combinatorial and chemotopic odorant coding in the zebrafish olfactory bulb visualized by optical imaging. *Neuron*, *18*(5), 737–752.

Galan, R. F., Sachse, S., Galizia, C. G., & Herz, A. V. M. (2004). Odor-driven attractor dynamics in the antennal lobe allow for simple and rapid olfactory pattern classification. *Neural Computation*, *16*(5), 999-1012.

Galizia, C. G., & Menzel, R. (2000). Odour perception in honeybees: coding information in glomerular patterns. *Current Opinion in Neurobiology*, *10*(4), 504-510.

Galizia, C. G., & Menzel, R. (2001). The role of glomeruli in the neural representation of odours: results from optical recording studies. *Journal of Insect Physiology*, *47*(2), 115-130.

Galizia, C. G., Nagler, K., Holldobler, B., & Menzel, R. (1998). Odour coding is bilaterally symmetrical in the antennal lobes of honeybees apis mellifera. *European Journal of Neuroscience*, *10*(9), 2964-2974.

Galizia, C. G., Sachse, S., & Mustaparta, H. (2000). Calcium responses to pheromones and plant odours in the antennal lobe of the male and female moth heliothis virescens. *Journal of Comparative Physiology A-Sensory Neural and Behavioral Physiology*, *186*(11), 1049-1063.

Galizia, C. G., Sachse, S., Rappert, A., & Menel, R. (1999). The glomerular code for odor representation is species specific in the honeybee apis mellifera. *Nature Neuroscience*, *2*(5), 473-478.

Gao, Q., Yuan, B. B., & Chess, A. (2000). Convergent projections of drosophila olfactory neurons to specific glomeruli in the antennal lobe. *Nature Neuroscience*, *3*(8), 780-785.

Getz, W. M., & Akers, R. P. (1997). Response of american cockroach (*Periplaneta americana*) olfactory receptors to selected alcohol odorants and their binary combinations. *Journal of Comparative Physiology A-Sensory Neural And Behavioral Physiology*, *180*(6), 701–709.

Getz, W. M., & Lutz, A. (1999). A neural network model of general olfactory coding in the insect antennal lobe. *Chemical Senses*, *24*(4), 351-372.

Hammer, M. (1993). An identified neuron mediates the unconditioned stimulus in associative olfactory learning in honeybees. *Nature*, *366*(6450), 59-63.

Hammer, M., & Menzel, R. (1995). Learning and memory in the honey bee. *Journal of Neuroscience*, *9*, 3154–3162.

Hansson, B. S. (1999). Functional characteristics of the antennal lobe. In B. S. Hansson (Ed.), *Insect olfaction* (p. 125-161). Springer.

Hansson, B. S., Almaas, T. J., & Anton, S. (1995). Chemical communication in heliothine moths .5. antennal lobe projection patterns of pheromone-detecting olfactory receptor neurons in the male heliothis-virescens (lepidoptera, noctuidae). *Journal of Comparative Physiology A-Sensory Neural and Behavioral Physiology*, *177*(5), 535-543.

Hansson, B. S., Ljungberg, H., Hallberg, E., & Lofstedt, C. (1992). Functional specialization of olfactory glomeruli in a moth. *Science*, *256*(5061), 1313-1315.

Hansson, B. S., Szocs, G., Schmidt, F., Francke, W., Lofstedt, C., & Toth, M. (1990). Electrophysiological and chemical-analysis of sex-pheromone communication-system of the mottled umber, *Erannis-defoliaria* (lepidoptera, geometridae). *Journal of Chemical Ecology*, *16*(6), 1887–1897.

Harris, M. O., & Foster, S. P. (1991). Wind-tunnel studies of sex pheromone-mediated behavior of the hessian fly (diptera, cecidomyiidae). *Journal of Chemical Ecology*, *17*(12), 2421-2435.

Hartlieb, E., & Anderson, P. (1999). Olfactory-released behaviours. In B. S. Hansson (Ed.), *Insect olfaction* (p. 315-349). Springer.

Hartlieb, E., Anton, S., & Hansson, B. S. (1997). Dose-dependent response characteristics of antennal lobe neurons in the male moth agrotis segetum (lepidoptera: Noctuidae). *Journal of Comparative Physiology A-Sensory Neural and Behavioral Physiology*, *181*(5), 469-476.

Heinbockel, T., Christensen, T. A., & Hildebrand, J. G. (1999). Temporal

tuning of odor responses in pheromone-responsive projection neurons in the brain of the sphinx moth manduca sexta. *Journal of Comparative Neurology*, *409*(1), 1–12.

Heinbockel, T., Christensen, T. A., & Hildebrand, J. G. (2004). Representation of binary pheromone blends by glomerulus-specific olfactory projection neurons. *Journal of Comparative Physiology A-Neuroethology Sensory Neural and Behavioral Physiology*, *190*, 1023–1037.

Homberg, U., Christensen, T. A., & Hildebrand, J. G. (1989). Structure and function of the deutocerebrum in insects. *Annual Review of Entomology*, *34*, 477-501.

Homberg, U., Montague, R. A., & Hildebrand, J. G. (1988). Anatomy of antenno-cerebral pathways in the brain of the sphinx moth manduca-sexta. *Cell and Tissue Research*, *254*(2), 255-281.

Homberg, U., & Muller, U. (1999). Neuroactive substances in the antennal lobe. In B. S. Hansson (Ed.), *Insect olfaction* (p. 181-206). Springer.

Hoskins, S. G., Homberg, U., Kingan, T. G., Christensen, T. A., & Hildebrand, J. G. (1986). Immunocytochemistry of gaba in the antennal lobes of the sphinx moth manduca-sexta. *Cell and Tissue Research*, *244*(2), 243–252.

Hosler, J. S., & Smith, B. H. (2000). Blocking and the detection of odor components in blends. *Journal of Experimental Biology*, *203*(18), 2797-2806.

Jönsson, M., & Anderson, P. (1999). Electrophysiological response to herbivour-induced host plant volatiles in the moth *Spodoptera littoralis*. *Physiological Entomology*, *24*, 377-385.

Joerges, J., Kuttner, A., Galizia, C. G., & Menzel, R. (1997). Representations of odours and odour mixtures visualized in the honeybee brain. *Nature*, *387*(6630), 285–288.

Johnson, B. A., & Leon, M. (2000). Modular representations of odorants in the glomerular layer of the rat olfactory bulb and the effects of stimulus concentration. *Journal of Comparative Neurology*, *422*(4), 496-509.

Kaissling, K., & Kramer, E. (1990). Sensory basis of pheromone-mediated orientation in moths. *Verhandlungen der Deutschen Zoologischen Gesellschaft*, *83*, 109–131.

Kaissling, K. E. (1998). Flux detectors versus concentration detectors: Two types of chemoreceptors. *Chemical Senses*, *23*(1), 99-111.

Kaissling, K. E., Meng, L. Z., & Bestmann, H. J. (1989). Responses of bombykol receptor-cells to (z,e)-4,6-hexadecadiene and linalool. *Journal of Comparative Physiology A-Sensory Neural And Behavioral Physiology*, *165*(2), 147–154.

Kang, J. S., & Caprio, J. (1991). Electro-olfactogram and multiunit olfactory

receptor responses to complex mixtures of amino acids in the channel catfish, *Ictalurus punctatus*. *The Journal of General Physiology*, *98*(4), 699–721.

Kang, J. S., & Caprio, J. (1997). In vivo responses of single olfactory receptor neurons of channel catfish to binary mixtures of amino acids. *Journal of Neurophysiology*, *77*(1), 1–8.

Kay, L. M., Lowry, C. A., & Jacobs, H. A. (2003). Receptor contributions to configural and elemental odor mixture perception. *Behavioral Neuroscience*, *117*(5), 1108-1114.

Keil, T. A. (1999). Morphology and development of the peripheral olfactory organs. In B. S. Hansson (Ed.), *Insect olfaction* (p. 5-48). Springer.

Kerguelen, V., & Carde, R. T. (1997). Manoeuvres of female brachymeria intermedia flying towards host-related odours in a wind tunnel. *Physiological Entomology*, *22*(4), 344-356.

King, J. R., Christensen, T. A., & Hildebrand, J. G. (2000). Response characteristics of an identified, sexually dimorphic olfactory glomerulus. *Journal of Neuroscience*, *20*(6), 2391–2399.

Kuenen, L. P. S., & Carde, R. T. (1994). Strategies for recontacting a lost pheromone plume - casting and upwind flight in the male gypsy-moth. *Physiological Entomology*, *19*(1), 15-29.

Laing, D. G. (1989). *Perception of complex smells and tastes.* (D. Laing, W. Cain, R. McBride, & B. Ache, Eds.). New York: Academic Press.

Laing, D. G., & Francis, G. W. (1989). The capacity of humans to identify odors in mixtures. *Physiology & Behavior*, *46*(5), 809-814.

Laing, D. G., & Livermore, B. A. (1992). A perceptual analysis of complex chemical signals in humans. In R. Doty & D. Muller-Schwartz (Eds.), *Chemical signals in vertebrates.* (p. 587-593). New York: Plenum Press.

Laing, D. G., Panhuber, H., & Slotnick, B. M. (1989). Odor masking in the rat. *Physiology & Behavior*, *45*(4), 689-694.

Laing, D. G., Panhuber, H., Willcox, M. E., & Pittman, E. A. (1984). Quality and intensity of binary odor mixtures. *Physiology & Behavior*, *33*(2), 309–319.

Laurent, G., & Davidowitz, H. (1994, September). Encoding of olfactory information with oscillating neural assemblies. *Science*, *265*(5180), 1872–1875.

Laurent, G., Stopfer, M., Friedrich, R. W., Rabinovich, M. I., Volkovskii, A., & Abarbanel, H. D. I. (2001). Odor encoding as an active, dynamical process: Experiments, computation, and theory. *Annual Review of Neuroscience*, *24*, 263-297.

Linster, C., & Cleland, T. A. (2004). Configurational and elemental odor mixture perception can arise from local inhibition. *Journal of Compu-*

tational Neuroscience, *16*(1), 39-47.

Linster, C., & Dreyfus, G. (1996). A model for pheromone discrimination in the insect antennal lobe: Investigation of the role of neuronal response pattern complexity. *Chemical Senses*, *21*(1), 19-27.

Linster, C., Kerszberg, M., & C, M. (1994). Pheromone detection, ratio discrimination and oscillations: a new approach to olfactory coding. In F. Eeckman (Ed.), *Computation in neurons and neural systems* (pp. 179–184). Kluwer Academic Publishers.

Linster, C., & Masson, C. (1996). A neural model of olfactory sensory memory in the honeybee's antennal lobe. *Neural Computation*, *8*(1), 94-114.

Linster, C., Masson, C., Kerszberg, M., Personnaz, L., & Dreyfus, G. (1992). A formal model of the insect olfactory macroglomerulus: simulations and analytical results. In C. Giles, S. Hanson, & J. Cowan (Eds.), *Advances in neural information processing systems, 5* (p. 239-252). Morgan Kaufmann.

Linster, C., Masson, C., Kerszberg, M., Personnaz, L., & Dreyfus, G. (1993). Computational diversity in a formal model of the insect olfactory macroglomerulus. *Neural Computation*, *5*(2), 228-241.

Linster, C., Sachse, S., & Galizia, G. (2005). Computational modeling suggests that response properties rather than spatial position determine connectivity between olfactory glomeruli. *Journal of Neurophysiology*, *93*, 3410–3417.

Linster, C., & Smith, B. H. (1997). A computational model of the response of honey bee antennal lobe circuitry to odor mixtures: overshadowing, blocking and unblocking can arise from lateral inhibition. *Behavioural Brain Research*, *87*(1), 1-14.

Linster, C., & Smith, B. H. (1999). Generalization between binary odor mixtures and their components in the rat. *Physiology & Behavior*, *66*(4), 701-707.

Lofstedt, C., Vanderpers, J. N. C., Lofqvist, J., Lanne, B. S., Appelgren, M., Bergstrom, G., *et al.* (1982). Sex-pheromone components of the turnip moth, *Agrotis-segetum*, lepidoptera, noctuidae - chemical-identification, electro-physiological evaluation and behavioral activity. *Journal of Chemical Ecology*, *8*(10), 1305–1321.

MacLeod, K., & Laurent, G. (1996, November). Distinct mechanisms for synchronization and temporal patterning of odor-encoding neural assemblies. *Science*, *274*(5289), 976–979.

Malnic, B., Hirono, J., Sato, T., & Buck, L. B. (1999). Combinatorial receptor codes for odors. *Cell*, *96*(5), 713-723.

Masson, C., & Linster, C. (1995). Towards a cognitive understanding of odor

discrimination: Combining experimental and theoretical approaches. *Behavioural Processes*, *35*(1-3), 63-82.

Meister, M., & Bonhoeffer, T. (2001). Tuning and topography in an odor map on the rat olfactory bulb. *Journal of Neuroscience*, *21*(4), 1351–1360.

Menzel, R. (1993). Associative learning in honey bees. *Apidologie*, *24*, 157–168.

Mombaerts, P., Wang, F., Dulac, C., Chao, S. K., Nemes, A., Mendelsohn, M., *et al.* (1996). Visualizing an olfactory sensory map. *Cell*, *87*(4), 675-686.

Moskowitz, H. R., & Barbe, C. D. (1977). Profiling of odor components and their mixtures. *Sensory Processes*, *1*(3), 212–226.

Muller, D., Abel, R., Brandt, R., Zockler, M., & Menzel, R. (2002). Differential parallel processing of olfactory information in the honeybee, apis mellifera l. *Journal of Comparative Physiology A-Neuroethology Sensory Neural and Behavioral Physiology*, *188*(5), 359-370.

Murlis, J., Elkinton, J. S., & Carde, R. T. (1992). Odor plumes and how insects use them. *Annual Review of Entomology*, *37*, 505-532.

Ochieng, S. A., Park, K. C., & Baker, T. C. (2002). Host plant volatiles synergize responses of sex pheromone-specific olfactory receptor neurons in male *Helicoverpa zea*. *Journal of Comparative Physiology A-Neuroethology Sensory Neural And Behavioral Physiology*, *188*(4), 325–333.

Oka, Y., Omura, M., Kataoka, H., & Touhara, K. (2004). Olfactory receptor antagonism between odorants. *EMBO Journal*, *23*(1), 120-126.

Pearce, T. C., Chong, K. Y., Verschure, P. F. M., Bermudez I Badia, S., Carlsson, M. A., Chanie, E., *et al.* (2004). Chemotactic search in complex environments: From insects to real-world apaplications. In J. W. Gardner & J. Yinon (Eds.), *Electronic noses & sensors for the detection of explosives* (pp. 181–208). Kluwer.

Quero, C., Fadamiro, H. Y., & Baker, T. C. (2001). Responses of male helicoverpa zea to single pulses of sex pheromone and behavioural antagonist. *Physiological Entomology*, *26*(2), 106-115.

Rabinovich, M., Huerta, R., Volkovskii, A., Abarbanel, H. D. I., Stopfer, M., & Laurent, G. (2000). Dynamical coding of sensory information with competitive networks. *Journal of Physiology-Paris*, *94*(5-6), 465-471.

Rabinovich, M., Volkovskii, A., Lecanda, P., Huerta, R., Abarbanel, H. D. I., & Laurent, G. (2001). Dynamical encoding by networks of competing neuron groups: Winnerless competition. *Physical Review Letters*, *87*(6), 068102.

Rencher, A. C. (2002a). Cluster analysis. In *Methods of multivariate analysis* (second ed., p. 451-503). Wiley-Interscience.

Rencher, A. C. (2002b). Discriminant analysis: Description of group seperation. In *Methods of multivariate analysis* (second ed., p. 270-298). Wiley-Interscience.

Rencher, A. C. (2002c). Multivariate analysis of variance. In *Methods of multivariate analysis* (second ed., p. 156-247). Wiley-Interscience.

Rencher, A. C. (2002d). Principal component analysis. In *Methods of multivariate analysis* (second ed., p. 380-407). Wiley-Interscience.

Rospars, J. P., & Hildebrand, J. G. (2000). Sexually dimorphic and isomorphic glomeruli in the antennal lobes of the sphinx moth manduca sexta. *Chemical Senses*, *25*(2), 119-129.

Rubin, B. D., & Katz, L. C. (1999). Optical imaging of odorant representations in the mammalian olfactory bulb. *Neuron*, *23*(3), 499–511.

Sachse, S., & Galizia, C. G. (2003). The coding of odour-intensity in the honeybee antennal lobe: local computation optimizes odour representation. *European Journal of Neuroscience*, *18*(8), 2119-2132.

Sachse, S., Rappert, A., & Galizia, C. G. (1999). The spatial representation of chemical structures in the antennal lobe of honeybees: steps towards the olfactory code. *European Journal of Neuroscience*, *11*(11), 3970-3982.

Sadek, M. M., Hansson, B. S., Rospars, J. P., & Anton, S. (2002). Glomerular representation of plant volatiles and sex pheromone components in the antennal lobe of the female spodoptera littoralis. *Journal of Experimental Biology*, *205*(10), 1363-1376.

Stengle, M., Ziegelberger, G., Boekhoff, I., & Krieger, J. (1999). Perireceptor events and transduction mechanisms in insect olfaction. In B. S. Hansson (Ed.), *Insect olfaction* (p. 49-66). Springer.

Steullet, P., & Derby, C. D. (1997). Coding of blend ratios of binary mixtures by olfactory neurons in the florida spiny lobster, panulirus argus. *Journal of Comparative Physiology A-Sensory Neural and Behavioral Physiology*, *180*(2), 123-135.

Stewart, G. W. (1998). The qr decomposition and least squares. In *Matrix algorithms* (p. 251-358). SIAM.

Tabor, R., Yaksi, E., Weislogel, J. M., & Friedrich, R. W. (2004). Processing of odor mixtures in the zebrafish olfactory bulb. *Journal of Neuroscience*, *24*(29), 6611-6620.

Todd, J. L., & Baker, T. C. (1999). Function of peripheral olfactory organs. In B. S. Hansson (Ed.), *Insect olfaction* (p. 67-96). Springer.

Uchida, N., Takahashi, Y. K., Tanifuji, M., & Mori, K. (2000). Odor maps in the mammalian olfactory bulb: domain organization and odorant structural features. *Nature Neuroscience*, *3*(10), 1035–1043.

Valeur, P. G., & Lofstedt, C. (1996, April). Behaviour of male oriental fruit

moth, grapholita molesta, in overlapping sex pheromone plumes in a wind tunnel. *Entomologia Experimentalis et Applicata*, *79*(1), 51–59.

Vickers, N. J., Christensen, T. A., Baker, T. C., & Hildebrand, J. G. (2001). Odour-plume dynamics influence the brain's olfactory code. *Nature*, *410*(6827), 466–470.

Vosshall, L. B. (2001). The molecular logic of olfaction in drosophila. *Chemical Senses*, *26*(2), 207-213.

Vosshall, L. B., Wong, A. M., & Axel, R. (2000). An olfactory sensory map in the fly brain. *Cell*, *102*(2), 147-159.

Wang, J. W., Wong, A. M., Flores, J., Vosshall, L. B., & Axel, R. (2003). Two-photon calcium imaging reveals an odor-evoked map of activity in the fly brain. *Cell*, *112*(2), 271-282.

Ward, J. H. (1963, March). Hierarchical grouping to optimize an objective function. *Journal of the American Statistical Association*, *58*(301), 236-244.

Wilson, H. R. (1999a). Action potentials and limit cycles. In *Spikes, decisions, and actions* (p. 116-135). Oxford University Press.

Wilson, H. R. (1999b). First order linear differential equations. In *Spikes, decisions, and actions* (p. 13-27). Oxford University Press.

Wilson, H. R. (1999c). Nonlinear oscillations. In *Spikes, decisions, and actions* (p. 136-155). Oxford University Press.

Wiltrout, C., Dogra, S., & Linster, C. (2003). Configurational and nonconfigurational interactions between odorants in binary mixtures. *Behavioral Neuroscience*, *117*(2), 236-245.

Wu, W. Q., Anton, S., Lofstedt, C., & Hansson, B. S. (1996). Discrimination among pheromone component blends by interneurons in male antennal lobes of two populations of the turnip moth, *Agrotis segetum*. *Proceedings of the National Academy of Sciences of the United States of America*, *93*(15), 8022-8027.

Wu, W. Q., Hansson, B. S., & Lofstedt, C. (1995). Electrophysiological and behavioral evidence for a 4th sex-pheromone component in the turnip moth, *Agrotis-segetum*. *Physiological Entomology*, *20*(1), 81–92.

Yu, D. H., Ponomarev, A., & Davis, R. L. (2004). Altered representation of the spatial code for odors after olfactory classical conditioning: Memory trace formation by synaptic recruitment. *Neuron*, *42*(3), 437-449.